Reduced Basis Methods for nonlinear Inverse Problems

Dissertation
zur Erlangung des Doktorgrades
der Naturwissenschaften

vorgelegt beim Fachbereich Informatik und Mathematik
der Johann Wolfgang Goethe-Universität
in Frankfurt am Main

von

Dominik Karl Garmatter
aus Heilbronn-Neckargartach

Frankfurt am Main 2018
(D 30)

vom Fachbereich Informatik und Mathematik der

Johann Wolfgang Goethe-Universität als Dissertation angenommen.

Dekan: Prof. Dr. Andreas Bernig

Gutachter: Prof. Dr. Bastian von Harrach
Prof. Dr. Bernard Haasdonk
Prof. Dr. Jin Keun Seo

Datum der Disputation: 27.06.2018

Contents

Introduction

Partial differential equations (PDEs) are the mathematical language in which we nowadays describe many phenomena observed in physics, biology and other sciences. Usually, one knows the present surroundings, e. g. certain parameters, and wants to determine a physical quantity by solving the corresponding PDE. Although this so-called *forward problem* is of large interest on its own and the correct modeling and numerical implementation of such problems is of great importance in many branches of today's industry and economy, this work shall deal with so-called *inverse coefficient problems for partial differential equations*. In this inverse context, one observes or measures the physical quantity and wants to identify the underlying set of parameters.

We formulate an exemplary model problem, where Ω denotes the object of interest: given the thermal heat conductivity σ on Ω (the parameter) find the temperature distribution u (the physical quantity) fulfilling the PDE

$$\nabla \cdot (\sigma \nabla u) = 1 \quad \text{in } \Omega \qquad u = 0 \quad \text{on } \partial\Omega, \tag{0.1}$$

with $\partial\Omega$ denoting the boundary of the domain Ω. The corresponding *inverse model problem* then reads: given the temperature distribution u over Ω, find the corresponding thermal heat conductivity σ such that (0.1) is fulfilled.

Hadamard [Had14] once formulated the following criteria for a *well-posed* mathematical problem: existence of a solution, uniqueness of the solution and the continuous dependency of the solution on the data (small changes in the data should only lead to small changes in the solution). Furthermore, he suggested to only tackle well-posed problems and ignore *ill-posed* problems, that are problems where at least one of the criteria is violated. Unfortunately, many inverse problems for partial differential equations, for instance the inverse model problem described above, are known to be ill-posed. The ill-posedness often occurs in the solution not depending continuously on the data, such that small measurement errors in the data (which are present in any real-world context) can lead to arbitrarily large errors in the reconstruction that is the solution of the inverse problem.

A simple approach to solve an inverse problem is the following: guess a set of parameters, solve the corresponding forward problem, test how well this solution does represent the observed data and repeat this process until the PDE solution for a set of parameters is a satisfactory fit for the data. Apart from the obvious inefficiency of guessing a set of parameters, this approach fails as soon as the inverse

problem is ill-posed and measurement errors are present. Nevertheless, it illuminates a scheme that is prevalent in many modern solution algorithms for inverse problems: the forward problem has to be solved multiple or many times in order to solve the inverse problem. We mention the class of *regularization algorithms*, see, e.g., [KNS08, EHN96, Rie03] for a thorough overview, whose representatives not only choose a new set of parameters in a sophisticated way but also provide stable reconstructions for ill-posed inverse problems and noise-corrupted data.

Having to frequently solve the forward problem is the most time-consuming part of the solution process of an inverse problem such that the main motivation of this work arises from this connection: we want to speed up the solution process of inverse problems by reducing the computational time required for a solution of the forward problem. To be more precise, we want to utilize an approximation to the forward solution that can be cheaply computed. As a result, we will develop novel algorithms that will combine existing solution algorithms for inverse problems with the approach of utilizing an approximative forward solution. To obtain such an approximation, we choose the *reduced basis method* which is a model order reduction technique.

Given a parametrized PDE, for instance let this be (0.1) with $\sigma \in \mathcal{P}$ being the parameter in the parameter domain $\mathcal{P}$ and $u^\sigma \in Y$ being the corresponding solution of the PDE residing in the solution space Y, there is an associated *solution manifold* $\mathcal{M} := \{u^\sigma \mid \sigma \in \mathcal{P}\}$. The aim of the classical reduced basis method is the construction of a low-dimensional subspace $Y_N \subset Y$, the *global reduced basis space*, such that Y_N approximates the solution manifold $\mathcal{M}$. The *reduced basis approximation* u_N^σ of u^σ is then the Galerkin projection of u^σ onto Y_N. Typically, the reduced basis space is the linear span of so-called *snapshots* that are solutions of the PDE for parameters that are of significance for the problem. Figure 1 illustrates the reduced basis method in a schematic way and we refer to[RHP08, Haa17] for a detailed overview of the method.

Let us return to the ill-posed inverse model problem. In Chapter 1, we will employ the nonlinear *Landweber method*, see, e.g., [HNS95, Han14] for an investigation of this basic iterative regularization algorithm, to solve it and then develop a novel algorithm that combines the Landweber method with the reduced basis method. The naive idea for such an algorithm would be what we want to call the *direct approach*: construct a global reduced basis space for the PDE (0.1) and substitute every solution of (0.1) in the Landweber method with corresponding reduced basis approximations. Of course, the applicability of this direct approach is reliant on the possibility of constructing a global reduced basis space for the corresponding forward problem.

In the inverse model problem however, one wants to recover a high-resolution image of the thermal conductivity. In a numerical approach, this leads to a high-dimensional parameter domain $\mathcal{P}$ where one pixel of the image corresponds to one dimension in the parameter domain and it is well-known that parameter domains

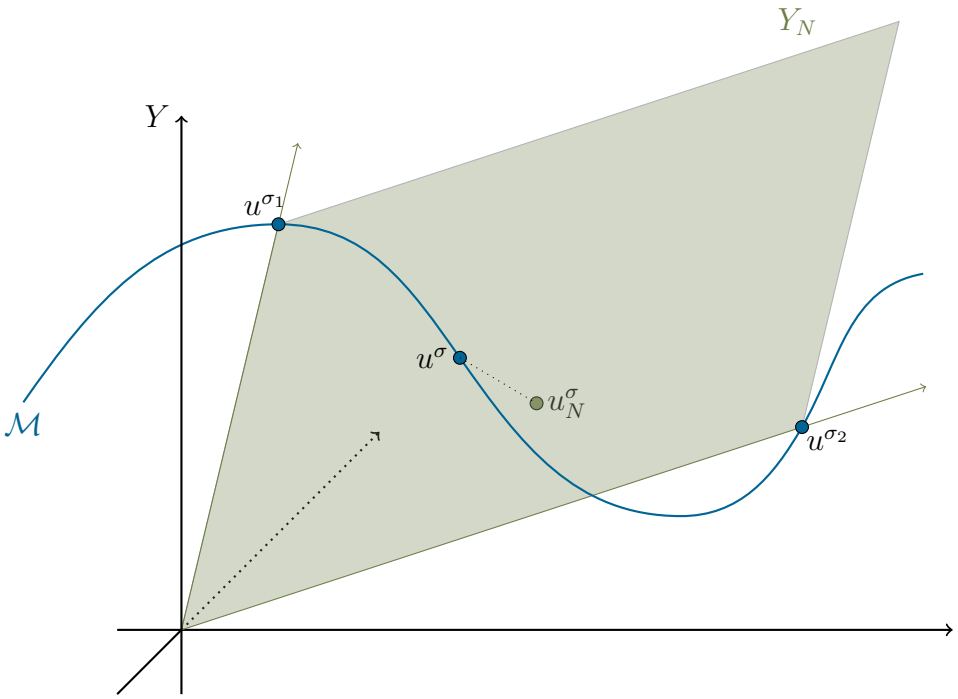

Figure 1: Schematic overview of the reduced basis method. The reduced basis space Y_N is the linear span of the snapshots u^{σ_1}, u^{σ_2} and u_N^{σ}, the reduced basis approximation of u^{σ}, is illustrated as the orthogonal projection of u^{σ} onto Y_N.

of high or arbitrary dimension represent an enormous difficulty in reduced basis methods. We will discuss why a global reduced basis space cannot be constructed for our imaging problem such that the mentioned direct approach is not feasible in this context. This leads to the first achievement of this work: the development of a general approach that applies reduced basis methods to high-dimensional parameter domains in the context of inverse imaging problems. New algorithms that are combinations of existing solution algorithms for (ill-posed) inverse problems and an *adaptive reduced basis approach* will be the result. We will describe the basics of this adaptive reduced basis approach in the following.

Iterative regularization methods such as the Landweber method produce a sequence of iterates starting with an initial guess and ending with the exact solution or an approximation to it. In any case, this sequence resides inside a bounded, a-priori unknown, subdomain of the parameter domain $\mathcal{P}$ and the associated forward solutions of the PDE reside in an a-priori unknown part of the solution manifold $\mathcal{M}$. In order to substitute these forward solutions by reduced basis approximations, it is therefore sufficient to construct a *local reduced basis space* that approximates only this unknown part of $\mathcal{M}$ instead of the whole solution manifold as it is the case with a global reduced basis space. The challenge in constructing such a local reduced basis space is: how can such a space be constructed, if the to be approximated part

of $\mathcal{M}$ and the associated part of $\mathcal{P}$ are a-priori unknown? To resolve this issue, we will exploit the inherent ability of the solution algorithm of the inverse problem to find new parameters that are relevant for the solution of the inverse problem. The following steps are the foundation of the adaptive reduced basis approach:

1. Given a reduced basis space Y_N, project the solution algorithm of the inverse problem onto Y_N.
2. Run this projected algorithm to generate new iterates until either the current iterate is accepted as the solution to the inverse problem or the approximation quality of Y_N has to be improved.
3. In the former case, accept the current iterate as a solution to the inverse problem and terminate. In the latter case, use the current iterate to enrich Y_N using the corresponding forward solution and go to the first step.

Chapter 1 will thoroughly work out this idea and the novel *Reduced Basis Landweber method* will be the result. In a numerical investigation this method will be compared to the original Landweber method and we will find out that the Reduced Basis Landweber method is more than an order faster than the Landweber method while possessing the same reconstruction quality as the Landweber method. Figure 2 depicts a preview of the numerical results regarding the similarity of the reconstructions.

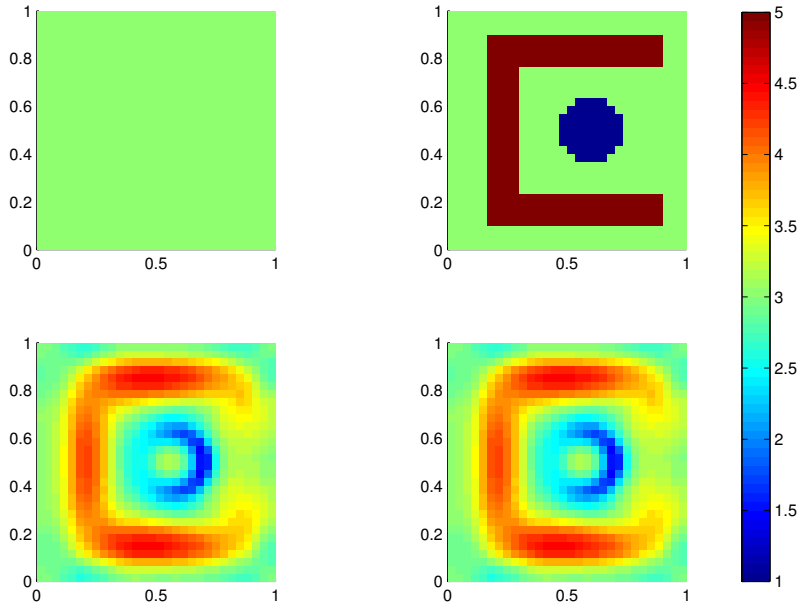

Figure 2: The initial guess (top left), the true solution (top right), the reconstructions via the Reduced Basis Landweber method (bottom left) and via the Landweber method (bottom right).

Magnetic Resonance Electrical Impedance Tomography

The simplicity of the inverse model problem and the Landweber method are beneficial for the development of the adaptive reduced basis framework for inverse imaging problems and serve the purpose of a clear explanation of the approach. The second Chapter of this work shall investigate the approach applied to a practicably reasonable and complex problem and especially provide a deep theoretical investigation towards convergence of the resulting novel method. To this end, the second part of this work is devoted to the problem of Magnetic Resonance Electrical Impedance Tomography (MREIT).

MREIT is an imaging modality developed during the past three decades. The imaging subject resides inside an MRI scanner and surface electrodes are attached to it. The aim of the method is the recovery of the electrical conductivity of the subject. The necessary data is generated by injecting electrical current through an electrode and the generated current flow then results in a change of the magnetic flux density $\mathbf{B} = (B_x, B_y, B_z)$ which can be observed by the MRI scanner. Measuring this magnetic field yields a full set of internal data of the subject and enables the reconstruction of high-resolution images of the subject's electrical conductivity.

The idea for MREIT originates from the Electrical Impedance Tomography (EIT), see, e.g., [CIN99, NGI88, AGL11, Lio04, Uhl09] for a broad overview, where one wants to determine the electrical conductivity of the subject from current-to-voltage measurements taken at the electrodes attached to the subject. Although the setup of EIT is easier (no MRI scanner is required), the problem is severely ill-posed such that the resolution of the resulting reconstructions is usually rather low. This drawback of EIT was the historical motivation for the development of MREIT.

In this work, we will investigate the B_z-based inverse problem of MREIT, where it is assumed that only B_z is available with the z-direction being the direction of the main magnetic field of the MRI scanner (obtaining the whole magnetic field $\mathbf{B}$ requires undesired rotations of the imaging subject inside the scanner). In the early 2000s, Seo et al. [SYWK03] proposed the *Harmonic B_z Algorithm* as a numerical solution algorithm for this B_z-based inverse problem of MREIT and we mention that this algorithm has since then been extensively studied, see, e.g., [OLW$^+$03, KPSW06, WS08, LSSW07, LSW10, SW11] and the references therein.

We will examine this practically reasonable inverse problem together with the Harmonic B_z Algorithm as its solution algorithm and, referring to Theorem 2.2.12, provide a convergence result that extents the existing convergence theory, see [LSSW07, LSW10], towards an approximative Harmonic B_z Algorithm. It will be proven that this approximative Harmonic B_z Algorithm converges as soon as the utilized approximation to the forward solution fulfills a regularity and a quality condition. Aside from these conditions it is up to the user to choose the type of approximation. The second achievement of this work is the consequence: numerical convergence of the Harmonic B_z Algorithm (for instance when a suitable finite element approximation

is utilized in a numerical implementation). We want to highlight that convergence results for other solution algorithms of inverse problems (if there exists one) usually assume the knowledge of the exact forward solution such that numerical convergence of the associated algorithm can not be concluded. Therefore, the statement proven in Theorem 2.2.12 can be seen as a step towards numerical convergence of other solution algorithms for inverse problems.

Since the type of approximation in this theoretical investigation will not matter, the convergence of the novel *Reduced Basis Harmonic B_z Algorithm*, which will be developed as a combination of the Harmonic B_z Algorithm and our adaptive reduced basis approach, is also achieved. In a numerical investigation, we will see that the Reduced Basis Harmonic B_z Algorithm is again faster than the Harmonic B_z Algorithm while retaining the approximation quality of the original algorithm. Therefore, our adaptive reduced basis approach applied to this real-world problem is also viable. Figure 3 depicts a preview of the numerical results regarding the reconstruction quality when perfect data is assumed, where we will also consider noisy data in the actual section.

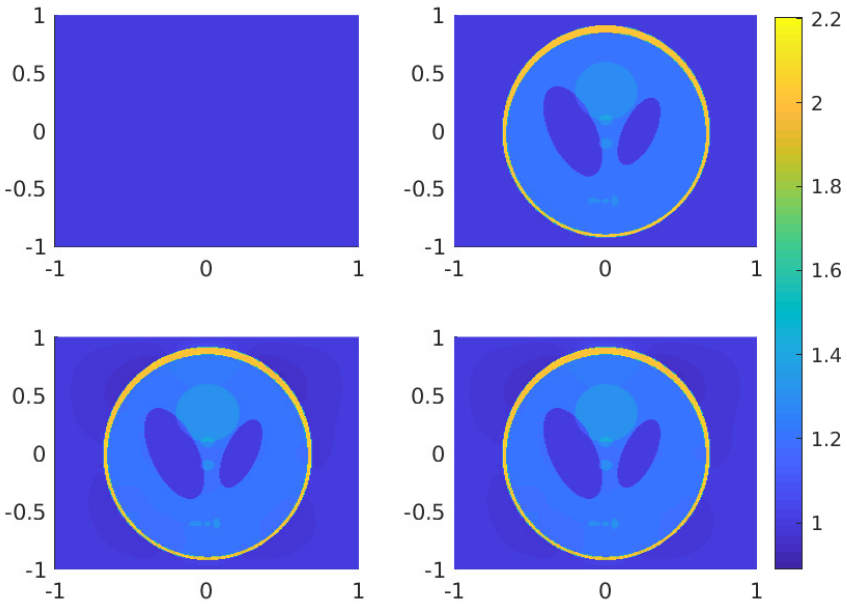

Figure 3: The initial guess (top left), the true solution (top right), the reconstructions via the Harmonic B_z Algorithm (bottom left) and via the Reduced Basis Harmonic B_z Algorithm (bottom right).

Overview

Chapter 1 will deal with the inverse model problem and the nonlinear Landweber method as its solution algorithm. It will thoroughly work out the adaptive reduced basis approach and explain how it is applied to the nonlinear Landweber method in order to present the novel *Reduced Basis Landweber method*. In-depth numerical results will demonstrate that the new method is indeed faster than the original Landweber method without loss of accuracy in the reconstruction of the thermal conductivity as well as further enhance the understanding of the adaptive reduced basis approach.

Chapter 2 will deal with the inverse problem of MREIT and the Harmonic B_z Algorithm as its solution algorithm. It will provide a rigorous theoretical investigation of the inverse problem of MREIT resulting in a convergence result for an approximative Harmonic B_z Algorithm and thus implying numerical convergence of the Harmonic B_z Algorithm. On the other hand, it will introduce the novel *Reduced Basis Harmonic B_z Algorithm* as the combination of the adaptive reduced basis framework and the existing solution algorithm. Since the theoretical result will indeed be valid for any approximation that fulfills certain criteria, convergence of the Reduced Basis Harmonic B_z Algorithm is also obtained. Numerical results for the latter algorithm will demonstrate that our general adaptive reduced basis approach is valid in this complex framework as well.

Published results

All results included in this work have been published or are accepted for publication. The first publication is joint work with my supervisor Prof. Dr. Bastian von Harrach as well as Prof. Dr. Bernard Haasdonk (Professor for Numerical Mathematics at the University of Stuttgart). The second publication is joint work with my supervisor Prof. Dr. Bastian von Harrach.

The results of Chapter 1 have been published in the journal Inverse Problems under the title "A reduced basis Landweber method for nonlinear inverse problems" [GHH16]. The article was selected as one of the Inverse Problems Highlights of 2016.

The results of Chapter 2 are accepted for publication in the SIAM Journal on Imaging Sciences (SIIMS) under the title "Magnetic Resonance Electrical Impedance Tomography (MREIT): convergence and reduced basis approach" [GH18].

Chapter 1

A Reduced Basis Landweber method for nonlinear inverse problems

Sections 1.1 - 1.3 and Sections 1.5 - 1.6 are, up to minor changes, Sections 1-3, 5 and the appendix of the article [GHH16]. Section 1.4 is largely based on Section 4 of the same article, but has been slightly reworked to include Section 1.4.2.

1.1 Introduction

The numerical solution of nonlinear inverse problems such as the identification of a parameter in a partial differential equation (PDE) from a noisy solution of the PDE via iterative regularization methods, e.g., the Landweber method or Newton-type methods, see, e.g., [KNS08, EHN96, Rie03] for a detailed overview, usually requires numerous amounts of forward solutions of the respective PDE. Since this can be very time-consuming, it is highly desirable to speed up the solution process.

The reduced basis method, see, e.g., [RHP08, Haa17] for a general survey, is a model order reduction technique that can yield a significant decrease in the computational time of the PDE solution, especially in a many-query context. The classical reduced basis framework aims at constructing a global reduced basis space that is a low-dimensional subspace of the solution space of the PDE providing accurate approximations to the PDE-solution for every parameter in the parameter domain. A possible way to construct such a space is to select *meaningful* parameters and choose the corresponding PDE-solutions, the so-called *snapshots*, as basis vectors of the reduced basis space. Via Galerkin projection of the problem onto the reduced basis space, the reduced basis approximation can be computed. An offline/online decomposition of the procedure allows for the efficient and rapid computation of the reduced basis approximation for many different parameters. Using a global reduced basis space, one can replace the expensive forward solution or a functional evaluation of it with the corresponding reduced basis quantity in the solution procedure of a given inverse problem. We call this the direct approach and it has successfully been applied to various problems, see, e.g., [NRHP10, Ngu05, HKL$^+$13], but we

want to stress that in those references the parameter space was bounded and of low dimension, which is required for the construction of a global reduced basis space.

In this chapter, we want to apply the reduced basis method to a parameter identification problem with a very high-dimensional and unbounded parameter space. To this end we want to study the inverse model problem: given a solution $u(x)$, $x \in \Omega$, of

$$\nabla \cdot (\sigma(x)\nabla u(x)) = 1, \quad x \in \Omega, \quad \text{and} \quad u(x) = 0, \quad x \in \partial\Omega, \tag{1.1}$$

identify the parameter $\sigma(x)$, with $\Omega \subset \mathbb{R}^2$ a bounded domain. This is an example of recovering an image of the thermal conductivity in the stationary heat equation with constant heat source. Typically, instead of u a noisy measurement u^δ is known, with $\|u - u^\delta\| \leq \delta$ and noise level $\delta > 0$. Since this problem is ill-posed, regularization techniques have to be applied. We choose the nonlinear Landweber method.

The aim of this chapter is the development of a new method to solve nonlinear inverse problems with high-dimensional parameter spaces, where our approach is based on the ideas developed by Druskin and Zaslavsky [DZ07]. We will combine the nonlinear Landweber method with the main ideas of the reduced basis method: instead of constructing a global reduced basis space, providing accurate approximations for every parameter in the parameter domain, as it is usually the case in reduced basis methods, see, e.g., [DH15], we will adaptively construct a small problem-specific reduced basis space that may only be useful for the reconstruction of a single conductivity. This will break the typical offline/online framework of reduced basis methods. A critical question then will be the selection of the snapshots for this problem-oriented space. We will develop termination criteria that, together with the nonlinear Landweber method projected onto the current reduced basis space, will not only select meaningful parameters for space enrichment but also serve the solution of the posed inverse problem. Therefore, we adaptively enrich our reduced basis space to fit the region of the parameter space that is required to reconstruct the desired conductivity, while also reconstructing it. This will allow for the numerical treatment of very high-dimensional parameter spaces. We note that the nonlinear Landweber method being a regularization method has been extensively studied and analyzed, see, e.g., [HNS95, EHN96, KNS08, Han14].

Ideas similar to our adaptive approach have been applied to a parameter estimation problem arising from the modeling of lithium ion batteries [Las14], a subsonic aerodynamic shape optimization problem [ZF15], both leading to an optimization problem constrained with a nonlinear PDE, and a Bayesian inversion approach, where the parameter is modelled as a random variable, using Markov chain Monte Carlo (MCMC) methods [CMW14].

The remainder of this chapter is organized as follows. In Section 1.2 we will present a mathematical formulation of the model problem, for which the nonlinear Landweber method is known to converge locally. Section 1.3 contains a brief discretization as well as the key ingredients of the classical reduced basis method. Section 1.4 contains

a short discussion about the direct approach for high-dimensional parameter spaces as well as the development of the new method, comments on its implementation and detailed numerical results. Final conclusions are drawn in Section 1.5.

1.2 Problem formulation

We present a well-known setting in which the Landweber method applied to (1.1) does converge locally. Throughout this section we assume $\Omega \subset \mathbb{R}^2$ to be a bounded domain with C^2-boundary. Following [IK94, Han97, KSS09], we choose the parameter space

$$H^2_+(\Omega) := \{\sigma(x) \in H^2(\Omega) \mid \operatorname{ess\,inf} \sigma(x) > 0\},$$

with $H^2(\Omega)$ the usual Sobolev space. Since Ω has a C^2-boundary, $H^2(\Omega)$ embeds continuously into $L^\infty(\Omega)$, cf. [AF03, Theorem 4.12], such that taking the essential infimum of a function in $H^2(\Omega)$ is a continuous mapping and $H^2_+(\Omega)$ is an open subset of $H^2(\Omega)$. We consider the PDE: for given $\sigma(x) \in H^2_+(\Omega)$ find the (weak) solution $u \in H^1_0(\Omega)$ of

$$\nabla \cdot (\sigma(x)\nabla u(x)) = 1.$$

The corresponding parameter-to-solution map is defined as

$$\mathcal{F} : \mathcal{D}(\mathcal{F}) := H^2_+(\Omega) \subset H^2(\Omega) \longrightarrow L^2(\Omega) \tag{1.2a}$$

$$\mathcal{F}(\sigma) = u \quad u \in H^1_0(\Omega) \subset L^2(\Omega) \text{ solving} \tag{1.2b}$$

$$b(u, w; \sigma) = f(w) \quad \text{for all } w \in H^1_0(\Omega), \tag{1.2c}$$

$$b(u, w; \sigma) := \int_\Omega \sigma \nabla u \cdot \nabla w \, dx, \quad f(w) := -\int_\Omega w \, dx. \tag{1.2d}$$

The associated *inverse problem* is

$$\text{for } u \in L^2(\Omega) \text{ find } \sigma \in H^2_+(\Omega) \text{ such that } \mathcal{F}(\sigma) = u. \tag{1.3}$$

Typically, instead of u a noisy measurement $u^\delta \in L^2(\Omega)$ is known, with $\|u^\delta - u\|_{L^2(\Omega)} \leq \delta$ and noise level $\delta > 0$, such that regularization techniques have to be applied since simple inversion fails due to the ill-posedness of the problem. Throughout this chapter we assume the knowledge of δ.

Remark 1.2.1. *(i) For $\sigma \in H^2_+(\Omega)$ we have $|b(u, u; \sigma)| \geq \alpha(\sigma) \|u\|^2_{L^2(\Omega)}$, with $\alpha(\sigma) := \frac{\operatorname{ess\,inf} \sigma(x)}{C^2_{PF}} > 0$, where C_{PF} is the Poincaré-Friedrich constant of Ω. Therefore, the bilinear form $b(\cdot, \cdot\,; \sigma)$ is coercive for all $\sigma \in H^2_+(\Omega)$. Since $H^2(\Omega)$ embeds continuously into $L^\infty(\Omega)$, b is also continuous for every $\sigma \in H^2_+(\Omega)$ with continuity constant $\gamma(\sigma) := \operatorname{ess\,sup} \sigma(x) < \infty$. The linear form f is continuous as well such that the Lax-Milgram theorem guarantees existence and uniqueness of a solution of (1.2) in $H^1_0(\Omega)$.*

(ii) $L^2(\Omega)$ *is chosen as the image space of* $\mathcal{F}$ *because we consider it to be more realistic for a measurement* $u^\delta \in L^2(\Omega)$ *to be close to the exact data* $u \in H_0^1(\Omega)$ *in the* L^2*-norm rather than in the* H^1*-norm.*

(iii) We acknowledge that the inverse problem stated in (1.3) *is actually a linear problem since the data* $u \in L^2(\Omega)$ *is known over the whole domain* Ω*. The problem becomes truly nonlinear if the data is only known on a proper subdomain* $\tilde{\Omega} \subset \Omega$*. We formulate this* partial inverse problem

$$\text{for } u \in L^2(\tilde{\Omega}) \text{ find } \sigma \in H_+^2(\Omega) \text{ such that } \tilde{\mathcal{F}}(\sigma) = u, \tag{1.4}$$

with $\tilde{\mathcal{F}} := E \circ \mathcal{F}$ *and a restriction operator* $E : L^2(\Omega) \longrightarrow L^2(\tilde{\Omega})$*. Since the scope of this chapter is the connection of iterative regularization methods and the reduced basis method, we will continue to consider* (1.3) *for reasons of simplicity. Still, the resulting method derived in Section 1.4 is applicable to the partial problem* (1.4) *and we will provide corresponding numerical results in Section 1.4.4.*

(iv) We mention that in the chosen setting (but also in general) the inverse problem (1.3) *(and more so* (1.4)*) is not uniquely solvable. In [IK94] Ito and Kunisch provide an overview of existing results on this topic and show the injectivity of* $\mathcal{F}$ *with respect to a reference parameter under certain assumptions. A recent result on the uniqueness of* (1.3) *with* C^2*-parameter is given by Knowles [Kno99], where his techniques are based on the work of Richter [Ric81].*

If we consider $\mathcal{D}(\mathcal{F}) = L_+^\infty(\Omega) \subset L^2(\Omega)$ as definition space of $\mathcal{F}$, it is a well-known result that for each $\sigma \in L_+^\infty(\Omega)$ and each direction $\kappa \in L^2(\Omega)$ with $\sigma + \kappa \in L_+^\infty(\Omega)$ (note that $L_+^\infty(\Omega)$ is not an open subset of $L^2(\Omega)$)

$$\lim_{\|\kappa\|_\infty \to 0} \frac{\|\mathcal{F}(\sigma+\kappa) - \mathcal{F}(\sigma) - \mathcal{F}'(\sigma)\kappa\|_{L^2(\Omega)}}{\|\kappa\|_\infty} = 0 \tag{1.5}$$

holds, with a linear and continuous operator $\mathcal{F}'(\sigma)$ given by

$$\mathcal{F}'(\sigma)(\cdot) : L^2(\Omega) \longrightarrow L^2(\Omega) \tag{1.6a}$$

$$\mathcal{F}'(\sigma)\kappa = v \quad v \in H_0^1(\Omega) \subset L^2(\Omega) \text{ solving} \tag{1.6b}$$

$$b(v, w; \sigma) = g(w; \kappa) \quad \text{for all } w \in H_0^1(\Omega), \tag{1.6c}$$

$$b(v, w; \sigma) := \int_\Omega \sigma \nabla v \cdot \nabla w \, dx, \quad g(w; \kappa) := -\int_\Omega \kappa \nabla u^\sigma \cdot \nabla w \, dx, \tag{1.6d}$$

where u^σ abbreviates $\mathcal{F}(\sigma)$. Section 1.6 contains a proof of the above statement. Since $H^2(\Omega)$ embeds continuously into $L^\infty(\Omega)$ and $H_+^2(\Omega)$ is an open subset of $H^2(\Omega)$, (1.5) holds for every $\sigma \in H_+^2(\Omega)$ and $\kappa \in H^2(\Omega)$, where $\mathcal{F}'(\sigma)$ considered as an operator from $H^2(\Omega)$ to $L^2(\Omega)$ is the Fréchet derivative of $\mathcal{F}$.

To numerically solve (1.3), we consider the nonlinear Landweber iteration that is based on the fix point equation

$$\sigma = \Xi(\sigma) := \sigma + \omega \mathcal{F}'(\sigma)^*(u - \mathcal{F}(\sigma)),$$

where $\mathcal{F}'(\sigma)^*$ denotes the adjoint of $\mathcal{F}'(\sigma)$ and $\omega > 0$ is a damping parameter. With given noisy data $u^\delta \in L^2(\Omega)$ we can only expect to reconstruct an approximative solution σ^δ to an exact solution $\sigma^+ \in H^2_+(\Omega)$ of (1.3). The *damped nonlinear Landweber iteration* is defined via

$$\sigma^\delta_{n+1} = \sigma^\delta_n + \omega \mathcal{F}'(\sigma^\delta_n)^*(u^\delta - \mathcal{F}(\sigma^\delta_n)), \quad n = 0, 1, \dots \tag{1.7}$$

with starting value $\sigma^\delta_0 \in H^2_+(\Omega)$, which may incorporate a-priori knowledge of σ^+, and damping parameter ω chosen as $\omega \leq \|\mathcal{F}'(\sigma^+)\|^{-2}$. Since we consider noisy data, the iteration (1.7) has to be stopped properly to prevent error amplification. We choose the well-known discrepancy principle: accept the iterate $\sigma^\delta_{n^*(\delta,u^\delta)}$ as a solution to (1.3), if it fulfills

$$\|\mathcal{F}(\sigma^\delta_{n^*(\delta,u^\delta)}) - u^\delta\|_{L^2(\Omega)} \leq \tau\delta \leq \|\mathcal{F}(\sigma^\delta_n) - u^\delta\|_{L^2(\Omega)} \tag{1.8}$$

for $n = 0, 1, \dots, n^*(\delta, u^\delta) - 1$, with $\tau > 2$. In this setting the damped nonlinear Landweber iteration applied to (1.3) for noisy data is known to locally converge.

Proposition 1.2.2. *Let $\sigma^+ \in \mathcal{D}(\mathcal{F})$ be a solution of $\mathcal{F}(\sigma) = u$. Then, there exists a radius $\rho > 0$ such that the following holds for every starting value $\sigma^\delta_0 \in \mathcal{B}_\rho(\sigma^+)$: if the damped nonlinear Landweber iteration applied to noisy data $u^\delta \in L^2(\Omega)$ is stopped with $n^*(\delta, u^\delta)$ according to* (1.8)*, then $\sigma^\delta_{n^*(\delta,u^\delta)}$ converges to some solution $\hat{\sigma}$ of $\mathcal{F}(\sigma) = u$ as $\delta \to 0$.*

Proof. Since $H^2(\Omega)$ embeds continuously into $L^\infty(\Omega)$ and therefore $H^2_+(\Omega)$ is open as mentioned in the beginning of the section, we can always find an open ball $\mathcal{B}_{r_1}(\sigma^+) \subset \mathcal{D}(\mathcal{F}) = H^2_+(\Omega)$ around σ^+ with $r_1 > 0$ such that $\operatorname{ess\,inf}(\sigma) > c_1$ for all $\sigma \in \mathcal{B}_{r_1}(\sigma^+)$, where c_1 depends on $\operatorname{ess\,inf}(\sigma^+)$. Furthermore, the triangle inequality yields $\|\sigma\|_{H^2(\Omega)} \leq \|\sigma - \sigma^+\|_{H^2(\Omega)} + \|\sigma^+\|_{H^2(\Omega)} < r_1 + \|\sigma^+\|_{H^2(\Omega)} =: c_2$ for every $\sigma \in \mathcal{B}_{r_1}(\sigma^+)$. We mention that $H^2_+(\Omega)$ is convex. Hanke showed in [Han97, Corollary 3.2] that

$$\|\mathcal{F}(\sigma) - \mathcal{F}(\tilde{\sigma}) - \mathcal{F}'(\tilde{\sigma})(\sigma - \tilde{\sigma})\|_{L^2(\Omega)} \leq C\|\sigma - \tilde{\sigma}\|_{H^2(\Omega)}\|\mathcal{F}(\sigma) - \mathcal{F}(\tilde{\sigma})\|_{L^2(\Omega)}$$

holds for all $\sigma, \tilde{\sigma} \in \mathcal{B}_{r_1}(\sigma^+)$, where C depends on c_1, c_2 and Ω. Therefore, there exist $0 < r_2 \leq r_1$ and $\eta < \frac{1}{2}$ such that the *tangential cone condition*

$$\|\mathcal{F}(\sigma) - \mathcal{F}(\tilde{\sigma}) - \mathcal{F}'(\tilde{\sigma})(\sigma - \tilde{\sigma})\|_{L^2(\Omega)} \leq \eta\|\mathcal{F}(\sigma) - \mathcal{F}(\tilde{\sigma})\|_{L^2(\Omega)}$$

is true for all $\sigma, \tilde{\sigma} \in \mathcal{B}_{r_2}(\sigma^+)$. We now choose τ in (1.8) as

$$\tau > 2\frac{1+\eta}{1-\eta} > 2.$$

Finally, we can find $0 < r_3 \leq r_2$ such that $\sqrt{\omega}\|\mathcal{F}'(\sigma)\| \leq \frac{\|\mathcal{F}'(\sigma)\|}{\|\mathcal{F}'(\sigma^+)\|} \leq 1$ for all $\sigma \in \mathcal{B}_{r_3}(\sigma^+)$. We now choose $\rho = \frac{r_3}{3}$ such that for every $\sigma^\delta_0 \in \mathcal{B}_\rho(\sigma^+)$ all assumptions of [EHN96, Theorem 11.5] are fulfilled and the assertion follows. □

Remark 1.2.3. *(i) Hanke [Han14] extends the convergence result of [EHN96, Theorem 11.5] to choices $\tau > 1$. In the same article Hanke also mentions that the solution $\hat{\sigma}$ found with Proposition 1.2.2 depends on the starting value σ_0^δ and does not need to coincide with σ^+ if $F'(\sigma^+)$ happens to have a nontrivial null space.*

(ii) Since in a practical application σ^+ is unknown, we will make a heuristic choice of the damping parameter ω in Section 1.4.4.

1.3 Reduced basis methods

Before we introduce the key ingredients of the classical reduced basis method and for further numerical treatment, we discretize our model problem.

1.3.1 Discretization

We introduce a standard finite element space and a discrete parameter space. Note that the unit square, despite lacking a C^2-boundary, still meets the demands on the domain required for the theory in Section 1.2. Therefore, we choose $\Omega := [0,1]^2$ as computational domain for the remainder of this chapter.

Definition 1.3.1. For a given $n \in \mathbb{N}$, $n \geq 2$, we choose a uniform triangulation of Ω with $(n+2)^2$ grid nodes x_i and I_{in} the index set of inner nodes. We use piecewise linear nodal basis functions, denoted as φ_i, $i \in I_{in}$, on the inner nodes. The discrete function space Y then is defined via

$$Y := \{u : \Omega \to \mathbb{R} \mid u(x) = \sum_{i \in I_{in}} u_i \varphi_i(x),\ u_i \in \mathbb{R},\ i \in I_{in}\}.$$

Y is equipped with the L^2-norm and and for $u \in Y$ let $\boldsymbol{u} = (u_i)_{i \in I_{in}} \in \mathbb{R}^{n^2}$ denote the vector of coefficients.

Definition 1.3.2. For a given square number $p = q^2$, $q \in \mathbb{N}$, we divide Ω into a uniform partition of p square subdomains Ω_i, $i = 1, \ldots, p$, and define $\mathcal{P}_p$ via

$$\mathcal{P}_p := \{\sigma : \Omega \to \mathbb{R} \mid \sigma(x) = \sum_{i=1}^{p} \sigma_i \chi_{\Omega_i}(x),\ \sigma_i \in \mathbb{R}_+ := (0, \infty),\ i = 1, \ldots p\},$$

with χ_{Ω_i} being the characteristic function on the subdomain Ω_i. $\mathcal{P}_p$ is equipped with the L^2-norm and for $\sigma \in \mathcal{P}_p$ let $\boldsymbol{\sigma} = (\sigma_i)_{i=1}^p \in \mathbb{R}_+^p$ denote the vector of coefficients.

The following discrete problems will have $\mathbb{R}_+^p$ and $\mathbb{R}^p$ as definition space. Note the isomorphisms between $\mathbb{R}_+^p$ and $\mathcal{P}_p$ as well as $\mathbb{R}^p$ and its (analogously to Definition

1.3.2 defined) function space. Furthermore, we recall that b, f and g are the bilinear and linear forms introduced in Section 1.2 and the stability constants of b, f and g carry over to Y and $\mathbb{R}^p_+$ such that existence and uniqueness of the discrete problems are guaranteed via the Lax-Milgram theorem. The *discrete forward operator* is given by

$$F : \mathbb{R}^p_+ \longrightarrow Y, \quad \boldsymbol{\sigma} \longmapsto u^\sigma, \, \boldsymbol{u} = (u_i^\sigma)_{i \in I_{in}} \text{ solving} \tag{1.9a}$$

$$\boldsymbol{B}(\boldsymbol{\sigma})\boldsymbol{u} = \boldsymbol{f} \text{ with } (\boldsymbol{B}(\boldsymbol{\sigma}))_{ij} := b(\varphi_i, \varphi_j; \sigma), \, (\boldsymbol{f})_i := f(\varphi_i), \, i, j \in I_{in}. \tag{1.9b}$$

The associated *discrete inverse problem* is

$$\text{for } u^\sigma \in Y \text{ find } \boldsymbol{\sigma} \in \mathbb{R}^p_+ \text{ such that (1.9) is fulfilled.} \tag{1.10}$$

In the upcoming sections u^σ, the solution of (1.9), will simply be denoted by u. For $\boldsymbol{\sigma} \in \mathbb{R}^p_+$, the *Jacobian* $F'(\boldsymbol{\sigma})$ is given by

$$F'(\boldsymbol{\sigma})(\cdot) : \mathbb{R}^p \longrightarrow Y, \quad \boldsymbol{\kappa} \longmapsto v_\kappa^\sigma, \, \boldsymbol{v} = \left(v_{\kappa,i}^\sigma\right)_{i \in I_{in}} \text{ solving} \tag{1.11a}$$

$$\boldsymbol{B}(\boldsymbol{\sigma})\boldsymbol{v} = \boldsymbol{g}(\boldsymbol{\kappa}) \text{ with } \boldsymbol{B}(\boldsymbol{\sigma}) \text{ as in (1.9) and } (\boldsymbol{g}(\boldsymbol{\kappa}))_i := g(\varphi_i; \kappa), \, i \in I_{in}. \tag{1.11b}$$

Remark 1.3.3. *(i) The discrete setting introduced in this section deviates from the continuous setting introduced in Section 1.2, where the forward operator $\mathcal{F}$ was a mapping from $H^2_+(\Omega)$ to $L^2(\Omega)$. Here, the discrete forward operator F is a mapping from a finite-dimensional subspace $\mathcal{P}_p$ of $L^2(\Omega)$ into another finite-dimensional subspace Y of $L^2(\Omega)$. This choice is made since it resembles the common numerical setting for the inverse problem tackled in this chapter, where no continuity for the searched for diffusion coefficient can be assumed. Do note that due to this choice the result of Proposition 1.2.2 does not need to hold in this discrete setting. Also, to our knowledge, it is an open question if the tangential cone condition required in the proof of Proposition 1.2.2 holds in this discrete setting.*

(ii) Since we use the L^2-norm instead of the energy-norm on Y, it is $\alpha(\boldsymbol{\sigma}) := \frac{\min(\boldsymbol{\sigma})}{C_{PF}^2} > 0$, for all $\sigma \in \mathcal{P}_p$, the coercivity constant of b with respect to Y. For $\Omega = [0,1]^2$, we refer to the proof of [AF03, Thm. 6.30] and choose $C_{PF} = \frac{1}{\sqrt{2}}$ such that we use $\alpha(\boldsymbol{\sigma}) = 2\min(\boldsymbol{\sigma}) > 0$ for all $\sigma \in \mathcal{P}_p$ throughout this chapter.

1.3.2 The reduced basis method

Reduced basis methods aim at constructing a low-dimensional subspace Y_N of Y, with $N = \dim Y_N \ll \dim Y = n^2$, such that the reduced basis solution u_N is an accurate approximation of u, the high-dimensional forward solution of (1.9). Typically, Y_N will consist of *snapshots* that are solutions of (1.9) to *meaningful* parameters. We will not discuss the construction of Y_N in this section but assume a reduced basis space to be given. In order to give a brief overview of the reduced

basis method, this section is kept very generic. For a detailed survey of the reduced basis method we refer to [RHP08, Haa17].

Definition 1.3.4. Let a forward operator (1.9) and a reduced basis space $Y_N \subset Y$, with $\dim Y_N = N$ and basis $\Psi_N := \{\psi_1, \dots, \psi_N\}$, be given. We define the *discrete reduced forward operator*

$$F_N : \mathbb{R}^p_+ \longrightarrow Y_N, \quad \boldsymbol{\sigma} \longmapsto u_N^\sigma = \sum_{i=1}^N u_{N,i}^\sigma \psi_i, \ \boldsymbol{u}_N = (u_{N,i}^\sigma)_{i=1}^N \text{ solving} \tag{1.12a}$$

$$\boldsymbol{B}_N(\boldsymbol{\sigma})\boldsymbol{u}_N = \boldsymbol{f}_N \text{ with } (\boldsymbol{B}_N(\boldsymbol{\sigma}))_{ij} := b(\psi_i, \psi_j; \sigma), \ (\boldsymbol{f}_N)_i := f(\psi_i), \tag{1.12b}$$

for $i, j = 1, \dots, N$. We call u_N^σ the *reduced basis approximation* and will often write u_N instead.

Remark 1.3.5. *(i) Existence and uniqueness of* (1.12) *follow from the properties of* (1.9).

(ii) If the reduced basis Ψ_N is orthonormal, $\operatorname{cond}(\boldsymbol{B}_N(\boldsymbol{\sigma})) \leq \frac{\gamma(\boldsymbol{\sigma})}{\alpha(\boldsymbol{\sigma})}$ *holds independent of N with $\boldsymbol{B}_N(\boldsymbol{\sigma})$ defined in* (1.12).

For the sake of completeness, we include the proof of the well-known rigorous error estimator for the reduced basis error, here measured in the L^2-norm, $\|u - u_N\|_{L^2(\Omega)}$, cf. [RHP08] or [Haa17, Propositions 2.20 & 2.24].

Lemma 1.3.6. *For $\sigma \in \mathcal{P}_p$ we define the residual $r(\cdot;\sigma) \in Y'$ via*

$$r(v;\sigma) := f(v) - b(u_N, v; \sigma), \quad v \in Y.$$

Then, let $v_r \in Y$ denote the Riesz-representative of $r(\cdot;\sigma)$, i.e.,

$$\langle v_r, v \rangle_{L^2(\Omega)} = r(v;\sigma), \ v \in Y, \quad \|v_r\|_{L^2(\Omega)} = \|r(\cdot;\sigma)\|_{Y'}.$$

Then, the error $u - u_N \in Y$ is bounded for all $\sigma \in \mathcal{P}_p$ by

$$\|u - u_N\|_{L^2(\Omega)} \leq \Delta_N(\boldsymbol{\sigma}) := \frac{\|v_r\|_{L^2(\Omega)}}{\alpha(\boldsymbol{\sigma})}. \tag{1.13}$$

Proof. Introducing the notation $e := u - u_N$, we calculate

$$b(e, v; \sigma) = b(u, v; \sigma) - b(u_N, v, \sigma) = f(v) - b(u_N, v; \sigma) = r(v;\sigma) \quad \text{for all } v \in Y.$$

Testing this equation with $e \in Y$ yields

$$\alpha(\boldsymbol{\sigma})\|e\|^2_{L^2(\Omega)} \leq b(e, e; \sigma) = r(e;\sigma) \leq \|r(\cdot;\sigma)\|_{Y'}\|e\|_{L^2(\Omega)} = \|v_r\|_{L^2(\Omega)}\|e\|_{L^2(\Omega)}.$$

Division by $\|e\|_{L^2(\Omega)}$ and $\alpha(\boldsymbol{\sigma})$ concludes the proof. □

We want to remind the reader that this is an estimator for the error between the reduced basis approximation and the discrete forward solution. Since the construction method for Y_N in Section 1.4 will be snapshot-based, we note an important property of such methods, the *reproduction of solutions*. It guarantees exactness in the reduced basis approximation for parameters whose snapshots are part of Y_N.

Lemma 1.3.7. *Let $\sigma \in \mathcal{P}_p$, $F(\boldsymbol{\sigma})$, $F_N(\boldsymbol{\sigma})$ be solutions of* (1.9) *and* (1.12) *and $\boldsymbol{e}_i \in \mathbb{R}^N$ the i-th unit vector. Then the following holds*

(a) if $F(\boldsymbol{\sigma}) \in Y_N$ then $F_N(\boldsymbol{\sigma}) = F(\boldsymbol{\sigma})$.

(b) if $F(\boldsymbol{\sigma}) = \psi_i \in \Psi_N$ then $\boldsymbol{u}_N = \boldsymbol{e}_i \in \mathbb{R}^N$.

Proof. Both statements immediately follow from (1.9) and (1.12), see, e.g., [Haa17, Proposition 2.21]. □

To conclude this brief overview of the reduced basis method, we present both offline/online decompositions of (1.12) and the error estimator (1.13) that allow for the rapid computation of u_N and Δ_N. The essential assumption for those decompositions is that the bilinear form b and the linear form f are *parameter-separable*, which is fulfilled by (1.9).

Corollary 1.3.8. *Using the notation of Definition 1.3.2, the set*

$$\{\sigma^{(1)}(x), \dots, \sigma^{(p)}(x) \mid \sigma^{(i)}(x) = \chi_{\Omega_i}(x),\ i = 1, \dots, p\}$$

is a basis of $\mathcal{P}_p$ with corresponding coefficient vectors $\boldsymbol{\sigma}^{(i)} = \boldsymbol{e}_i \in \mathbb{R}^p$, $i = 1, \dots, p$, $\boldsymbol{e}_i$ being the i-th unit vector. Therefore, we can rewrite b and f as

$$b(u, v; \sigma) = \sum_{q=1}^{Q_b} \Theta_b^q(\boldsymbol{\sigma}) b^q(u, v), \quad f(v; \sigma) = \sum_{q=1}^{Q_f} \Theta_f^q(\boldsymbol{\sigma}) f^q(v),$$

for all $u, v \in Y$ and $\sigma \in \mathcal{P}_p$, with $Q_b = p$, $Q_f = 1$ coefficient functions $\Theta_b^q(\boldsymbol{\sigma}) := (\boldsymbol{\sigma})_q$, $q = 1, \dots, p$, $\Theta_f^1(\boldsymbol{\sigma}) := 1$ *and* components

$$b^q(u, v) := b(u, v; \sigma^{(q)}),\ q = 1, \dots p,\ f^1(v) := f(v),\ u, v \in Y.$$

If the bilinear form b and the linear form f can be rewritten this way, they are said to be parameter-separable. *Regarding the residual we set $Q_r := Q_f + N \cdot Q_b = 1 + N \cdot p$ and define the components of the residual $r^q \in Y'$, $q = 1, \dots, Q_r$ via*

$$\begin{aligned}(r^1, \dots, r^{Q_r}) &:= (f^1(\cdot), \dots, f^{Q_f}(\cdot), b^1(\psi_1, \cdot), \dots, b^{Q_b}(\psi_1, \cdot), \dots, \\ &\qquad b^1(\psi_N, \cdot), \dots, b^{Q_b}(\psi_N, \cdot)) \\ &= (f^1(\cdot), b^1(\psi_1, \cdot), \dots, b^{Q_b}(\psi_1, \cdot), \dots, b^1(\psi_N, \cdot), \dots, b^{Q_b}(\psi_N, \cdot)),\end{aligned}$$

and let $v_r^q \in Y$ denote the Riesz-representative of r^q. For $u_N^\sigma = \sum_{i=1}^N u_{N,i}^\sigma \psi_i$ a solution of (1.12) *we define the corresponding coefficient functions $\Theta_r^q(\boldsymbol{\sigma})$, $q = 1, \dots, Q_r$*

via

$$\begin{aligned}(\Theta_r^1, \dots, \Theta_r^{Q_r}) &:= (\Theta_f^1, \dots, \Theta_f^{Q_f}, -\Theta_b^1 u_{N,1}^\sigma, \dots, -\Theta_b^{Q_b} u_{N,1}^\sigma, \dots, \\ &\quad - \Theta_b^1 u_{N,N}^\sigma, \dots, -\Theta_b^{Q_b} u_{N,N}^\sigma) \\ &= (1, -(\boldsymbol{\sigma})_1 u_{N,1}^\sigma, \dots, -(\boldsymbol{\sigma})_p u_{N,1}^\sigma, \dots, -(\boldsymbol{\sigma})_1 u_{N,N}^\sigma, \dots, -(\boldsymbol{\sigma})_p u_{N,N}^\sigma).\end{aligned}$$

Using this, the residual r and its Riesz-representative v_r are parameter-separable as

$$r(v;\sigma) = \sum_{q=1}^{Q_r} \Theta_r^q(\boldsymbol{\sigma}) r^q(v), \quad v_r(\sigma) = \sum_{q=1}^{Q_r} \Theta_r^q(\boldsymbol{\sigma}) v_r^q.$$

For problems that are not parameter-separable, the empirical interpolation method [BMNP04] is available. The general idea of an offline/online decomposition is: compute all parameter independent quantities in a nonrecurring possibly expensive offline phase and then, for every new parameter, rapidly compute the desired quantity in the online phase. We first formulate the offline/online decomposition of (1.12).

Procedure 1.3.9 (Offline/online decomposition of (1.12))**.**

1. Offline phase (one-time)

(i) Generate reduced basis $\Psi_N = \{\psi_1, \dots, \psi_N\}$ and Y_N.

(ii) Galerkin projection of components onto Y_N, i.e., compute

$$\boldsymbol{B}_N^q := (b^q(\psi_i, \psi_j))_{i,j=1}^N \in \mathbb{R}^{N\times N} \quad \text{and} \quad \boldsymbol{f}_N^q := (f^q(\psi_i))_{i=1}^N \in \mathbb{R}^N.$$

2. Online phase (for each new $\sigma \in \mathcal{P}_p$)

(i) Evaluate coefficient functions $\Theta_b^q(\boldsymbol{\sigma})$, $\Theta_f^q(\boldsymbol{\sigma})$, assemble $\boldsymbol{B}_N(\boldsymbol{\sigma})$, $\boldsymbol{f}_N$ and solve linear system in (1.12).

(ii) Reconstruct reduced basis solution $u_N = \sum_{i=1}^N \boldsymbol{u}_{N,i}\psi_i$.

Since the online phase only involves linear combinations and the solution of a linear system of dimension N, with $N \ll n^2$, it is very cheap. We conclude with the offline/online decomposition of the residual norm $\|v_r\|_{L^2(\Omega)}$ and therefore the error estimator.

Procedure 1.3.10 (Offline/online decomposition of (1.13))**.**

1. Offline phase: *After the offline phase of Procedure 1.3.9, compute the matrix* $\boldsymbol{G}_r := \left(\langle v_r^q, v_r^{q'}\rangle_{L^2(\Omega)}\right)_{q,q'=1}^{Q_r}$.

2. Online phase: *For given $\sigma \in \mathcal{P}_p$ and corresponding u_N^σ, evaluate* $\boldsymbol{\Theta}_r := (\Theta_r^i(\boldsymbol{\sigma}))_{i=1}^{Q_r} \in \mathbb{R}^{Q_r}$ *and compute* $\|v_r\|_{L^2(\Omega)} = \sqrt{\boldsymbol{\Theta}_r^\mathsf{T} \boldsymbol{G}_r \boldsymbol{\Theta}_r}$.

1.4 Reduced Basis Landweber (RBL) method

Before we develop the Reduced Basis Landweber (RBL) method, we introduce needed results and clearly explain why the alternative direct approach that was mentioned in Section 1.1 is not viable for our parameter identification problem.

1.4.1 Preliminaries

With the notation introduced in Section 1.3.1 the nonlinear Landweber iteration defined in (1.7) applied to (1.10) is reasonable. As mentioned in Section 1.2 we consider the damped nonlinear Landweber iteration with damping parameter $\omega > 0$ terminated with the discrepancy principle as it is stated in Algorithm 1.

Algorithm 1 Landweber($\boldsymbol{\sigma}_{start}, \tau$)

1: $n := 0,\ \boldsymbol{\sigma}_0^\delta := \boldsymbol{\sigma}_{start}$
2: **while** $\|F(\boldsymbol{\sigma}_n^\delta) - u^\delta\|_{L^2(\Omega)} > \tau\delta$ **do**
3: $\quad \boldsymbol{\sigma}_{n+1}^\delta := \boldsymbol{\sigma}_n^\delta + \omega F'(\boldsymbol{\sigma}_n^\delta)^*(u^\delta - F(\boldsymbol{\sigma}_n^\delta))$
4: $\quad n := n + 1$
5: **end while**
6: **return** $\boldsymbol{\sigma}_{LW} := \boldsymbol{\sigma}_n^\delta$

In the upcoming sections we will write σ_{LW} to denote the element in $\mathcal{P}_p$ corresponding to $\boldsymbol{\sigma}_{LW}$. We introduce a *dual problem* that allows for a simple calculation of the Landweber update in line 3 of Algorithm 1.

Proposition 1.4.1. *For $\boldsymbol{\sigma} \in \mathbb{R}_+^p$, $\boldsymbol{\kappa} \in \mathbb{R}^p$ and $l \in Y$ it holds*

$$\langle \boldsymbol{\kappa}, F'(\boldsymbol{\sigma})^* l \rangle_2 = \langle F'(\boldsymbol{\sigma})\boldsymbol{\kappa}, l \rangle_{L^2(\Omega)} = \int_\Omega \kappa \nabla u^\sigma \cdot \nabla u_l^\sigma \, dx, \tag{1.14}$$

with $F'(\boldsymbol{\sigma})^*$ the adjoint of $F'(\boldsymbol{\sigma})$ and $u_l^\sigma \in Y$ the unique solution of the discrete dual problem

$$\boldsymbol{B}(\boldsymbol{\sigma})\boldsymbol{u} = \boldsymbol{m}(\boldsymbol{l}) \text{ with } \boldsymbol{B}(\boldsymbol{\sigma}) \text{ as in (1.9) and} \tag{1.15a}$$

$$(\boldsymbol{m}(\boldsymbol{l}))_i := m(\varphi_i; l) := -\int_\Omega \varphi_i \, l \, dx,\ i \in I_{in}. \tag{1.15b}$$

Proof. Note that $u_l^\sigma \in Y$ solving (1.15) is equivalent to u_l^σ solving $b(u_l^\sigma, v; \sigma) = m(v)$ for all $v \in Y$. The first equality in (1.14) is the definition of the adjoint. The second equality follows from (1.11) and (1.15)

$$\begin{aligned}\langle F'(\boldsymbol{\sigma})\boldsymbol{\kappa}, l \rangle_{L^2(\Omega)} &= \int_\Omega F'(\boldsymbol{\sigma})\boldsymbol{\kappa} \, l \, dx = \int_\Omega v_\kappa^\sigma \, l \, dx = -\int_\Omega \sigma \nabla u_l^\sigma \cdot \nabla v_\kappa^\sigma \, dx \\ &= \int_\Omega \kappa \nabla u^\sigma \cdot \nabla u_l^\sigma \, dx.\end{aligned}$$

□

Using Proposition 1.4.1, we calculate the Landweber update in line 3 of Algorithm 1. For $\sigma \in \mathcal{P}_p$, $l \in Y$ let $u^\sigma = \sum_{i \in I_{in}} u_i^\sigma \varphi_i$ and $u_l^\sigma = \sum_{i \in I_{in}} u_{l,i}^\sigma \varphi_i \in Y$ be solutions of (1.9) and (1.15) with corresponding coefficient vectors $\boldsymbol{u}^\sigma = (u_i^\sigma)_{i \in I_{in}}$ and $\boldsymbol{u}_l^\sigma = (u_{l,i}^\sigma)_{i \in I_{in}}$ such that it holds for $\boldsymbol{\kappa} \in \mathbb{R}^p$

$$\langle \boldsymbol{\kappa}, F'(\boldsymbol{\sigma})^* l \rangle_2 = \int_\Omega \kappa \nabla u^\sigma \cdot \nabla u_l^\sigma \, dx = \sum_{i,j \in I_{in}} u_i^\sigma u_{l,j}^\sigma \int_\Omega \kappa \nabla \varphi_i \cdot \nabla \varphi_j \, dx \tag{1.16a}$$

$$= \sum_{i,j \in I_{in}} u_i^\sigma u_{l,j}^\sigma b(\varphi_i, \varphi_j; \kappa) = (\boldsymbol{u}^\sigma)^\intercal \boldsymbol{B}(\boldsymbol{\kappa}) \boldsymbol{u}_l^\sigma. \tag{1.16b}$$

Therefore, we can evaluate $F'(\boldsymbol{\sigma})^* l$ for given $\sigma \in \mathcal{P}_p$, $l \in Y$ by consecutively inserting a basis vector of $\mathbb{R}^p$ as the parameter $\boldsymbol{\kappa}$. Following Corollary 1.3.8, we choose the standard basis of $\mathbb{R}^p$ such that $\boldsymbol{B}(\boldsymbol{\kappa})$ in (1.16) is the k-th component matrix $\boldsymbol{B}^k := \left(b^k(\varphi_i, \varphi_j)\right)_{i,j \in I_{in}}$ if $\boldsymbol{\kappa}$ is the k-th unit vector. Using this, the calculation of the Landweber update in line 3 of Algorithm 1 consists of the following steps.

Procedure 1.4.2 (Landweber update)**.** *1. Compute $u^{\sigma_n^\delta}$ the primal forward solution of* (1.9)*. Define $l := u^\delta - u^{\sigma_n^\delta}$.*

2. Compute $u_l^{\sigma_n^\delta}$ the dual forward solution of (1.15)*.*

3. Evaluate the Landweber update

$$\left(F'(\boldsymbol{\sigma}_n^\delta)^*(u^\delta - F(\boldsymbol{\sigma}_n^\delta))\right)_k = (\boldsymbol{u}^{\sigma_n^\delta})^\intercal \boldsymbol{B}^k \boldsymbol{u}_l^{\sigma_n^\delta}, \; k = 1, \dots, p.$$

1.4.2 Intermission: a direct approach

Let us shortly outline the direct approach that was mentioned in Section 1.1 and explain why it is not applicable in the present context. Due to Procedure 1.4.2, every Landweber step contains two forward solutions and Algorithm 1 as an iterative regularization algorithm provides a many-query context such that the application of reduced basis methods is intuitive. The direct approach consists of constructing one *global reduced basis space*, yielding accurate reduced basis approximations for all $\sigma \in \mathcal{P}_p$, per forward problem and replacing the corresponding forward solutions required in the Landweber iteration with their reduced counterparts. We note that this methodology surely could be applied to other regularization algorithms as well and that similar techniques have successfully been applied to problems with a low-dimensional parameter space, see, e.g., [NRHP10, Ngu05, HKL$^+$13].

We formulate the well-known *greedy algorithm*, see, e.g., [VPRP03, RHP08, Haa17], as a basic construction method for global reduced basis spaces, where Δ_N denotes the error estimator defined in Lemma 1.3.6, $\varepsilon_{tol} > 0$ a tolerance determining the

Algorithm 2 greedy algorithm($M_{train},\ \varepsilon_{tol},\ \Delta_N$)

$Y_N := \{0\},\ \Psi_N := \emptyset$
repeat
  $\hat{\boldsymbol{\sigma}} := \arg\max_{\sigma \in M_{train}} \Delta_N(\boldsymbol{\sigma})$
  $\psi_N := F(\hat{\boldsymbol{\sigma}}),\ \Psi_N := \Psi_N \cup \{\psi_N\},\ Y_N := Y_N + \operatorname{span}\{\psi_N\}$
  $\varepsilon := \max_{\sigma \in M_{train}} \Delta_N(\boldsymbol{\sigma})$
until $\varepsilon \leq \varepsilon_{tol}$
return $\Psi_N,\ Y_N$

approximation quality of the resulting reduced basis space and $M_{train} \subset \mathcal{P}_p$ a finite set of sampling parameters.

Remembering the offline/online decomposition of the error estimator Δ_N presented in Procedure 1.3.10, $\hat{\boldsymbol{\sigma}}$ in Algorithm 2 can be rapidly computed if the finite training set M_{train} is of reasonable size. It is furthermore obvious that the quality of the space Y_N constructed with Algorithm 2 relies on the finite training set M_{train} covering $\mathcal{P}_p$. In our case $\mathcal{P}_p$ is unbounded and of dimension p (where p shall be large since it corresponds to the amount of pixels in an image), see Definition 1.3.2, such that it is impossible to find a suitable and numerically manageable training set M_{train} covering the whole parameter domain $\mathcal{P}_p$. Thus, the greedy algorithm can not be utilized to construct a global reduced basis space for the primal forward problem (1.9). Acknowledging that the greedy algorithm is a basic construction method for global reduced basis spaces, we refer to more sophisticated methods, see, e.g., [HSZ14, EPR10, HDO11, UVZ14], and mention that these would fail in this imaging context as well, although, referring to [Haa17, Remark 2.11] for more details on this discussion, high-dimensionality of the parameter domain alone is not prohibiting global reduced basis spaces.

Even if we would restrict ourselves to an undesired low-dimensional and bounded parameter domain (then resembling an undesired low-resolution image) such that a global reduced basis space for the primal forward problem (1.9) would be available, the dual problem would still pose a challenge. The right hand side of (1.15) is given by $(\boldsymbol{m}(\boldsymbol{l}))_i = m(\varphi_i; l)$, $i \in I_{in}$, with m defined in Proposition 1.4.1 and $l \in Y$. If one would want to construct a global reduced basis space for this dual problem the dependency of $\boldsymbol{m}$ on l would result in an extended parameter space $\tilde{\mathcal{P}}$ since $\boldsymbol{m}$ would additionally depend on $|I_{in}|$ parameters resembling the degrees of freedom of l. According to Procedure 1.4.2 each of those $|I_{in}|$ degrees of freedom of l indeed changes during a Landweber iteration such that $\tilde{\mathcal{P}}$ would be obtained by simply adding those $|I_{in}|$ dimensions to the existing parameter space $\mathcal{P}_p$. As already discussed, a global reduced basis space could not be constructed anymore for such a problem.

1.4.3 Development of the Reduced Basis Landweber method

One way to couple reduced basis methods and the nonlinear Landweber method is the direct approach that was discussed in the preceding Section 1.4.2 which had several drawbacks. In this section we want to develop a new method that overcomes these drawbacks via adaptive online updates of the reduced basis space during the solution process of the inverse problem. Online updates in model order reduction have also been considered recently in other contexts [DZ07, CMW14, Las14, ZF15].

We no longer aim at constructing a global reduced basis space that could be used for the reconstruction of every $\sigma \in \mathcal{P}_p$. Instead, for a given measurement, we aim at adaptively constructing a small problem-oriented reduced basis space $Y_{N,1}$ while also solving the associated inverse problem. Therefore, $Y_{N,1}$ aims only at a specific yet unknown region of $\mathcal{P}_p$ that is relevant for the solution of the inverse problem. This breaks the typical offline/online framework of reduced basis methods but the resulting method will still have offline and online segments. Nevertheless, the procedure provides considerable acceleration of the computational time.

For the construction of this problem-oriented space we use the nonlinear Landweber method projected onto the current reduced basis space as a criterion to select meaningful parameters. These are then used to enrich the reduced basis space with the corresponding snapshot. By this choice we construct a reduced basis space that is tailored around the inverse problem in the sense that it provides accurate reduced basis approximations for parameters lying in the a priori unknown region of the parameter space that is relevant for the solution of the inverse problem. Simultaneously the inverse problem is solved in this process. Since the Landweber method makes use of the adjoint of the derivative, we introduce a second reduced basis space $Y_{N,2}$ containing the required information. We gather these thoughts.

Procedure 1.4.3 (Adaptive reduced basis approach)**.** *1. Start with an initial value $\sigma_{start} \in \mathcal{P}_p$ and initial possibly empty spaces $Y_{N,1}$, $Y_{N,2}$.*

2. Update the spaces $Y_{N,1}$, $Y_{N,2}$ using the current iterate. In the first step use σ_{start}.

3. Solve the inverse problem up to a certain accuracy with the nonlinear Landweber method projected onto $Y_{N,1}$ and $Y_{N,2}$ and thus determine a new parameter for space enrichment.

4. If the current iterate fulfills (1.8)*, terminate, else go to step* 2*.*

For now, we treat the update of the reduced spaces and the projected Landweber method as modular blocks of our procedure and elaborate on these after the final algorithm has been presented. First, we need to find meaningful termination criteria for the projected nonlinear Landweber method in step 3 of Procedure 1.4.3. Let in the following $\sigma \in \mathcal{P}_p$ be the current iterate of the projected method.

Terminating with a high-dimensional discrepancy principle as soon as $\|F(\boldsymbol{\sigma}) - u^\delta\|_{L^2(\Omega)} \leq \tau\delta$ is out of question since we do not want to compute the expensive solution of (1.9) in each iteration. Instead, we want to terminate via a low-dimensional discrepancy principle as soon as $\|F_N(\boldsymbol{\sigma}) - u^\delta\|_{L^2(\Omega)} \leq \tau\delta$. Taking a look at

$$\|F(\boldsymbol{\sigma}) - u^\delta\|_{L^2(\Omega)} \leq \|F(\boldsymbol{\sigma}) - F_N(\boldsymbol{\sigma})\|_{L^2(\Omega)} + \|F_N(\boldsymbol{\sigma}) - u^\delta\|_{L^2(\Omega)}, \tag{1.17}$$

$$\|F_N(\boldsymbol{\sigma}) - u^\delta\|_{L^2(\Omega)} - \|F_N(\boldsymbol{\sigma}) - F(\boldsymbol{\sigma})\|_{L^2(\Omega)} \leq \|F(\boldsymbol{\sigma}) - u^\delta\|_{L^2(\Omega)}, \tag{1.18}$$

we can see that $\|F(\boldsymbol{\sigma}) - u^\delta\|_{L^2(\Omega)}$ and $\|F_N(\boldsymbol{\sigma}) - u^\delta\|_{L^2(\Omega)}$ are connected via the reduced basis error $\|F_N(\boldsymbol{\sigma}) - F(\boldsymbol{\sigma})\|_{L^2(\Omega)}$ that will grow over the course of the projected Landweber iteration since each consecutive iterate will be worse and worse approximated by the current set of reduced basis spaces. Therefore, we want to control this error which can be done using the rigorous error estimator Δ_N introduced in Lemma 1.3.6. As long as σ does not fulfill the reduced discrepancy principle $(\tau - 2)\delta$ is a reasonable upper bound for Δ_N since it follows from (1.18) that $\|F(\boldsymbol{\sigma}) - u^\delta\|_{L^2(\Omega)} > 2\delta$ (and therefore σ is rejected by (1.8) as well) as long as $\Delta_N(\boldsymbol{\sigma}) \leq (\tau - 2)\delta$. This is a strong motivation to suggest the termination of step 3 of Procedure 1.4.3 if one of the following criteria is met

$$\|F_N(\boldsymbol{\sigma}) - u^\delta\|_{L^2(\Omega)} \leq \tau\delta \quad \text{or} \quad \Delta_N(\boldsymbol{\sigma}) > (\tau - 2)\delta. \tag{1.19}$$

The latter *alternative termination criterion* in (1.19) is in fact a trust region criterion: as soon as the error estimator grows too large we cannot ensure that the error $\|F_N(\boldsymbol{\sigma}) - F(\boldsymbol{\sigma})\|_{L^2(\Omega)}$ stays small enough, thus we do not trust the current reduced basis spaces anymore (they might not produce feasible approximations anymore such that further iterations might be misleading) and enrich them using the current iterate.

We add these thoughts to Procedure 1.4.3 and call the resulting new method *Reduced Basis Landweber (RBL) method*, see Algorithm 3.

Remark 1.4.4. *(i) The reduced bases $\Psi_{N,1}$, $\Psi_{N,2}$ are orthonormalized to ensure numerical stability according to Remark 1.3.5.*

(ii) Computing $\Delta_N(\boldsymbol{\sigma}_i^\delta)$ is crucial regarding the total computational time of Algorithm 3. We will elaborate in Section 1.4.4.

(iii) The alternative termination criterion in (1.19) *guarantees that the reduced basis error stays very small. Due to* (1.17)*, we expect Algorithm 3 to terminate as soon as the inner repeat loop terminates with $\|F_N(\boldsymbol{\sigma}_i^\delta) - u^\delta\|_{L^2(\Omega)} \leq \tau\delta$.*

(iv) A possible drawback of the alternative termination criterion could be the error estimator being inefficient, i.e., in the notation of Lemma 1.3.6,

$$\frac{\Delta_N(\boldsymbol{\sigma}_i^\delta)}{\|e\|_{L^2(\Omega)}}$$

Algorithm 3 RBL($\boldsymbol{\sigma}_{start}, \tau, \Psi_{N,1}, \Psi_{N,2}$)

1: $n := 0,\ \boldsymbol{\sigma}_0^\delta := \boldsymbol{\sigma}_{start},\ Y_{N,1} := \text{span}(\Psi_{N,1}),\ Y_{N,2} := \text{span}(\Psi_{N,2})$
2: **while** $\|F(\boldsymbol{\sigma}_n^\delta) - u^\delta\|_{L^2(\Omega)} > \tau\delta$ **do**
3: compute $\psi_{n,2}$ as described in (1.20)
4: $\Psi_{N,1} := \Psi_{N,1} \cup \{F(\boldsymbol{\sigma}_n^\delta)\},\ \Psi_{N,2} := \Psi_{N,2} \cup \{\psi_{n,2}\}$
5: $Y_{N,1} = \text{span}\{\Psi_{N,1}\},\ Y_{N,2} = \text{span}\{\Psi_{N,2}\}$
6: $i := 1,\ \boldsymbol{\sigma}_i^\delta := \boldsymbol{\sigma}_n^\delta$
7: **repeat**
8: compute $s_{n,i}$ as described in Procedure 1.4.5
9: $\boldsymbol{\sigma}_{i+1}^\delta := \boldsymbol{\sigma}_i^\delta + \omega s_{n,i}$
10: $i := i + 1$
11: **until** $\|F_N(\boldsymbol{\sigma}_i^\delta) - u^\delta\|_{L^2(\Omega)} \leq \tau\delta$ **or** $\Delta_N(\boldsymbol{\sigma}_i^\delta) > (\tau - 2)\delta$
12: $\boldsymbol{\sigma}_{n+1}^\delta := \boldsymbol{\sigma}_i^\delta$
13: $n := n + 1$
14: **end while**
15: **return** $\boldsymbol{\sigma}_{RBL} := \boldsymbol{\sigma}_n^\delta$

being large. This could result in a premature termination of the repeat loop, wasting possible cheap repeat loop iterations and possibly causing more than necessary expensive while loop iterations.

(v) Analogous to Algorithm 1 we write σ_{RBL} to denote the element in $\mathcal{P}_p$ corresponding to $\boldsymbol{\sigma}_{RBL}$.

We want to elaborate on line 3 and 8 of Algorithm 3 with respect to our chosen model problem. Regarding the space update of $Y_{N,2}$, we refer to Procedure 1.4.2 and choose snapshots of the dual problem for the basis update $\psi_{n,2}$ of $Y_{N,2}$

$$\text{enrich } \Psi_{N,2} \text{ with } \psi_{n,2} = u_l^{\sigma_n^\delta} \text{ solving (1.15) for } l := u^\delta - F(\boldsymbol{\sigma}_n^\delta). \tag{1.20}$$

The *reduced Landweber update* in line 8 of Algorithm 3 is done along the lines of Procedure 1.4.2 as well: for given spaces $Y_{N,1} = \text{span}\{\psi_{1,1}, \ldots, \psi_{1,N_1}\}$, $Y_{N,2} = \text{span}\{\psi_{2,1}, \ldots, \psi_{2,N_2}\}$ and current iterate $\boldsymbol{\sigma}_i^\delta$, we replace the forward solutions of (1.9) and (1.15) with their reduced counterparts. This is summarized in the following Procedure.

Procedure 1.4.5 (Reduced Landweber update)**.** *1. Compute $F_N(\sigma_i^\delta) = u_N^{\sigma_i^\delta}$ the primal reduced basis approximation via* (1.12) *using $Y_{N,1}$ as reduced basis space. Define $l := u^\delta - u_N^{\sigma_i^\delta}$.*

2. Compute the dual reduced basis approximation $u_{N,l}^{\sigma_i^\delta} = \sum_{j=1}^{N_2} u_{N,l,j}^{\sigma_i^\delta} \psi_{2,j}$ with $\boldsymbol{u}_{N,l}^{\sigma_i^\delta} =$

$(u_{N,l,j}^{\sigma_i^\delta})_{j=1}^{N_2}$ *solving the small linear system*

$$\tilde{\boldsymbol{B}}_N(\boldsymbol{\sigma}_i^\delta)\boldsymbol{u}_{N,l}^{\sigma_i^\delta} = \tilde{\boldsymbol{m}}_N(\boldsymbol{l}) \quad \textit{with} \tag{1.21a}$$

$$(\tilde{\boldsymbol{B}}_N(\boldsymbol{\sigma}_i^\delta))_{j,k} := b(\psi_{2,j}, \psi_{2,k}; \sigma_i^\delta) \quad \textit{and} \quad (\tilde{\boldsymbol{m}}_N(\boldsymbol{l}))_j := m(\psi_{2,j}; l), \tag{1.21b}$$

for $j, k = 1, \dots, N_2$.

3. *Evaluate the* reduced Landweber update $s_{n,i}$ *via*

$$(s_{n,i})_k = (\boldsymbol{u}_N^{\sigma_i^\delta})^\intercal \boldsymbol{Q}^k \boldsymbol{u}_{N,l}^{\sigma_i^\delta},\ k = 1, \dots, p,$$

with $\boldsymbol{Q}^k = b^k(\psi_{1,i}, \psi_{2,j})_{i,j=1}^{N_1,N_2} \in \mathbb{R}^{N_1 \times N_2}$ *being parameter independent.*

Since both reduced problems (1.12) and (1.21) are offline/online decomposable, i.e., the online phases are of complexity polynomial in N_1 and N_2, independent of n^2, and the matrices $\boldsymbol{Q}^k$, $k = 1, \dots p$, can be computed as soon as the reduced spaces are updated in line 4, the projected reduced Landweber method in the repeat loop from line 7 to 10 can be implemented in an efficient and cheap way. It only consists of the online phases of (1.12) and (1.21) and the reduced Landweber update in step 3 of Procedure 1.4.5. In this sense the repeat loop is the online segment of Algorithm 3, where we elaborate on the computational cost of the error estimator Δ_N in the upcoming section. The remainder of the algorithm is then the offline segment since, with the enrichment of the reduced basis spaces, i.e., computing solutions of (1.9) and (1.15), and the projection onto the new set of reduced basis spaces, it involves computations depending on n^2.

We conclude this section with final remarks about the RBL method.

Remark 1.4.6. *(i) For a fixed* $\sigma \in \mathcal{P}_p$ *let* $\langle \cdot, \cdot \rangle_\sigma := b(\cdot, \cdot; \sigma)$ *denote the energy scalar product and* $P_\sigma : Y \longrightarrow Y_{N,1}$ *the corresponding orthogonal projection. With* $Y_{N,1} = \operatorname{span}\{\psi_{1,1}, \dots, \psi_{1,N_1}\}$ *it holds for all* $i = 1, \dots, N_1$

$$\begin{aligned} &\langle P_\sigma(F(\sigma)) - F(\sigma), \psi_{1,i} \rangle_\sigma = 0 \\ \Leftrightarrow\, &b(P_\sigma(F(\sigma)) - F(\sigma), \psi_{1,i}; \sigma) = 0 \\ \Leftrightarrow\, &b(P_\sigma(F(\sigma)), \psi_{1,i}; \sigma) = f(\psi_{1,i}) \end{aligned}$$

such that $P_\sigma \circ F(\sigma)$ *is a solution of* (1.12) *and therefore* $u_N^\sigma = F_N(\sigma) = P_\sigma \circ F(\sigma)$*, since the solution of* (1.12) *is unique. Using this and the fact that* $P_\sigma \in \mathcal{L}(Y, Y_{N,1})$ *is an orthogonal projection, it is easy to see that* $F_N'(\sigma) = P_\sigma \circ F'(\sigma)$ *and (for* $l \in Y_{N,1}$*)* $F_N'(\sigma)^* l = F'(\sigma)^*(P_\sigma^* l) = F'(\sigma)^* l$*. Therefore, the reduced Landweber update* $s_{n,i}$ *calculated in step* 3 *of Procedure 1.4.5 does not coincide with the expression* $F_N'(\boldsymbol{\sigma}_i^\delta)^*(u^\delta - F_N(\boldsymbol{\sigma}_i^\delta))$ *(see Procedure 1.4.2). The consequence here is, that in general there is no closed expression of the iteration scheme of the RBL method. Instead, the main idea of the RBL method is to determine what kind of PDE solutions are required for the update of the Landweber method and replace them with suitable reduced basis approximations.*

(ii) In [Sch98] Scherzer proposes a different methodology where one employs a sequence $\{X_N\}_{N\in\mathbb{N}_0}$ of nested subspaces of X (the infinite dimensional parameter space) with $\bigcup_{N\in\mathbb{N}_0} X_N$ being dense in X. The orthonormal projection P_N on those spaces is then used to develop a multi-level discrete Landweber method. In [dHQS15] a similar approach is made for a steepest descent method in Banach spaces. As we can see our approach can not be formulated in such a way and the convergence theory developed in the mentioned works can not be adapted to the RBL method.

(iii) Because of (i) and (ii), we postpone a theoretical investigation of the RBL method to future work.

1.4.4 Experiments

We want to compare Algorithms 1 & 3. To this end we choose a specific setting to which all experiments refer. We use the parameter space $\mathcal{P}_{900}$, $n = 149$ for the finite element space Y and want to reconstruct

$$\begin{aligned}\sigma^+(\boldsymbol{x}) :=& 3 + 2\chi_{\Omega^{(1)}}(\boldsymbol{x}) - 2\chi_{\Omega^{(2)}}(\boldsymbol{x}) \quad \boldsymbol{x}\in\Omega \text{ with subdomains}\\ \Omega^{(1)} =& [5/30, 9/30]\times[3/30, 27/30]\\ &\cup\left([9/30, 27/30]\times([3/30, 7/30]\cup[23/30, 27/30])\right),\\ \Omega^{(2)} =& \{\boldsymbol{x}\in\Omega \mid \|(18/30, 15/30)^\intercal - \boldsymbol{x}\|_2 < 4/30\}.\end{aligned}$$

This is a piecewise constant function with background 3, contrast 2 on the C-shaped subdomain $\Omega^{(1)}$ and contrast -2 on the disk $\Omega^{(2)}$. The starting value $\sigma_{start}\equiv 3$ as well as the function σ^+ are visualized in the top left and bottom left of Figure 4. The noisy measurement u^δ is generated in the following way: we compute the PDE-solution for σ^+ using Comsol® and evaluate it at the nodes of the finite element space Y. Afterwards we add uniformly distributed random noise with a certain noise level. If not specified differently we add 1% relative noise (corresponding to $1.243\cdot 10^{-4}$ absolute noise) and choose $\tau = 2.5$ in this section. Note that the noise is only added on the inner nodes of the discretization since we assume that the homogeneous Dirichlet data are known and measured correctly. The damping parameter ω is heuristically chosen as $\omega = \frac{1}{2}(\|F'(\boldsymbol{\sigma}_{start})\|)^{-1}$ with the $\frac{1}{2}$ resembling local uniform boundedness. Note that $\|F'(\boldsymbol{\sigma}_{start})\| \ll 1$ such that ω actually serves as a speed-up of the iteration. The numerical experiments are done using Matlab® in conjunction with the libraries RBmatlab and KerMor, which both can be found online[1].

In the following, three experiments will be carried out in the above *full* setting. Additionally, the same experiments are done for the (accordingly modified) versions of Algorithms 1 & 3 applied to the partial inverse problem (1.4) introduced in

[1] http://www.ians.uni-stuttgart.de/MoRePaS/software/

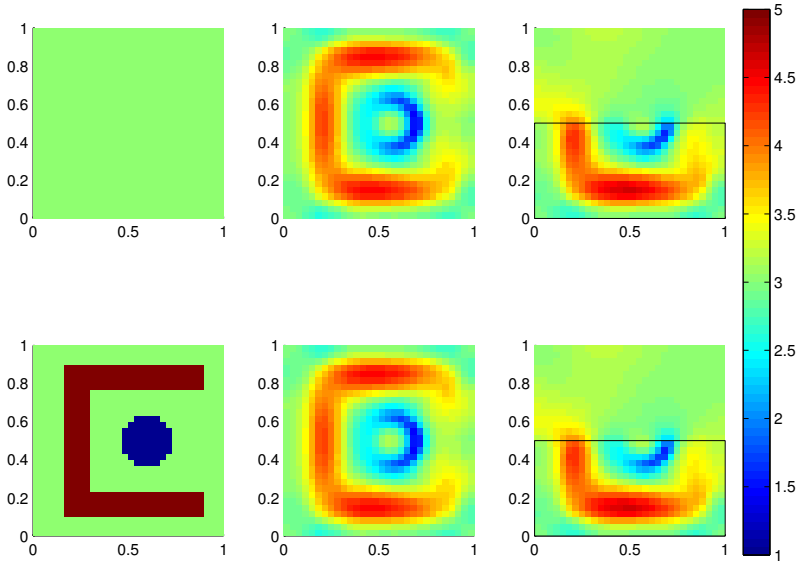

Figure 4: The reconstructions of σ^+ in the full setting via Algorithm 3 (top middle) and Algorithm 1 (bottom middle), as well as the starting value σ_{start} (top left) and the exact value σ^+ (bottom left). The reconstruction in the partial setting via Algorithm 3 (top right) and Algorithm 1 (bottom right) including the subdomain $\tilde{\Omega}$ as a black box.

Remark 1.2.1. In this *partial* setting, we use the same numerical setting as above but measure the data only on the subdomain $\tilde{\Omega} = [0,1] \times [0,0.5]$, add 1% relative noise (corresponding to $8.786 \cdot 10^{-5}$ absolute noise) and use $\tilde{\omega} = \frac{1}{2}(\|\tilde{F}'(\boldsymbol{\sigma}_{start})\|)^{-1}$ as damping parameter. Figures 4 & 5 as well as Table 1 contain results for both (partial and full) settings where our discussion will focus on the full setting.

Figure 4 shows the reconstructions of σ^+ in the full setting via Algorithm 3 in the top middle and via Algorithm 1 in the bottom middle. In addition the reconstructions in the partial setting via Algorithm 3 in the top right and via Algorithm 1 in the bottom right are shown, where the black box indicates the subdomain $\tilde{\Omega}$.

Concerning the middle column, we cannot distinguish the two reconstructions visually from each other, which is also stated by $\|\sigma_{RBL} - \sigma_{LW}\|_{L^2(\Omega)} \approx 1.118 \cdot 10^{-5}$, such that both algorithms numerically yield the same reconstruction. The shape and location of as well as the contrast on $\Omega^{(1)}$ are well reconstructed. Regarding $\Omega^{(2)}$, only the location is well reconstructed. The contrast is not fitting everywhere and there is another small circular inclusion with opposite sign inside of $\Omega^{(2)}$. In the partial setting we have a good reconstruction on $\tilde{\Omega}$ and some indications of a reconstruction close to $\tilde{\Omega}$.

Next, we want to compare the Algorithms with respect to the computational time: for Algorithm 1 we measure the total time, the amount of iterations until the discrepancy principle is reached and therefore the time per iteration, as well as the total amount of forward solves. Due to Procedure 1.4.2, both discretized problems

Setting	time (s)	# Iterations		time per Iter. (s)		# forward solves
LW, full	187189	608067		0.308		1216134
		outer	inner	outer	inner	
RBL, full	14661	20	608083	3.705	0.024	40
LW, partial	173759	580129		0.299		1160258
		outer	inner	outer	inner	
RBL, partial	10638	20	580133	3.670	0.018	40

Table 1: Runtime comparison of Algorithms 1 & 3 in the full and partial setting.

(1.9) and (1.15) are considered here. For Algorithm 3, we are interested in the total time and therefore the speed-up compared to Algorithm 1, the amount of and the time per outer iteration (line 2 - 14 excluding the repeat-loop from line 7 - 11), as well as the amount of and the time per inner iteration (one step of the repeat-loop from line 7 - 11) and again the total amount of high-dimensional forward solves. Table 1 contains the respective information.

In the full setting the RBL method needs around 4 hours and the Landweber method needs around 52 hours of computational time resulting in a speed-up of 13. Due to (1.19), the reduced spaces are very accurate such that the amount of inner iterations of Algorithm 3 roughly coincides with the amount of iterations of Algorithm 1. We want to highlight that Algorithm 3 only needed 40 expensive forward solves compared to the 1216134 forward solves required for Algorithm 1. If we look at the average iteration times of Algorithm 3, it becomes clear that sufficient inner iterations have to be made per outer iteration for Algorithm 3 to pay off in time. We will see in our next experiment that this is the case in the chosen setting. Regarding the average time per inner iteration, we have to mention our implementation of the error estimator (1.13): we do not use the offline/online decomposition presented in Procedure 1.3.10 since this would result in each online phase to contain a vector-matrix-vector multiplication of dimension $Q_r = N_1 \cdot p + 1$, with $p = 900$ and $N_1 = \dim Y_{N,1}$. But the matrix in this multiplication is full as we can see in Corollary 1.3.8, which prohibits this approach. Therefore, we compute the Riesz-representative and its norm in each inner iteration according to Lemma 1.3.6 such that the online segment of Algorithm 3 is not completely independent of n^2 in this example and roughly 50% of the total computational time is spent in computing the error estimator in the inner loop. Hence, it might be interesting to develop termination criteria that still guarantee accurate reduced basis spaces but are less expensive. Similar conclusions can be drawn for the partial setting as it can be seen in Table 1.

In the third experiment we want to see that both Algorithms 1 & 3 behave the same way, with the latter simply being faster. To this end we define the nonlinear Landweber update $\boldsymbol{s}_{n,LW} := F'(\boldsymbol{\sigma}_n^\delta)^*(u^\delta - F(\boldsymbol{\sigma}_n^\delta))$ in addition to the update of the RBL method (here denoted by $s_{n,RBL}$) described in Procedure 1.4.5. Figure 5 shows

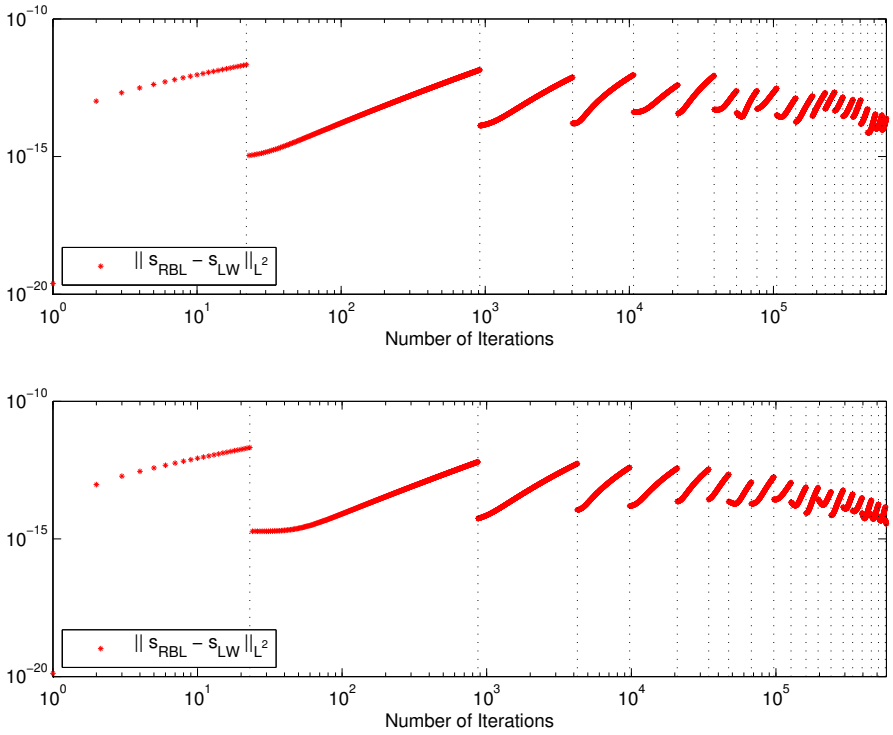

Figure 5: Update error $\|s_{n,RBL} - s_{n,LW}\|_{L^2(\Omega)}$ over the course of the iteration for the full setting (top) and the partial setting (bottom).

the *update error* $\|s_{n,RBL} - s_{n,LW}\|_{L^2(\Omega)}$ over the course of the iteration. The plot also includes a vertical dashed line whenever an outer iteration in Algorithm 3 is performed.

We observe the expected behaviour: the more inner iterations of the RBL method are performed for a given set of spaces, the worse the update error gets until one of the termination criteria is met. Note that in this test the alternative termination criterion always triggered except in the very end where the reduced discrepancy principle is reached. With $\|F_N(\boldsymbol{\sigma}_{RBL}) - F(\boldsymbol{\sigma}_{RBL})\|_{L^2(\Omega)} \approx 1.296 \cdot 10^{-8}$ and (1.17), the high-dimensional discrepancy principle in line 2 of Algorithm 3 is then met as well and the whole algorithm terminates. According to Remark 1.4.4 this behaviour was expected. If we look at the iteration sequence in Figure 5 we can observe two further aspects: the more outer iterations are performed, the better the set of reduced spaces fits the region of the parameter space relevant for the solution of the inverse problem, resulting in the update error to decrease as a whole. Finally, the space updates are performed more frequently in the beginning of the iteration sequence (note the logarithmic scale of the iteration axis) to quickly adapt to the region of interest. Once the spaces are well suited, more and more inner iterations per outer iteration can be performed, resulting in Algorithm 3 to outperform Algorithm 1 by more than an order with respect to the computational time. Again, similar observations can be made in the partial setting as it can be seen on the bottom of

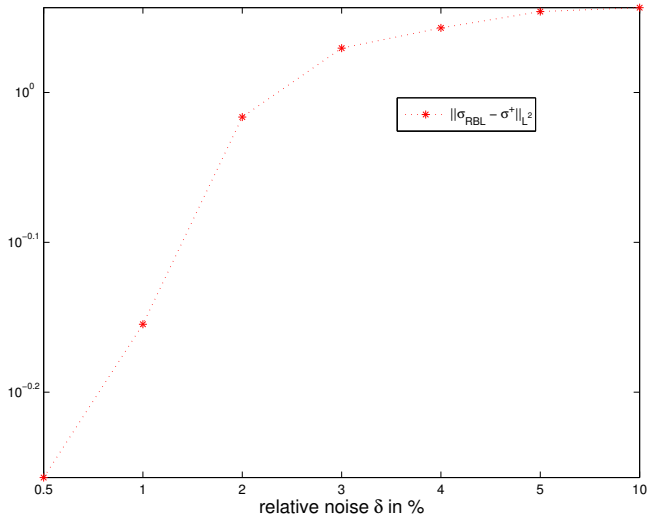

Figure 6: Error $\|\sigma_{RBL} - \sigma^+\|_{L^2(\Omega)}$ over the decreasing relative noise level δ.

Figure 5.

In Remark 1.4.6 we justified the current lack of a theoretical investigation of the RBL method. Still, we can provide an experiment regarding its numerical regularization property. In the usual full setting the error $\|\sigma_{RBL} - \sigma^+\|_{L^2(\Omega)}$ is shown over the decreasing relative noise level δ in Figure 6.

By this we can conclude that a numerical regularization property is present for the RBL method.

1.5 Conclusion

For the problem of reconstructing the conductivity in the stationary heat equation it was investigated how reduced basis methods and the nonlinear Landweber method can be combined to reduce the overall computational time. A direct approach was shortly discussed to be inapplicable in the presence of high-dimensional parameter spaces. A new approach, the RBL method, was presented. It combined adaptive space enrichment of the reduced basis spaces with the nonlinear Landweber method. Using the RBL method, high-resolution images of the conductivity could be reconstructed, with the method being as accurate as the nonlinear Landweber method but roughly 13 times faster. Future work should contain a theoretical investigation of the RBL method including convergence theory as well as the application of its methodology to other inverse problems and more sophisticated regularization algorithms.

1.6 Proof of the Fréchet derivative of $\mathcal{F}$

We prove the statement made in (1.5) of Section 1.2.

For $\sigma \in L^\infty_+(\Omega)$ and $\kappa \in L^2(\Omega)$ with $\sigma + \kappa \in L^\infty_+(\Omega)$ let u^σ, $u^{\sigma+\kappa}$ denote the corresponding solutions of (1.2), v^σ_κ the solution of (1.6) and $\underline{c} := \operatorname{ess\,inf}(\sigma)$. Note that u^σ solving (1.2) is equivalent to u^σ solving $b(u^\sigma, v; \sigma) = f(v)$ for all $v \in H^1_0(\Omega)$. It holds for all $w \in H^1_0(\Omega)$

$$\begin{aligned} &\int_\Omega (\sigma+\kappa)(\nabla u^{\sigma+\kappa} \cdot \nabla w) - (\sigma \nabla u^\sigma \cdot \nabla w)\, dx = 0 \\ \Leftrightarrow &\int_\Omega \sigma(\nabla(u^{\sigma+\kappa} - u^\sigma) \cdot \nabla w)\, dx = -\int_\Omega \kappa \nabla u^{\sigma+\kappa} \cdot \nabla w\, dx. \end{aligned} \tag{1.22}$$

The test function $w = u^{\sigma+\kappa} - u^\sigma$ in (1.22) and the Hölder inequality yield

$$\begin{aligned} &\underline{c}\|\nabla(u^{\sigma+\kappa} - u^\sigma)\|^2_{L^2(\Omega)} \le \int_\Omega \sigma \nabla(u^{\sigma+\kappa} - u^\sigma) \cdot \nabla(u^{\sigma+\kappa} - u^\sigma)\, dx \\ &= -\int_\Omega \kappa \nabla u^{\sigma+\kappa} \cdot \nabla(u^{\sigma+\kappa} - u^\sigma)\, dx \le \|\kappa\|_\infty \|\nabla u^{\sigma+\kappa}\|_{L^2(\Omega)} \|\nabla(u^{\sigma+\kappa} - u^\sigma)\|_{L^2(\Omega)} \\ &\Leftrightarrow \|\nabla(u^{\sigma+\kappa} - u^\sigma)\|_{L^2(\Omega)} \le \frac{\|\kappa\|_\infty}{\underline{c}} \|\nabla u^{\sigma+\kappa}\|_{L^2(\Omega)}. \end{aligned}$$

Similar arguments for $\sigma + \kappa$ and test function $w = u^{\sigma+\kappa}$ in (1.2) together with the inequality of Poincaré-Friedrich and the notation $c := \|1\|_{L^2(\Omega)}$ yield

$$\begin{aligned} \underline{c}\|\nabla u^{\sigma+\kappa}\|^2_{L^2(\Omega)} &\le \int_\Omega (\sigma+\kappa)(\nabla u^{\sigma+\kappa} \cdot \nabla u^{\sigma+\kappa})\, dx = -\int_\Omega 1 \cdot u^{\sigma+\kappa}\, dx \\ &\le \|1\|_{L^2(\Omega)} \|u^{\sigma+\kappa}\|_{L^2(\Omega)} \le c \cdot C_{PF} \|\nabla u^{\sigma+\kappa}\|_{L^2(\Omega)}. \end{aligned}$$

Introducing the constant $C' := \frac{c \cdot C_{PF}}{\underline{c}^2}$ we get

$$\|\nabla(u^{\sigma+\kappa} - u^\sigma)\|_{L^2(\Omega)} \le C' \|\kappa\|_\infty. \tag{1.23}$$

With (1.23) and the definition of v^σ_κ in (1.6) it follows

$$\begin{aligned} &\int_\Omega \sigma \nabla(u^{\sigma+\kappa} - u^\sigma) \cdot \nabla w - \sigma \nabla v^\sigma_\kappa \cdot \nabla w\, dx \\ &= -\int_\Omega \kappa \nabla u^{\sigma+\kappa} \cdot \nabla w\, dx + \int_\Omega \kappa \nabla u^\sigma \cdot \nabla w\, dx \\ \Leftrightarrow &\int_\Omega \sigma \nabla(u^{\sigma+\kappa} - u^\sigma - v^\sigma_\kappa) \cdot \nabla w\, dx = \int_\Omega \kappa \nabla(u^\sigma - u^{\sigma+\kappa}) \cdot \nabla w\, dx. \end{aligned} \tag{1.24}$$

The test function $w = u^{\sigma+\kappa} - u^\sigma - v^\sigma_\kappa$ in (1.24), the Hölder inequality and (1.23)

yield

$$\begin{aligned}\underline{c}\|\nabla(u^{\sigma+\kappa}-u^{\sigma}-v_{\kappa}^{\sigma})\|_{L^2(\Omega)}^2 & \\ &\leq \int_{\Omega}\sigma\nabla(u^{\sigma+\kappa}-u^{\sigma}-v_{\kappa}^{\sigma})\cdot\nabla(u^{\sigma+\kappa}-u^{\sigma}-v_{\kappa}^{\sigma})\,dx \\ &= \int_{\Omega}\kappa\nabla(u^{\sigma}-u^{\sigma+\kappa})\cdot\nabla(u^{\sigma+\kappa}-u^{\sigma}-v_{\kappa}^{\sigma})\,dx \\ &\leq \|\kappa\|_{\infty}\|\nabla(u^{\sigma}-u^{\sigma+\kappa})\|_{L^2(\Omega)}\|\nabla(u^{\sigma+\kappa}-u^{\sigma}-v_{\kappa}^{\sigma})\|_{L^2(\Omega)},\end{aligned}$$

such that

$$\|\nabla(u^{\sigma+\kappa}-u^{\sigma}-v_{\kappa}^{\sigma})\|_{L^2(\Omega)} \leq \frac{1}{\underline{c}}\|\kappa\|_{\infty}\|\nabla(u^{\sigma}-u^{\sigma+\kappa})\|_{L^2(\Omega)} \leq \frac{C'}{\underline{c}}\|\kappa\|_{\infty}^2.$$

Using the inequality of Poincaré-Friedrich again and introducing $C'' := \frac{C_{PF}\cdot C'}{\underline{c}}$ we get

$$\|u^{\sigma+\kappa}-u^{\sigma}-v_{\kappa}^{\sigma}\|_{L^2(\Omega)} \leq C_{PF}\|\nabla(u^{\sigma+\kappa}-u^{\sigma}-v_{\kappa}^{\sigma})\|_{L^2(\Omega)} \leq C''\|\kappa\|_{\infty}^2.$$

Since C'' is independent of κ the statement follows

$$\begin{aligned}\lim_{\|\kappa\|_{\infty}\to 0}\frac{\|\mathcal{F}(\sigma+\kappa)-\mathcal{F}(\sigma)-\mathcal{F}'(\sigma)\kappa\|_{L^2(\Omega)}}{\|\kappa\|_{\infty}} &= \lim_{\|\kappa\|_{\infty}\to 0}\frac{\|u^{\sigma+\kappa}-u^{\sigma}-v_{\kappa}^{\sigma}\|_{L^2(\Omega)}}{\|\kappa\|_{\infty}} \\ &\leq \lim_{\|\kappa\|_{\infty}\to 0}\frac{C''\|\kappa\|_{\infty}^2}{\|\kappa\|_{\infty}} = 0.\end{aligned}$$

Chapter 2

Magnetic Resonance Electrical Impedance Tomography (MREIT): Convergence and Reduced Basis Approach

Sections 2.1, 2.2 and 2.4 are, up to minor changes, Sections 1, 2 and 4 of the article [GH18]. Section 2.3 is largely based on Section 3 of the same article, but has been slightly reworked to account for Section 1.4.

2.1 Introduction

Magnetic resonance electrical impedance tomography (MREIT) is an imaging modality developed over the course of the last three decades. In order to obtain data, surface electrodes are attached onto the imaging subject, e.g., the human body, while the object resides inside an MRI scanner. Injecting current through the electrodes then results in a change of the magnetic flux density $\mathbf{B} = (B_x, B_y, B_z)$ inside the subject and the MRI scanner can detect this change in the magnetic field. The aim of the method is the determination of the electrical conductivity σ of the imaging subject from this measured data. This chapter deals with the B_z-based MREIT approach, which is feasible in practice: it is assumed that only B_z is available where the z-direction is the direction of the main magnetic field of the MRI scanner (earlier techniques utilized the whole magnetic field $\mathbf{B}$, but cumbersome subject rotations are then necessary to acquire all three components). In order to solve the inverse problem of determining σ from B_z, one can apply the well-known *Harmonic B_z Algorithm*, which was proposed by Seo et al. [SYWK03] and has since been extensively studied, see, e.g., [OLW$^+$03, KPSW06, WS08, LSSW07, LSW10, SW11] and the references therein.

The historical motivation for the development of MREIT techniques is the Electrical impedance tomography (EIT), see, e.g., [CIN99, NGI88, AGL11, Lio04, Uhl09] for

a broad overview. EIT is known to be severely ill-posed and nonlinear such that the spatial resolution of a reconstruction is (usually) poor (on the other hand, EIT shines with an excellent temporal resolution, cf. time-difference EIT in the above-cited works). Consequently, improving the spatial resolution of conductivity images was the driving force for the development of MREIT techniques.

Before the contributions of this chapter to the field of research are described, the basic setting and the key identity of the Harmonic B_z Algorithm are recapitulated. Let the imaging subject reside in a bounded domain $\Omega \subset \mathbb{R}^3$ with two pairs of surface electrodes attached to it, and let $E_1^{\pm}$, $E_2^{\pm}$ denote the respective parts of $\partial\Omega$ where the electrodes are attached. Furthermore, let $\sigma \in C^1(\overline{\Omega})$. Each of the two input currents I_1, I_2 (one per electrode pair) induces a magnetic field and the respective z-components B_z^1, B_z^2 are the observable data. The physical motivation for B_z-based MREIT is the implicit connection between the unknown conductivity σ and the observable data B_z^1, B_z^2 via the *Biot-Savart law*: for $j = 1, 2$, where j specifies the active electrode pair throughout this chapter, and $\mathbf{r} = (x, y, z) \in \Omega$, it is

$$B_z^j(\mathbf{r}) = \frac{\mu_0}{4\pi} \int_\Omega \sigma(\mathbf{r}) \frac{(x - x')\frac{\partial u_j^\sigma}{\partial y}(\mathbf{r}') - (y - y')\frac{\partial u_j^\sigma}{\partial x}(\mathbf{r}')}{|\mathbf{r} - \mathbf{r}'|^3} \mathrm{d}\mathbf{r}',$$

with μ_0 the magnetic constant of the free space. u_j^σ denotes the electrical potential that satisfies the *shunt model*, i.e.,

$$\begin{aligned}
&\nabla \cdot (\sigma \nabla u_j^\sigma) = 0 \quad \text{in} \quad \Omega \\
&I_j = \int_{E_j^+} \sigma \frac{\partial u_j^\sigma}{\partial \mathbf{n}} \mathrm{d}s = -\int_{E_j^-} \sigma \frac{\partial u_j^\sigma}{\partial \mathbf{n}} \mathrm{d}s, \quad \nabla u_j^\sigma \times \mathbf{n} = 0 \quad \text{on} \quad E_j^+ \cup E_j^-, \\
&\sigma \frac{\partial u_j^\sigma}{\partial \mathbf{n}} = 0 \quad \text{on} \quad \partial\Omega \setminus \overline{\left(E_j^+ \cup E_j^-\right)},
\end{aligned}$$

where $\mathbf{n}$ denotes the outward unit normal vector and $\times$ denotes the cross product. The Harmonic B_z Algorithm is then an iteration based upon the following identity (here in the logarithmic formulation), which is obtained by applying the curl-operator on both sides of Ampère's law:

$$\nabla_{xy} \ln \sigma = \frac{1}{\mu_0} (\sigma \mathbb{A}[\sigma])^{-1} \begin{pmatrix} \nabla^2 B_z^1 \\ \nabla^2 B_z^2 \end{pmatrix}, \quad \text{with} \quad \mathbb{A}[\sigma] = \begin{pmatrix} \frac{\partial u_1}{\partial y} & -\frac{\partial u_1}{\partial x} \\ \frac{\partial u_2}{\partial y} & -\frac{\partial u_2}{\partial x} \end{pmatrix}, \tag{2.1}$$

where ∇^2 always denotes the Laplace operator throughout this chapter and ∇_{xy} is the gradient in x and y direction.

For locally cylindrical subjects with a conductivity that is hardly changing alongside the z-direction, the corresponding MREIT problem can entirely be formulated in two space dimensions, see, e.g., [LSSW07, LSW10]. This chapter will consider this two-dimensional MREIT problem, which is feasible in practice for the limbs and the thorax of the human body.

Now, the contribution to the field made in this chapter is the following: although there have been many advanced numerical studies in MREIT, the convergence analysis did so far only consider the idealized case in which the exact forward solution u_j^σ is available for the Harmonic B_z Algorithm. Of course, this is not the case in a numerical study (where, for instance, only a finite element approximation is available), such that numerical convergence of the algorithm remains an open question. This chapter provides a rigorous and complete mathematical framework as well as a convergence result for the inverse problem in question. The convergence result is based on and at the same time an extension of the existing convergence theory, see [LSSW07, LSW10], such that the usage of an approximation of u_j^σ in the Harmonic B_z Algorithm is sufficient for convergence. As a consequence, actual numerical convergence of the algorithm is achieved. Furthermore, the potential to use an approximative forward solution instead of the exact one opens up the possibility of combining the existing Harmonic B_z Algorithm with model order reduction techniques in order to develop novel algorithms that retain the accuracy in the reconstruction but are computationally faster.

The reduced basis method is in Section 1.3.2 recalled for the shunt model, where the main task of the method was the construction of a low-dimensional reduced basis space, e.g., via snapshots that are forward solutions for relevant parameters, followed by Galerkin projection onto this space. The novel algorithm will then utilize the adaptive reduced basis approach which was outlined for the nonlinear Landweber method in Section 1.4.3 and is based on ideas developed in [DZ07, CMW14, Las14, ZF15]: new parameter values for the enrichment of the reduced basis space are found by projecting the inversion algorithm onto it and iterating this projected algorithm. By alternately updating the reduced basis space and running the onto this space reprojected inversion algorithm, the solution of the inverse problem and the construction of the reduced basis space are achieved simultaneously. We mention a recent work [SAS17] which aims at speeding up the image reconstruction in MREIT by presenting an undersampled MREIT method that allows for a reduced data acquisition time.

The remainder of this chapter is organized as follows. In Section 2.2 the forward and inverse problem in question are presented. Required results for the convergence theorem are derived and the theorem itself is proven. Section 2.3 contains a short recollection of the reduced basis method as well as the development of the novel algorithm including numerical results. Conclusions are drawn in Section 2.4.

2.2 Magnetic Resonance Electrical Impedance Tomography (MREIT)

This section provides the mathematical framework, i.e., the forward and the inverse problem of MREIT, the solution algorithms for the inverse problem, and the conver-

gence theorem including various minor results. As mentioned in Section 2.1, the focus of this chapter is a convergence analysis for the two-dimensional MREIT problem (and in Section 2.3 the speed-up of the Harmonic B_z Algorithm), such that the mathematical setting will be chosen accordingly. We refer to [SW11, SYWK03, LSSW07] for a detailed motivation as well as an overview of the MREIT problem.

2.2.1 Problem formulation

For the remainder of this chapter, let $\Omega_c \subset\subset \Omega_I \subset\subset \Omega \subset \mathbb{R}^2$ be $C^{1,\alpha}$-domains with $\alpha \in (0,1)$, let $E_1^{\pm}$, $E_2^{\pm}$ denote the respective parts of $\partial\Omega$ where the electrodes are attached, and let I_1, I_2 be the input currents corresponding to the electrodes, see Figure 7 for an exemplary setting of an electrode configuration and the domains. Later on, Ω_c will serve as contrast domain, where the unknown true conductivity is allowed to change from a constant background. Ω_I will be an intermediate domain between Ω_c and Ω, which will be necessary for various theoretical arguments throughout this chapter.

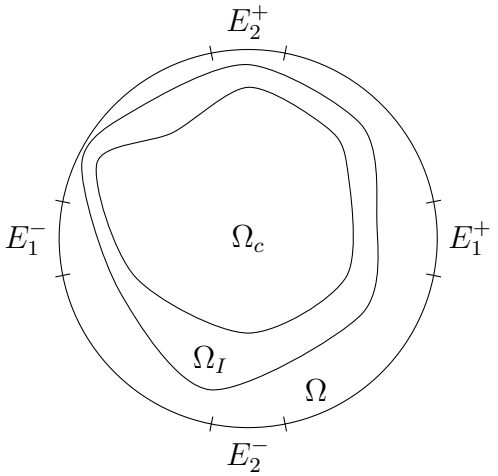

Figure 7: Exemplary setting of the domains $\Omega_c \subset\subset \Omega_I \subset\subset \Omega \subset \mathbb{R}^2$ and attached electrodes $E_j^{\pm}$, $j = 1, 2$.

We consider the parameter space

$$\mathcal{P} := \{\sigma \in C^{1,\alpha}(\overline{\Omega}) \mid \sigma(x) > 0,\, x \in \overline{\Omega}\}$$

and want to stress that this rather restrictive choice is made with sight on the convergence theory to be developed in Sections 2.2.2 & 2.2.3.

For the sake of completeness we include a proof of the fact, that a solution of the shunt model can be obtained as a scaled solution of a standard boundary value problem, see, e.g., [LSSW07, Lemma 2.1].

Lemma 2.2.1. *For $\sigma \in \mathcal{P}$, let u_j^σ fulfill*

$$\nabla \cdot (\sigma \nabla u_j^\sigma) = 0 \quad \text{in } \Omega \tag{2.2a}$$

$$u_j^\sigma|_{E_j^+} = 1, \quad u_j^\sigma|_{E_j^-} = 0 \tag{2.2b}$$

$$\sigma \nabla u_j^\sigma \cdot \mathbf{n} = 0 \quad \text{on } \partial\Omega \backslash \overline{E_j^+ \cup E_j^-}, \tag{2.2c}$$

where $j = 1, 2$ specifies the active electrode pair $E_j^\pm$ and corresponding input current I_j. Then,

$$\tilde{u}_j^\sigma = \frac{I_j}{\int_{E_j^+} \sigma \frac{\partial u_j^\sigma}{\partial \mathbf{n}} \mathrm{d}s} u_j^\sigma \tag{2.3}$$

is a solution of the two-dimensional shunt model

$$\nabla \cdot (\sigma \nabla u) = 0 \quad \text{in} \quad \Omega \tag{2.4a}$$

$$I_j = \int_{E_j^+} \sigma \frac{\partial u}{\partial \mathbf{n}} \mathrm{d}s = -\int_{E_j^-} \sigma \frac{\partial u}{\partial \mathbf{n}} \mathrm{d}s, \quad \nabla u \times \mathbf{n} = 0 \quad \text{on} \quad E_j^+ \cup E_j^-, \tag{2.4b}$$

$$\sigma \frac{\partial u}{\partial \mathbf{n}} = 0 \quad \text{on} \quad \partial\Omega \setminus \overline{\left(E_j^+ \cup E_j^-\right)}. \tag{2.4c}$$

Proof. u_j^σ as a weak solution of (2.2) has Neumann boundary values $\sigma \frac{\partial u_j^\sigma}{\partial \mathbf{n}} \in H^{-1/2}(\partial\Omega)$ such that

$$\int_\Omega \sigma \nabla u_j^\sigma \cdot \nabla w \mathrm{d}x = \int_{\partial\Omega} \sigma \frac{\partial u_j^\sigma}{\partial \mathbf{n}} w \mathrm{d}s$$

holds for all $w \in H^1(\Omega)$ and choosing $w \equiv 1$ as well as utilizing (2.2c) yields

$$\int_{E_j^+} \sigma \frac{\partial u_j^\sigma}{\partial \mathbf{n}} \mathrm{d}s = -\int_{E_j^-} \sigma \frac{\partial u_j^\sigma}{\partial \mathbf{n}} \mathrm{d}s.$$

As a consequence, $\tilde{u}_j^\sigma = \frac{I_j}{\int_{E_j^+} \sigma \frac{\partial u_j^\sigma}{\partial \mathbf{n}} \mathrm{d}s} u_j^\sigma$ fulfills the shunt model (2.4). □

Remark 2.2.2. *(i) Finding a solution u_j^σ of (2.2) is equivalent to finding*

$$u \in H^1_{D_j}(\Omega) := \{u \in H^1(\Omega) \mid u|_{E_j^+} = 1,\, u|_{E_j^-} = 0\}$$

solving

$$b(u, v; \sigma) = f(v), \quad \text{for all} \quad v \in H_0^1(\Omega), \tag{2.5a}$$

$$b(u, v; \sigma) := \int_\Omega \sigma \nabla u \cdot \nabla v dx, \quad f(v) := 0. \tag{2.5b}$$

Since $\sigma \in \mathcal{P}$, existence and uniqueness of a solution of (2.5) and therefore (2.2) follow via the Lax-Milgram theorem.

(ii) It is well known [SCI92] that the shunt model (2.4) *omits an (up to an additive constant) unique solution. Therefore, the gradient of a solution of* (2.4) *is uniquely determined and equivalent to the gradient of* (2.3).

(iii) Whenever we refer to a solution of (2.2)*, we refer to the scaled solution via* (2.3) *and will write not* $\tilde{u}$ *but* u.

Before we formulate the inverse problem in the upcoming section, we gather various known regularity results and estimates for the solutions of mixed boundary value problems in the following lemma, see [LSW10, Lemma 3.1]. It is easy to see, that the general problem (2.6) in the upcoming lemma covers the forward problem (2.2).

Lemma 2.2.3. *Denote by* Γ *any relatively open* $C^{1,\alpha}$*-portion of* $\partial\Omega$*. For the boundary value problem*

$$\nabla \cdot (\sigma \nabla u) = \sigma g \quad \text{in } \Omega \tag{2.6a}$$
$$u|_\Gamma = h \quad \text{on } \Gamma \tag{2.6b}$$
$$-\sigma \nabla u \cdot \mathbf{n} = 0 \quad \text{on } \partial\Omega \backslash \overline{\Gamma}, \tag{2.6c}$$

with $\sigma \in \mathcal{P}$*, and* $g \in L^2(\Omega)$*,* $h \in H^{1/2}(\Gamma)$*, it is* $u \in H^2(\Omega_I) \cap H^1(\Omega)$.

(a) If $h = 0$*, the following estimates hold*

$$\|u\|_{H^2(\Omega_I)} \leq C_1(\sigma)(\|u\|_{L^2(\Omega)} + \|g\|_{L^2(\Omega)}), \tag{2.7}$$
$$\|u\|_{H^1(\Omega)} \leq C_2(\sigma)\|g\|_{L^2(\Omega)}. \tag{2.8}$$

(b) If $g \in C(\Omega)$*, then* $u \in C^{1,\alpha}(\Omega)$ *with* $\alpha \in (0,1)$ *and*

$$\|\nabla u\|_{C^{0,\alpha}(\Omega_c)} \leq C_3(\sigma)(\|u\|_{C^{0,\alpha}(\Omega_I)} + \|g\|_{C(\Omega_I)}). \tag{2.9}$$

The functions $C_1(\sigma)$, $C_2(\sigma)$, $C_3(\sigma)$ *are known bounded functions with respect to* $\|\nabla \ln \sigma\|_{C(\Omega)}$.

Proof. $u \in H^2(\Omega_I) \cap H^1(\Omega)$ and (2.7) are direct consequences of [GT98, Theorem 8.8]. (2.8) can be obtained via the coercivity of the bilinear form and the continuity of the linear form of the variational problem associated with (2.6). Finally, $u \in C^{1,\alpha}(\Omega)$ is obtained by [GT98, Corollary 8.36] and the estimate (2.9) is generated by [GT98, Theorem 8.32] applied to $\Omega_c \subset\subset \Omega_I$. □

Do note, that all strong norms in this chapter, e.g., $\|\cdot\|_{C(\Omega)}$ or $\|\cdot\|_{C^{0,\alpha}(\Omega)}$, are always with respect to the closure of the specified domain.

2.2.2 Inverse problem and properties

For the remainder of this chapter, we assume that the unknown target conductivity $\sigma^\star$ fulfills $\sigma^\star \in \mathcal{P}$ with $\sigma^\star|_{\overline{\Omega}\backslash\Omega_c} = \sigma_b$, where $\sigma_b > 0$ is a known constant, and that the

associated data sets $B^1_{z,\star}$, $B^2_{z,\star}$ are available and fulfill (2.1), i.e.,

$$\nabla^2 B^j_{z,\star} = \mu_0 \left(\frac{\partial \sigma^\star}{\partial x} \frac{\partial u^\star_j}{\partial y} - \frac{\partial \sigma^\star}{\partial y} \frac{\partial u^\star_j}{\partial x} \right), \quad j = 1, 2, \tag{2.10}$$

holds in a pointwise sense inside Ω, where $u^\star_j$ denotes the solutions of (2.2) for $\sigma = \sigma^\star$. The *inverse problem of MREIT* then reads as follows:

$$\text{determine } \sigma^\star \text{ from the knowledge of } B^j_{z,\star},\ j = 1, 2. \tag{2.11}$$

Motivated by (2.1), we formulate the iteration sequence of the *Harmonic B_z Algorithm* with initial guess $\sigma^0 \in \mathcal{P}$.

Procedure 2.2.4 (Iteration sequence)**.** *1. Calculate the vector field*

$$\mathcal{V}^{n+1}(\mathbf{r}) := \begin{cases} \frac{1}{\mu_0} \left[(\sigma^n(\mathbf{r}) \mathbb{A}[\sigma^n](\mathbf{r}))^{-1} \begin{pmatrix} \nabla^2 B^1_{z,\star}(\mathbf{r}) \\ \nabla^2 B^2_{z,\star}(\mathbf{r}) \end{pmatrix} \right], & \mathbf{r} \in \Omega_I, \\ (0,0)^t, \quad \mathbf{r} \in \Omega \setminus \Omega_I, \end{cases}$$

in Ω, where $\mathbb{A}[\sigma^n](\mathbf{r}) = \begin{pmatrix} \frac{\partial u^n_1(\mathbf{r})}{\partial y} & -\frac{\partial u^n_1(\mathbf{r})}{\partial x} \\ \frac{\partial u^n_2(\mathbf{r})}{\partial y} & -\frac{\partial u^n_2(\mathbf{r})}{\partial x} \end{pmatrix}$ and u^n_j denotes the solution of the direct problem (2.2) for $\sigma = \sigma^n$.

2. Determine $\ln \sigma^{n+1}$ as the solution of

$$\nabla^2 \ln \sigma^{n+1} = \nabla \cdot \mathcal{V}^{n+1} \quad \text{in } \Omega \qquad \ln \sigma^{n+1} = \ln \sigma^\star \quad \text{on } \partial\Omega. \tag{2.12}$$

3. Define the new iterate $\sigma^{n+1} := \exp(\ln \sigma^{n+1}) > 0$.

Remark 2.2.5. *(i) We will often drop the dependency of $\mathcal{V}$ and $\mathbb{A}$ on $\mathbf{r} \in \Omega$ and understand those quantities in a pointwise sense.*

(ii) Procedure 2.2.4 differs from previous formulations of the Harmonic B_z Algorithm, see, e.g., [SYWK03, OLW+03, LSSW07, LSW10], by determining the new iterate as a solution of (2.12). We believe that there exists a formulation equivalent to (2.12) utilizing a suitable fundamental solution. Since this issue is not relevant for this work, it was not investigated.

(iii) As mentioned in [LSW10, Section 2.2], $\mathbb{A}[\sigma^n]$ is invertible in Ω_I (and Procedure 2.2.4 is well-defined) but does not need to be invertible up to the boundary. Furthermore, $\sigma^\star\,|_{\Omega \setminus \Omega_I} = \sigma_b$ together with (2.10) implies $\nabla^2 B^1_{z,\star} = \nabla^2 B^2_{z,\star} = 0$ in $\Omega \setminus \Omega_I$, such that it is reasonable to define $\mathcal{V}(\mathbf{r}) = 0$ for $\mathbf{r} \in \Omega \setminus \Omega_I$.

(iv) Regarding the uniqueness of the inverse problem (2.11), we refer to [SW11, Section 2.4.2].

(v) Throughout this chapter, the data $B^1_{z,\star}$, $B^2_{z,\star}$ is assumed to be known exactly. Denoising techniques have to be employed as soon as measurement noise is present in $B^1_{z,\star}$, $B^2_{z,\star}$ since the differentiation when obtaining $\nabla^2 B^1_{z,\star}$, $\nabla^2 B^2_{z,\star}$ will be sensitive to noise. We refer to [SYWK03, OLW+03, SW11, SGZ+05, LX11, SJLW11] for various articles that examine the problem of noise in MREIT.

(vi) $\sigma^\star$ is a fixed point of Procedure 2.2.4 in the sense that if $\sigma^n = \sigma^\star$, it is $\mathcal{V}^{n+1} = \nabla \ln \sigma^\star$, $\ln \sigma^{n+1} = \ln \sigma^\star$ and $\sigma^{n+1} = \sigma^\star$. Nonetheless, we want to stress that aside from this relation, $\mathcal{V}^{n+1} = 0$ in $\Omega \setminus \Omega_I$ does not imply that $\nabla \ln \sigma^{n+1} = 0$ in $\Omega \setminus \Omega_I$ as well.

It is the aim of this chapter to extend the existing convergence theory [LSSW07, LSW10], such that an approximative solution of the direct problem (2.2), e.g., a finite element approximation or a reduced basis approximation, can be used in Procedure 2.2.4 as well. To this end, we formulate the following iteration sequence of the *approximative Harmonic B_z Algorithm* with initial guess $\sigma^0 \in \mathcal{P}$.

Procedure 2.2.6 (Approximative iteration sequence)**.** *1. Calculate the approximative vector field*

$$\mathcal{V}_N^{n+1}(\mathbf{r}) := \begin{cases} \frac{1}{\mu_0} \left[(\sigma^n(\mathbf{r}) \mathbb{A}_N[\sigma^n](\mathbf{r}))^{-1} \begin{pmatrix} \nabla^2 B^1_{z,\star}(\mathbf{r}) \\ \nabla^2 B^2_{z,\star}(\mathbf{r}) \end{pmatrix} \right], & \mathbf{r} \in \Omega_I, \\ (0,0)^t, & \mathbf{r} \in \Omega \setminus \Omega_I, \end{cases}$$

in Ω, where $\mathbb{A}_N[\sigma^n](\mathbf{r}) = \begin{pmatrix} \frac{\partial u^n_{1,N}(\mathbf{r})}{\partial y} & -\frac{\partial u^n_{1,N}(\mathbf{r})}{\partial x} \\ \frac{\partial u^n_{2,N}(\mathbf{r})}{\partial y} & -\frac{\partial u^n_{2,N}(\mathbf{r})}{\partial x} \end{pmatrix}$ and $u^n_{j,N}$ denotes the yet-unspecified approximation to u^n_j, the exact solution of (2.2) for $\sigma = \sigma^n$.

2. Determine $\ln \sigma^{n+1}$ as the solution of

$$\nabla^2 \ln \sigma^{n+1} = \nabla \cdot \mathcal{V}_N^{n+1} \quad \text{in } \Omega \qquad \ln \sigma^{n+1} = \ln \sigma^\star \quad \text{on } \partial\Omega. \tag{2.13}$$

3. Define the new iterate $\sigma^{n+1} := \exp(\ln \sigma^{n+1}) > 0$.

Remark 2.2.7. *It is important to note that Procedures 2.2.4 & 2.2.6 produce different sequences of iterates $\{\sigma^1, \sigma^2, \dots\}$. Whenever we refer to u^n_j, the solution of the direct problem (2.2) for $\sigma = \sigma^n$, it is meant with respect to the underlying procedure.*

Since $u^n_{j,N}$ is an approximative solution of (2.2), the well-definedness of Procedure 2.2.6 cannot be obtained as in Remark 2.2.5 and we make the following assumption.

Assumption 2.2.8. *For the remainder of this chapter, we assume that Procedure 2.2.6 is well-defined. Explicitly, we require the matrices $\mathbb{A}_N[\sigma^n]$ to be invertible inside of Ω_I for all $n = 0, 1, 2, \ldots$*

This assumption is reasonable since $\mathbb{A}_N[\sigma^n] = \mathbb{A}[\sigma^n] + (\mathbb{A}_N[\sigma^n] - \mathbb{A}[\sigma^n])$, and as long as the perturbation $\mathbb{A}_N[\sigma^n] - \mathbb{A}[\sigma^n]$ is small (e.g., when $u^n_{j,N}$ is a good approximation), the invertibility of $\mathbb{A}_N[\sigma^n]$ might hold through the respective property of $\mathbb{A}[\sigma^n]$.

With sight on the convergence theory in Section 2.2.3, we investigate the regularity of the iterates and the vector fields defined during Procedures 2.2.4 & 2.2.6.

Theorem 2.2.9. *(a) The iterates σ^{n+1} defined by Procedure 2.2.4 with initial guess $\sigma^0 \in \mathcal{P}$ fulfill $\sigma^{n+1} \in \mathcal{P}$ for $n = 0, 1, 2, \ldots$*

(b) As long as the approximations $u^n_{j,N}$ in Procedure 2.2.6 fulfill $u^n_{j,N} \in C^{1,\alpha}(\Omega_I)$, the iterates σ^{n+1} defined by Procedure 2.2.6 with initial guess $\sigma^0 \in \mathcal{P}$ fulfill $\sigma^{n+1} \in \mathcal{P}$ for $n = 0, 1, 2, \ldots$

Proof.

(a) With $\sigma^\star \in \mathcal{P}$ we can apply Lemma 2.2.3 to derive $u_1^\star$, $u_2^\star \in C^{1,\alpha}(\Omega_I)$. Noticing that the product of Hölder-continuous functions is Hölder-continuous, (2.10) yields $\nabla^2 B^1_{z,\star}$, $\nabla^2 B^2_{z,\star} \in C^{0,\alpha}(\Omega_I)$. Repeating the same argument for $\sigma^0 \in \mathcal{P}$ and associated forward solutions and combining it with the fact that for any $v \in C^{0,\alpha}(\Omega_I)$ with $v(\mathbf{r}) \neq 0$, $\forall \mathbf{r} \in \Omega_I$, it is $\frac{1}{v} \in C^{0,\alpha}(\Omega_I)$, we can deduce $\mathcal{V}^1 \in C^{0,\alpha}(\Omega_I)$ (componentwise). Since $\sigma^\star$ is already constant in $\overline{\Omega} \setminus \Omega_c$, it is $\nabla^2 B^1_{z,\star} = \nabla^2 B^1_{z,\star} = 0$ in $\overline{\Omega} \setminus \Omega_c$ and together with $\Omega_c \subset\subset \Omega_I \subset\subset \Omega$ it is actually $\mathcal{V}^1 \in C^{0,\alpha}(\overline{\Omega})$. Since $\ln \sigma^1$ is defined as the solution of (2.12), its regularity is a consequence of the regularity of the right-hand side, and [GT98, Theorem 8.34] yields the desired result. The remaining statement follows via induction.

(b) The proof works analogously: the regularity assumption $u^n_{j,N} \in C^{1,\alpha}(\Omega_I)$ together with Assumption 2.2.8 yields the regularity of the vector field, and the regularity of the iterates of Procedure 2.2.6 follows from [GT98, Theorem 8.34].

□

As a conclusion of this section, we gather properties of the iterates of Procedure 2.2.6 which are interesting on their own and especially useful for the convergence proof in the upcoming section.

Lemma 2.2.10. *Let the approximations in Procedure 2.2.6 fulfill $u^n_{j,N} \in C^{1,\alpha}(\Omega_I)$ such that Theorem 2.2.9 holds.*

(a) There exists a constant $C^\dagger \geq 1$ that does not depend on n, such that

$$\| \ln \sigma^{n+1} - \ln \sigma^\star \|_{C^{1,\alpha}(\Omega_c)} \leq C^\dagger \, \| \mathcal{V}_N^{n+1} - \nabla \ln \sigma^\star \|_{C^{0,\alpha}(\Omega_c)}, \; n = 0, 1, 2, \ldots \quad (2.14)$$

(b) There exists a constant $C^\ddagger \geq 1$ that does not depend on n, such that

$$\|\ln\sigma^{n+1} - \ln\sigma^\star\|_{C^{1,\alpha}(\Omega)} \leq C^\ddagger \|\ln\sigma^{n+1} - \ln\sigma^\star\|_{C^{1,\alpha}(\Omega_c)},\ n = 0, 1, 2, \ldots \quad (2.15)$$

(c) It holds for $n = 0, 1, 2, \ldots$ that given an estimate $\|\ln\sigma^\star - \ln\sigma^n\|_{C^1(\Omega_c)} \leq K\epsilon^{n+1}$, for some $0 < \epsilon < 1$ and $K \geq 1$, there exists a constant $\tilde{K} \geq 1$ that does not depend on n, such that

$$\|\frac{\sigma^\star - \sigma^n}{\sigma^n}\|_{C^1(\Omega_c)} \leq \tilde{K}\epsilon^{n+1}. \quad (2.16)$$

Proof.

(a) It is obvious that $\ln\sigma^{n+1} - \ln\sigma^\star$ solves

$$\begin{aligned} \nabla^2\ln\sigma^{n+1} - \nabla^2\ln\sigma^\star &= \nabla\cdot\left(\mathcal{V}_N^{n+1} - \nabla\ln\sigma^\star\right) \text{ in } \Omega, \\ \ln\sigma^{n+1} - \ln\sigma^\star &= 0 \text{ on } \partial\Omega, \end{aligned}$$

and via [GT98, (8.90)] the estimate

$$\|\ln\sigma^{n+1} - \ln\sigma^\star\|_{C^{1,\alpha}(\Omega_c)} \leq C\|\mathcal{V}_N^{n+1} - \nabla\ln\sigma^\star\|_{C^{0,\alpha}(\Omega)}$$

holds, where C is independent of $\mathcal{V}_N^{n+1}$ and thus n. Since $\sigma^\star$ is constant in $\overline{\Omega}\setminus\Omega_c$, it is $\nabla^2 B^1_{z,\star} = \nabla^2 B^2_{z,\star} = 0$ and thus $\mathcal{V}_N^{n+1} = 0$ in $\overline{\Omega}\setminus\Omega_c$ as well. Together with $C^\dagger := \max\{C, 1\} \geq 1$, it follows

$$\begin{aligned} \|\ln\sigma^{n+1} - \ln\sigma^\star\|_{C^{1,\alpha}(\Omega_c)} &\leq C^\dagger\|\mathcal{V}_N^{n+1} - \nabla\ln\sigma^\star\|_{C^{0,\alpha}(\Omega)} \\ &= C^\dagger\|\mathcal{V}_N^{n+1} - \nabla\ln\sigma^\star\|_{C^{0,\alpha}(\Omega_c)}. \end{aligned}$$

(b) Since $\mathcal{V}_N^{n+1} = 0$ in $\Omega\setminus\Omega_c$, $e^{n+1} := \ln\sigma^{n+1} - \ln\sigma^\star$ fulfills

$$\nabla^2 e^{n+1} = 0 \text{ in } \Omega\setminus\Omega_c, \qquad e^{n+1} = 0 \text{ on } \partial\Omega, \qquad e^{n+1} = e^{n+1} \text{ on } \partial\Omega_c.$$

Utilizing $\|e^{n+1}\|_{C^{1,\alpha}(\Omega)} \leq \|e^{n+1}\|_{C^{1,\alpha}(\Omega_c)} + \|e^{n+1}\|_{C^{1,\alpha}(\Omega\setminus\Omega_c)}$ and applying [GT98, (8.90)] to $\|e^{n+1}\|_{C^{1,\alpha}(\Omega\setminus\Omega_c)}$ yields

$$\|e^{n+1}\|_{C^{1,\alpha}(\Omega)} \leq (1 + \tilde{C})\|e^{n+1}\|_{C^{1,\alpha}(\Omega_c)} =: C^\ddagger\|e^{n+1}\|_{C^{1,\alpha}(\Omega_c)},$$

where $\tilde{C}$ stems from [GT98, (8.90)] and is independent of n, such that $C^\ddagger \geq 1$ is also independent of n.

(c) Regarding $\|\frac{\sigma^\star-\sigma^n}{\sigma^n}\|_{C(\Omega_c)}$, it is

$$\|\ln\sigma^\star - \ln\sigma^n\|_{C(\Omega_c)} \leq \|\ln\sigma^\star - \ln\sigma^n\|_{C^1(\Omega_c)} \leq K\epsilon^{n+1},$$

such that

$$e^{-K\epsilon^{n+1}} \leq \frac{\sigma^\star}{\sigma^n} \leq e^{K\epsilon^{n+1}} \quad \Leftrightarrow \quad e^{-K\epsilon^{n+1}} - 1 \leq \frac{\sigma^\star}{\sigma^n} - 1 \leq e^{K\epsilon^{n+1}} - 1 \quad (2.17)$$

holds pointwise in $\overline{\Omega_c}$. Therefore, it is

$$\|\frac{\sigma^\star - \sigma^n}{\sigma^n}\|_{C(\Omega_c)} \leq \max\{|e^{K\epsilon^{n+1}} - 1|,\, |e^{-K\epsilon^{n+1}} - 1|\}$$

and applying the mean value theorem to $f_1(x) := e^{Kx}$ and $f_2(x) := e^{-Kx}$ yields the existence of ξ_n^+, $\xi_n^- \in (0, \epsilon^{n+1}) \subset (0, \epsilon)$, such that

$$|e^{K\epsilon^{n+1}} - 1| = \epsilon^{n+1} K e^{K\xi_n^+} \quad \text{and} \quad |e^{-K\epsilon^{n+1}} - 1| = \epsilon^{n+1} K e^{-K\xi_n^-}.$$

Since $Ke^{-K\xi_n^-} \leq Ke^{K\xi_n^+} \leq Ke^{K\epsilon}$ for $n = 0, 1, 2, \ldots$, we define $\tilde{K} := Ke^{K\epsilon} \geq 1$ and conclude $\|\frac{\sigma^\star - \sigma^n}{\sigma^n}\|_{C(\Omega_c)} \leq \tilde{K}\epsilon^{n+1}$.
Regarding

$$\|\nabla\left(\frac{\sigma^\star}{\sigma^n} - 1\right)\|_{C(\Omega_c)} = \|\nabla\frac{\sigma^\star}{\sigma^n}\|_{C(\Omega_c)},$$

it is

$$\|\nabla\left(\ln\left(\frac{\sigma^\star}{\sigma^n}\right)\right)\|_{C(\Omega_c)} \leq \|\ln\sigma^\star - \ln\sigma^n\|_{C^1(\Omega_c)} \leq K\epsilon^{n+1},$$

such that

$$-K\epsilon^{n+1} \leq \frac{\sigma^n}{\sigma^\star}\nabla\left(\frac{\sigma^\star}{\sigma^n}\right) \leq K\epsilon^{n+1} \quad \Leftrightarrow \quad -\frac{\sigma^\star}{\sigma^n}K\epsilon^{n+1} \leq \nabla\left(\frac{\sigma^\star}{\sigma^n}\right) \leq \frac{\sigma^\star}{\sigma^n}K\epsilon^{n+1}$$

holds pointwise and componentwise. With (2.17), it is $\|\frac{\sigma^\star}{\sigma^n}\|_{C(\Omega_c)} \leq e^{K\epsilon^{n+1}}$ and we conclude

$$\|\nabla\left(\frac{\sigma^\star}{\sigma^n}\right)\|_{C(\Omega_c)} \leq e^{K\epsilon^{n+1}} K\epsilon^{n+1} \leq \tilde{K}\epsilon^{n+1}$$

and the statement follows.

□

Obviously, due to the first part of Theorem 2.2.9, the results of Lemma 2.2.10 can be obtained for the iterates of Procedure 2.2.4 as well.

2.2.3 Convergence of the approximative Harmonic B_z Algorithm

We gather supplementary results for the convergence theorem in the following lemma.

Lemma 2.2.11. *(a) For a $C^{1,\alpha}$-domain $\Omega \subset \mathbb{R}^2$ and a_1, a_2, a_3, $a_4 \in C^{0,\alpha}(\overline{\Omega})$*

$$\|\begin{pmatrix} a_1 & a_2 \\ a_3 & a_4 \end{pmatrix}\|_{C^{0,\alpha}(\Omega)} := 2 \max_{i=1,2,3,4}\left\{\|a_i\|_{C^{0,\alpha}(\Omega)}\right\}$$

is a submultiplicative matrix norm that is consistent with the vector norm

$$\| \begin{pmatrix} a_1 \\ a_2 \end{pmatrix} \|_{C^{0,\alpha}(\Omega)} := \max \left\{ \|a_1\|_{C^{0,\alpha}(\Omega)}, \|a_2\|_{C^{0,\alpha}(\Omega)} \right\}.$$

(b) There exists a constant $C_{\mathbb{A}} > 0$ such that $\|\mathbb{A}[\sigma^\star]^{-1}\|_{C^{0,\alpha}(\Omega_c)} \leq C_{\mathbb{A}}$.

Proof.

(a) The statement follows from standard arguments in matrix and vector norm theory such that we omit the proof.

(b) As mentioned in the proof of Theorem 2.2.9 it is $u_1^\star$, $u_2^\star \in C^{1,\alpha}(\Omega)$ and with the notation $\begin{pmatrix} a_1 & a_2 \\ a_3 & a_4 \end{pmatrix} := \mathbb{A}[\sigma^\star]$, it is

$$\begin{aligned} \|\mathbb{A}[\sigma^\star]^{-1}\|_{C^{0,\alpha}(\Omega_c)} &\leq 2 \|\frac{1}{\det \mathbb{A}[\sigma^\star]}\|_{C(\Omega_c)} \max_{i=1,2,3,4} \left\{ \|a_i\|_{C^{0,\alpha}(\Omega_c)} \right\} \\ &= 2 \|\frac{1}{\det \mathbb{A}[\sigma^\star]}\|_{C(\Omega_c)} \max_{j=1,2} \|\nabla u_j^\star\|_{C^{0,\alpha}(\Omega_c)}, \end{aligned}$$

where $\max_{j=1,2} \|\nabla u_j^\star\|_{C^{0,\alpha}(\Omega_c)}$ is finite. Furthermore, [LSW10, Proposition 2.1] which is based on [AR04, Proposition 2.10] yields the existence of a constant $\underline{\sigma}^\star > 0$ such that $\|\frac{1}{\det \mathbb{A}[\sigma^\star]}\|_{C(\Omega_c)} \leq \frac{1}{\underline{\sigma}^\star}$. Therefore, we obtain the result

$$\|\mathbb{A}[\sigma^\star]^{-1}\|_{C^{0,\alpha}(\Omega_c)} \leq \frac{2}{\underline{\sigma}^\star} \max_{j=1,2} \|\nabla u_j^\star\|_{C^{0,\alpha}(\Omega_c)} =: C_{\mathbb{A}}. \tag{2.18}$$

□

In the following, we present the main result of this chapter - the convergence result for Procedures 2.2.4 & 2.2.6. Do note, that this result is inspired by [LSW10, Theorem 3.2].

Theorem 2.2.12. *Let $\sigma^\star \in \mathcal{P} = \{\sigma \in C^{1,\alpha}(\overline{\Omega}) \mid \sigma(x) > 0,\, x \in \overline{\Omega}\}$ with $\sigma^\star|_{\overline{\Omega}\setminus\Omega_c} = \sigma_b$, σ_b a known constant, and recall that $C^\dagger$ was introduced in Lemma 2.2.10.*

(a) Considering Procedure 2.2.4, we obtain the following convergence result. There exists an $\epsilon > 0$, such that if $\|\nabla \ln \sigma^\star\|_{C^{0,\alpha}(\Omega)} < \epsilon$, the resulting sequence of iterates σ^n, $n = 1, 2, \ldots$, with initial guess $\sigma^0 = \sigma_b$, satisfies

$$\|\ln \sigma^n - \ln \sigma^\star\|_{C^{1,\alpha}(\Omega_c)} \leq C^\dagger \left(\frac{1}{2}\right)^n \epsilon, \quad n = 1, 2, \ldots$$

(b) Considering Procedure 2.2.6, we obtain the following convergence result. There exists an $\epsilon > 0$, such that if $\|\nabla \ln \sigma^\star\|_{C^{0,\alpha}(\Omega)} < \epsilon$ and the approximations $u_{j,N}^n$ fulfill

(i) $u_{j,N}^n \in C^{1,\alpha}(\Omega_I)$ *(regularity condition)*

(ii) $\|\nabla u_{j,N}^n - \nabla u_j^n\|_{C^{0,\alpha}(\Omega_c)} \leq \frac{\epsilon^{n+1}}{2C_{\mathbb{A}}}$ *(quality condition)*

throughout Procedure 2.2.6, the resulting sequence of iterates σ^n, $n = 1, 2, \ldots$, *with initial guess* $\sigma^0 = \sigma_b$, *satisfies*

$$\|\ln \sigma^n - \ln \sigma^\star\|_{C^{1,\alpha}(\Omega_c)} \leq C^\dagger \left(\frac{1}{2}\right)^n \epsilon, \quad n = 1, 2, \ldots$$

Proof.

(a) The exact forward solutions u_j^n utilized in Procedure 2.2.4 fulfill both requirements of the second part of this theorem (the regularity stems from Lemma 2.2.3 and the second requirement is trivial). Therefore, the first statement of this theorem is a consequence of the second statement.

(b) We prove by induction: there exists an $\epsilon \in (0, 1)$, such that if $\|\nabla \ln \sigma^\star\|_{C^{0,\alpha}(\Omega)} < \epsilon$ and both the regularity and the quality condition hold, there exists a $\theta < \frac{1}{2}$ depending on ϵ, such that

$$\|\ln \sigma^n - \ln \sigma^\star\|_{C^{1,\alpha}(\Omega_c)} \leq C^\dagger \theta^n \epsilon \leq C^\dagger \left(\frac{1}{2}\right)^n \epsilon$$

holds for $n = 1, 2, \ldots$, where ϵ and θ are fixed after the base case.
Base case ($n = 0$): Let u_j^n and $u_j^\star$ denote the solutions of (2.2) for $\sigma = \sigma^n$ and $\sigma^\star$ respectively, where (2.2) was a special case of (2.6) with $g = 0$, $\Gamma = E_j^+ \cup E_j^-$ and adequately chosen h. Furthermore, we introduce the notation $e^0 := \ln \sigma^0 - \ln \sigma^\star$, $w_j^0 := u_j^0 - u_j^\star$ and $w_{j,N}^0 := u_{j,N}^0 - u_j^\star$, where w_j^0 fulfills

$$\nabla \cdot (\sigma^0 \nabla w_j^0) = -\sigma^0 \nabla e^0 \cdot \nabla u_j^\star \quad \text{in } \Omega \tag{2.19a}$$

$$w_j^0|_{E_j^+} = 0, \quad w_j^0|_{E_j^-} = 0 \tag{2.19b}$$

$$-\sigma^0 \nabla w_j^0 \cdot \mathbf{n} = (\sigma^0 - \sigma^\star) \nabla u_j^\star \cdot \mathbf{n} = 0 \quad \text{on } \partial\Omega \backslash \overline{E_j^+ \cup E_j^-} \tag{2.19c}$$

since it is $\sigma^0 = \sigma_b$ and thus $\sigma^0 = \sigma^\star$ on $\partial\Omega$.

To obtain the desired result, we want to utilize (2.14) and derive a suitable estimate for $\|\mathcal{V}_N^1 - \nabla \ln \sigma^\star\|_{C^{0,\alpha}(\Omega_c)}$. According to Procedure 2.2.6, it is

$$\sigma^0 \mathbb{A}_N[\sigma^0] \mathcal{V}_N^1 = \frac{1}{\mu_0} \begin{pmatrix} \nabla^2 B_{z,\star}^1 \\ \nabla^2 B_{z,\star}^2 \end{pmatrix}$$

in Ω_c. Introducing the notation $W_N^0 := \mathbb{A}_N[\sigma^0] - \mathbb{A}[\sigma^\star]$ the above relation can be written as

$$(\sigma^0 I + \sigma^0 \mathbb{A}[\sigma^\star]^{-1} W_N^0) \mathcal{V}_N^1 = \frac{1}{\mu_0} \mathbb{A}[\sigma^\star]^{-1} \begin{pmatrix} \nabla^2 B_{z,\star}^1 \\ \nabla^2 B_{z,\star}^2 \end{pmatrix} = \nabla \sigma^\star,$$

where $I \in \mathbb{R}^{2\times 2}$ is the identity matrix and the last equality was explained (for the logarithmic formulation of Procedure 2.2.6) in Remark 2.2.5. Subtracting $(\sigma^0 I + \sigma^0 \mathbb{A}[\sigma^\star]^{-1} W_N^0)\nabla \ln \sigma^\star$ on both sides and dividing by σ^0 yields

$$(I + \mathbb{A}[\sigma^\star]^{-1} W_N^0)(\mathcal{V}_N^1 - \nabla \ln \sigma^\star) = \left(\left(\frac{\sigma^\star}{\sigma^0} - 1\right) I - \mathbb{A}[\sigma^\star]^{-1} W_N^0\right) \nabla \ln \sigma^\star. \tag{2.20}$$

In order to derive the invertibility of $I + \mathbb{A}[\sigma^\star]^{-1} W_N^0$ and also gain an upper bound on the matrix norm of its inverse via the Neumann series, we calculate

$$\begin{aligned}
\|\mathbb{A}[\sigma^\star]^{-1} W_N^0\|_{C^{0,\alpha}(\Omega_c)} &\leq 2\|\mathbb{A}[\sigma^\star]^{-1}\|_{C^{0,\alpha}(\Omega_c)} \max_{j=1,2} \|\nabla w_{j,N}^0\|_{C^{0,\alpha}(\Omega_c)} \\
&\leq \underbrace{2\|\mathbb{A}[\sigma^\star]^{-1}\|_{C^{0,\alpha}(\Omega_c)} \max_{j=1,2} \|\nabla w_j^0\|_{C^{0,\alpha}(\Omega_c)}}_{(*)} \\
&\quad + \underbrace{2\|\mathbb{A}[\sigma^\star]^{-1}\|_{C^{0,\alpha}(\Omega_c)} \max_{j=1,2} \|\nabla u_{j,N}^0 - \nabla u_j^0\|_{C^{0,\alpha}(\Omega_c)}}_{(**)}.
\end{aligned}$$

Defining $\hat{C} := \max\{C^\dagger, C^\ddagger\} \geq 1$, where $C^\dagger$ and $C^\ddagger$ have been introduced in Lemma 2.2.10, we make the initial choice of $\epsilon \in (0, \frac{1}{\hat{C}^2+1}) \subset\subset (0,1)$.

Regarding $(**)$, we combine the quality condition $\|\nabla u_{j,N}^0 - \nabla u_j^0\|_{C^{0,\alpha}(\Omega_c)} \leq \frac{\epsilon}{2C_{\mathbb{A}}}$ with (2.18) to obtain

$$2\|\mathbb{A}[\sigma^\star]^{-1}\|_{C^{0,\alpha}(\Omega_c)} \max_{j=1,2} \|\nabla u_{j,N}^0 - \nabla u_j^0\|_{C^{0,\alpha}(\Omega_c)} \leq 2C_{\mathbb{A}} \frac{\epsilon}{2C_{\mathbb{A}}} = \epsilon. \tag{2.21}$$

Regarding $(*)$, we want to derive an upper bound for $\|\nabla w_j^0\|_{C^{0,\alpha}(\Omega_c)}$ containing ϵ. Since w_j^0 is a solution of (2.19) which is covered by (2.6) with right-hand side $g = \nabla e^0 \cdot \nabla u_j^\star \in L^2(\Omega)$ (it is $u_j^\star \in H^1(\Omega)$ and $e^0 \in C^{1,\alpha}(\overline{\Omega})$), using (2.7) and (2.8) yields

$$\begin{aligned}
\|w_j^0\|_{H^2(\Omega_I)} &\leq C_1(\sigma^0)\left(\|\nabla e^0 \cdot \nabla u_j^\star\|_{L^2(\Omega)} + \|w_j^0\|_{H^1(\Omega)}\right) \\
&\leq C_1(\sigma^0)(1 + C_2(\sigma^0))\|\nabla e^0 \cdot \nabla u_j^\star\|_{L^2(\Omega)} \\
&\leq C_1(\sigma^0)(1 + C_2(\sigma^0))\|\nabla e^0\|_{C(\Omega)}\|u_j^\star\|_{H^1(\Omega)}.
\end{aligned}$$

The Sobolev embedding theorem [AF03, Theorem 4.12] yields the estimate $\|w_j^0\|_{C^{0,\alpha}(\Omega_I)} \leq C_s\|w_j^0\|_{H^2(\Omega_I)}$ with the embedding constant C_s, and together with (2.9) we obtain

$$\begin{aligned}
&\|\nabla w_j^0\|_{C^{0,\alpha}(\Omega_c)} \leq C_3(\sigma^0)[\|w_j^0\|_{C^{0,\alpha}(\Omega_I)} + \|\nabla e^0 \cdot \nabla u_j^\star\|_{C(\Omega_I)}] \\
&\leq C_3(\sigma^0)[C_s\|u_j^\star\|_{H^1(\Omega)} C_1(\sigma^0)(1 + C_2(\sigma^0)) + \|\nabla u_j^\star\|_{C^{0,\alpha}(\Omega_I)}]\|\nabla e^0\|_{C(\Omega)}.
\end{aligned}$$

Note that (2.9) is applicable here since $e^0 \in C^{1,\alpha}(\overline{\Omega})$ combined with $u_1^\star$, $u_2^\star \in C^{1,\alpha}(\Omega)$ yields $\nabla e^0 \cdot \nabla u_j^\star \in C(\Omega)$. At the same time, $\|u_j^\star\|_{H^1(\Omega)}$ and $\|\nabla u_j^\star\|_{C^{0,\alpha}(\Omega_I)}$ are finite, and we denote by

$$\tilde{G}(\sigma) := C_3(\sigma)[C_s\|u_j^\star\|_{H^1(\Omega)} C_1(\sigma)(1 + C_2(\sigma)) + \|\nabla u_j^\star\|_{C^{0,\alpha}(\Omega_I)}]$$

a (due to Lemma 2.2.3) known function that only depends on $\|\nabla \ln \sigma\|_{C(\Omega)}$. The expression

$$\sup_{\|\nabla \ln \sigma - \nabla \ln \sigma^\star\|_{C(\Omega)} \leq C^\dagger C^\ddagger \epsilon} \tilde{G}(\sigma)$$

is well-defined since $\|\nabla \ln \sigma - \nabla \ln \sigma^\star\|_{C(\Omega)} \leq C^\dagger C^\ddagger \epsilon$ implies the boundedness of $\|\nabla \ln \sigma\|_{C(\Omega)}$ via

$$\|\nabla \ln \sigma\|_{C(\Omega)} \leq \|\nabla \ln \sigma^\star\|_{C(\Omega)} + \|\nabla \ln \sigma - \nabla \ln \sigma^\star\|_{C(\Omega)} \leq (1 + C^\dagger C^\ddagger)\epsilon \leq 1,$$

where the last inequality stems from the initial choice of $\epsilon \in (0, \frac{1}{\hat{C}^2+1})$. Therefore, we define

$$\bar{G} := \sup_{\|\nabla \ln \sigma - \nabla \ln \sigma^\star\|_{C(\Omega)} \leq 1} \tilde{G}(\sigma),$$

and remembering $\|\nabla \ln \sigma^\star\|_{C^{0,\alpha}(\Omega)} < \epsilon$ it is

$$\|\nabla e^0\|_{C(\Omega)} \leq \|\nabla \ln \sigma^\star\|_{C^{0,\alpha}(\Omega)} < \epsilon \leq C^\dagger C^\ddagger \epsilon$$

since $C^\dagger$, $C^\ddagger \geq 1$, and we assert $\tilde{G}(\sigma^0) \leq \bar{G}$. With the definition of $\hat{C}$, the above result yields the estimate

$$\|\nabla w_j^0\|_{C^{0,\alpha}(\Omega_c)} \leq \tilde{G}(\sigma^0) \|\nabla e^0\|_{C(\Omega)} \leq \bar{G}\hat{C}^2\epsilon \tag{2.22}$$

and together with (2.18), we obtain

$$(*) = 2\|\mathbb{A}[\sigma^\star]^{-1}\|_{C^{0,\alpha}(\Omega_c)} \max_{j=1,2} \|\nabla w_j^0\|_{C^{0,\alpha}(\Omega_c)} \leq 2C_{\mathbb{A}}\bar{G}\hat{C}^2\epsilon. \tag{2.23}$$

We refine the initial choice of $\epsilon \in (0, \frac{1}{\hat{C}^2+1})$ and take ϵ small enough such that (with sight on (2.21)) $\max\{2C_{\mathbb{A}}\bar{G}\hat{C}^2\epsilon, \epsilon\} < \frac{1}{4}$. In total, it is

$$\|\mathbb{A}[\sigma^\star]^{-1} W_N^0\|_{C^{0,\alpha}(\Omega_c)} < \frac{1}{2}$$

and the Neumann series for $I + \mathbb{A}[\sigma^\star]^{-1}W_N^0$ is applicable. As a consequence, we obtain the following estimate which is based on (2.20), (2.21) as well as (2.23)

$$\begin{aligned}\|\mathcal{V}_N^1 - \nabla \ln \sigma^\star\|_{C^{0,\alpha}(\Omega_c)} \\ \leq 2\left(2\|\frac{\sigma^\star - \sigma^0}{\sigma^0}\|_{C^{0,\alpha}(\Omega_c)} + (2C_{\mathbb{A}}\bar{G}\hat{C}^2 + 1)\epsilon\right) \|\nabla \ln \sigma^\star\|_{C^{0,\alpha}(\Omega_c)}.\end{aligned}$$

Using $\sigma^0 = \sigma_b$, we calculate

$$\|e^0\|_{C(\Omega_c)} \leq \operatorname{diam}(\Omega_c) \|\nabla e^0\|_{C(\Omega_c)} = \operatorname{diam}(\Omega_c) \|\nabla \ln \sigma^\star\|_{C(\Omega_c)} \leq \operatorname{diam}(\Omega_c)\epsilon,$$

such that $\|e^0\|_{C^1(\Omega_c)} \leq (1+\operatorname{diam}(\Omega_c))\epsilon$ and (2.16) is applicable. Together with (2.14) and $\|\nabla \ln \sigma^\star\|_{C^{0,\alpha}(\Omega)} < \epsilon$, we obtain

$$\begin{aligned}\|\ln\sigma^1 - \ln\sigma^\star\|_{C^{1,\alpha}(\Omega_c)} &\leq C^\dagger \|\mathcal{V}_N^1 - \nabla \ln\sigma^\star\|_{C^{0,\alpha}(\Omega_c)} \\ &\leq C^\dagger 2\left(2\tilde{K} + 2C_{\mathbb{A}}\bar{G}\hat{C}^2 + 1\right)\epsilon^2,\end{aligned}$$

with $\tilde{K} \geq 1$ from (2.16). So far, $\epsilon \in (0, \frac{1}{\hat{C}^2+1})$ fulfills $\max\{2C_{\mathbb{A}}\bar{G}\hat{C}^2\epsilon,\, \epsilon\} < \frac{1}{4}$. We finalize our choice of ϵ and choose it small enough such that

$$\theta := 2\left(2\tilde{K} + 2C_{\mathbb{A}}\bar{G}\hat{C}^2 + 1\right)\epsilon < \frac{1}{2}$$

and obtain

$$\|\ln\sigma^1 - \ln\sigma^\star\|_{C^{1,\alpha}(\Omega_c)} \leq C^\dagger\theta\epsilon < C^\dagger\left(\frac{1}{2}\right)\epsilon.$$

Induction step ($n \to n+1$): Let us assume that

$$\|\ln\sigma^k - \ln\sigma^\star\|_{C^{1,\alpha}(\Omega_c)} \leq C^\dagger\theta^k\epsilon < C^\dagger\left(\frac{1}{2}\right)^k\epsilon$$

holds for $k = n$ and we want to verify the statement for $k = n+1$. We introduce the notation $e^n := \ln\sigma^n - \ln\sigma^\star$ and the above induction hypothesis reads

$$\|e^n\|_{C^{1,\alpha}(\Omega_c)} \leq C^\dagger\theta^n\epsilon = C^\dagger 2^n\left(2\tilde{K} + 2C_{\mathbb{A}}\bar{G}\hat{C}^2 + 1\right)^n\epsilon^{n+1}. \tag{2.24}$$

Correspondingly, we introduce the notation $w_j^n = u_j^n - u_j^\star$ as well as $w_{j,N}^n = u_{j,N}^n - u_j^\star$ and since $\sigma^n = \sigma^\star$ on $\partial\Omega$ due to (2.13), w_j^n meets

$$\begin{aligned}&\nabla\cdot(\sigma^n\nabla w_j^n) = -\sigma^n\nabla e^n\cdot\nabla u_j^\star \quad \text{in } \Omega \\ &w_j^n|_{E_j^+} = 0, \quad w_j^n|_{E_j^-} = 0 \\ &-\sigma^n\nabla w_j^n\cdot\mathbf{n} = (\sigma^n - \sigma^\star)\nabla u_j^\star\cdot\mathbf{n} = 0 \quad \text{on } \partial\Omega\backslash\overline{E_j^+\cup E_j^-}.\end{aligned}$$

Similar to (2.20), we obtain the equality

$$(I + \mathbb{A}[\sigma^\star]^{-1}W_N^n)(\mathcal{V}_N^{n+1} - \nabla\ln\sigma^\star) = \left(\left(\frac{\sigma^\star}{\sigma^n} - 1\right)I - \mathbb{A}[\sigma^\star]^{-1}W_N^n\right)\nabla\ln\sigma^\star,$$

with $W_N^n := \mathbb{A}_N[\sigma^n] - \mathbb{A}[\sigma^\star]$. As in the base case, we want to apply the Neumann series and therefore calculate

$$\begin{aligned}\|\mathbb{A}[\sigma^\star]^{-1}W_N^n\|_{C^{0,\alpha}(\Omega_c)} &\leq 2\|\mathbb{A}[\sigma^\star]^{-1}\|_{C^{0,\alpha}(\Omega_c)}\max_{j=1,2}\|\nabla w_{j,N}^n\|_{C^{0,\alpha}(\Omega_c)} \\ &\leq \underbrace{2\|\mathbb{A}[\sigma^\star]^{-1}\|_{C^{0,\alpha}(\Omega_c)}\max_{j=1,2}\|\nabla w_j^n\|_{C^{0,\alpha}(\Omega_c)}}_{(\diamond)} \\ &\quad + \underbrace{2\|\mathbb{A}[\sigma^\star]^{-1}\|_{C^{0,\alpha}(\Omega_c)}\max_{j=1,2}\|\nabla u_{j,N}^n - \nabla u_j^n\|_{C^{0,\alpha}(\Omega_c)}}_{(\diamond\diamond)}.\end{aligned}$$

Regarding ($\diamond$), due to the regularity condition $u_{j,N}^n \in C^{1,\alpha}(\Omega_I)$, Theorem 2.2.9 holds and with the regularity of σ^n Lemma 2.2.3 is applicable for w_j^n. Using the respective inequalities, similar to (2.22), we obtain

$$\|\nabla w_j^n\|_{C^{0,\alpha}(\Omega_c)} \leq \tilde{G}(\sigma^n)\,\|\nabla e^n\|_{C(\Omega)},$$

and (2.15) together with (2.24) yields

$$\|\nabla e^n\|_{C(\Omega)} \leq \|e^n\|_{C^{1,\alpha}(\Omega)} \leq C^{\ddagger}\|e^n\|_{C^{1,\alpha}(\Omega_c)} \leq C^{\dagger}C^{\ddagger}\epsilon < 1,$$

which implies $\tilde{G}(\sigma^n) \leq \bar{G}$. In total, we obtain

$$\|\nabla w_j^n\|_{C(\Omega_c)} \leq \bar{G}C^{\ddagger}C^{\dagger}\theta^n\epsilon.$$

Using this, (2.18) as well as $C^{\dagger}$, $C^{\ddagger} \leq \hat{C}$, and remembering the definition of θ, we obtain

$$2\,\|\mathbb{A}[\sigma^\star]^{-1}\|_{C^{0,\alpha}(\Omega_c)} \max_{j=1,2} \|\nabla w_j^n\|_{C^{0,\alpha}(\Omega_c)} \leq 2C_{\mathbb{A}}\bar{G}\hat{C}^2\theta^n\epsilon \leq \theta^{n+1} < \frac{1}{2^{n+1}} \leq \frac{1}{4}.$$

Regarding ($\diamond\diamond$), the quality condition $\|\nabla u_{j,N}^n - \nabla u_j^n\|_{C^{0,\alpha}(\Omega_c)} \leq \frac{\epsilon^{n+1}}{2C_{\mathbb{A}}}$ together with (2.18) yields

$$2\,\|\mathbb{A}[\sigma^\star]^{-1}\|_{C^{0,\alpha}(\Omega_c)} \max_{j=1,2} \|\nabla u_{j,N}^n - \nabla u_j^n\|_{C^{0,\alpha}(\Omega_c)} \leq 2C_{\mathbb{A}}\frac{\epsilon^{n+1}}{2C_{\mathbb{A}}} = \epsilon^{n+1}$$

and we can assert (ϵ is at least smaller than $\frac{1}{4}$)

$$\|\mathbb{A}[\sigma^\star]^{-1}W_N^n\|_{C^{0,\alpha}(\Omega_c)} < \frac{1}{2}.$$

Therefore, the Neumann series is once again applicable, and together with the previous estimates as well as (2.16) and the definition of θ we derive

$$\begin{aligned}
&\|\mathcal{V}_N^{n+1} - \nabla \ln \sigma^\star\|_{C^{0,\alpha}(\Omega_c)} \\
&\leq 2\left(2\tilde{K}\epsilon^{n+1} + 2\,\|\mathbb{A}[\sigma^\star]^{-1}\|_{C^{0,\alpha}(\Omega_c)} \max_{j=1,2} \|\nabla w_{j,N}^n\|_{C^{0,\alpha}(\Omega_c)}\right) \|\nabla \ln \sigma^\star\|_{C^{0,\alpha}(\Omega_c)} \\
&\leq 2\epsilon^{n+1}\left(2\tilde{K} + 2C_{\mathbb{A}}\bar{G}\hat{C}^2 2^n \left(2\tilde{K} + 2C_{\mathbb{A}}\bar{G}\hat{C}^2 + 1\right)^n + 1\right)\epsilon \\
&\leq 2\epsilon^{n+1}2^n\left(2\tilde{K} + 2C_{\mathbb{A}}\bar{G}\hat{C}^2 + 1\right)^{n+1}\epsilon = \theta^{n+1}\epsilon.
\end{aligned}$$

Combining this with (2.14) yields

$$\begin{aligned}
\|\ln \sigma^{n+1} - \ln \sigma^\star\|_{C^{1,\alpha}(\Omega_c)} &\leq C^{\dagger}\,\|\mathcal{V}_N^{n+1} - \nabla \ln \sigma^\star\|_{C^{0,\alpha}(\Omega_c)} \\
&\leq C^{\dagger}\theta^{n+1}\epsilon < C^{\dagger}\left(\frac{1}{2}\right)^{n+1}\epsilon,
\end{aligned}$$

and the statement is correct for $k = n + 1$.

□

Remark 2.2.13. *Theorem 2.2.12 extends [LSW10, Theorem 3.2] in the following ways:*

(i) The first part of Theorem 2.2.12 replicates the statement of [LSW10, Theorem 3.2]. Do note that as mentioned in Remark 2.2.5 there is no direct correlation between either $\mathcal{V}^{n+1}$ *or* $\mathcal{V}_N^{n+1}$ *and* $\nabla \ln \sigma^{n+1}$ *such that* $\mathcal{V}^{n+1} = \mathcal{V}_N^{n+1} = 0$ *in* $\Omega \backslash \Omega_c$ *cannot be abused to generate a result on the iteration error in the background* $\Omega \setminus \Omega_c$.

(ii) The second part of Theorem 2.2.12 ensures actual numerical convergence of the Harmonic B_z *Algorithm. Remembering Remark 2.2.7,* u_j^n *in the quality condition is the solution of* (2.2) *for* $\sigma = \sigma^n$ *with* σ^n *originating from Procedure 2.2.6 such that the quality condition does relate to, for instance, a discretization error. If the approximations* $u_{j,N}^n$ *are, for example, finite element approximations, the regularity condition indicates what type of finite elements should be utilized to obtain a convergent numerical scheme, and the quality condition specifies the required approximation quality i.e., the fineness of the mesh.*

(iii) The required bound on $\|\nabla \ln \sigma^\star\|_{C^{0,\alpha}(\Omega)}$ *together with* $\sigma^\star \in \mathcal{P}$ *translates to the contrast in* $\sigma^\star$ *from the background* σ_b *not being too large. In this sense the initial guess* $\sigma^0 = \sigma_b$ *cannot be too far away from* $\sigma^\star$*, and the convergence result acquired with Theorem 2.2.12 has to be interpreted as a local convergence result.*

(iv) Theorem 2.2.12 can be formulated for a broader class of initial guesses, possessing the properties necessary for the proof. Since the known background σ_b *is indeed the natural choice here (and fulfills the requirements), we did formulate the result with* $\sigma^0 = \sigma_b$.

2.3 Reduced basis methods for MREIT

Throughout Section 2.2 an unspecified approximation to the forward solution u_j^σ was used. In this section, we want to choose a specific approximation via the reduced basis method, the model order reduction technique already introduced for discretized problems in Section 1.3.2. Utilizing the reduced basis method, we develop a novel algorithm, where it is the aim to speed up the existing Harmonic B_z Algorithm, and Theorem 2.2.12 will guarantee the convergence of this new method if the respective conditions are met. Finally, a numerical comparison of the novel algorithm and the existing one will be carried out.

2.3.1 The reduced basis method

As introduced in Remark 2.2.2, there are two different forward problems (one for each electrode configuration), to which we want to apply the reduced basis method. Since this short section wants to repeat the basics of the method in the given continuous setting, again referring to [RHP08, Haa17] for a detailed survey, we formulate it for only one of the two forward problems. W.l.o.g. we choose $Y := H^1_{D_1}(\Omega)$ as the solution space in (2.5) and write u or u^σ instead of u_1^σ whenever we refer to (2.5) in this section. Of course, the method can be analogously formulated for the second solution space $H^1_{D_2}(\Omega)$.

The aim of the reduced basis method is the construction of an accurate reduced basis approximation u_N^σ of u^σ, the solution of (2.5), where $u_N^\sigma \in Y_N \subset Y$, with Y_N the reduced basis space being of low dimension. We will discuss our method of constructing Y_N in the upcoming section and assume its existence in this section.

Definition 2.3.1. Given the forward problem (2.5) and a reduced basis space $Y_N \subset Y$, with $\dim Y_N = N$ and basis $\Psi_N := \{\psi_1, \dots, \psi_N\}$, we define the *reduced forward problem*: for $\sigma \in \mathcal{P}$ find $u_N^\sigma \in Y_N$, the solution of

$$b(u_N, v; \sigma) = f(v) \quad \text{for all} \quad v \in Y_N. \tag{2.25}$$

We call u_N^σ the *reduced basis approximation* and will often write u_N instead.

Since (2.25) is simply the Galerkin projection of (2.5) onto Y_N, a closed subspace of Y, existence and uniqueness of a solution of (2.25) follow from the properties of (2.5).

To give a better impression of (2.25) and insight into its numerical implementation, we define the *discrete reduced forward problem*.

Proposition 2.3.2. *For a given reduced forward problem* (2.25) *and* $\sigma \in \mathcal{P}$*, we define*

$$\mathbf{B}_N(\sigma) := (b(\psi_j, \psi_i; \sigma))_{i,j=1}^N \in \mathbb{R}^{N\times N}, \quad \mathbf{f}_N := (f(\psi_i))_{i=1}^N \in \mathbb{R}^N.$$

Solving the linear system

$$\mathbf{B}_N(\sigma)\mathbf{u}_N^\sigma = \mathbf{f}_N \tag{2.26}$$

for $\mathbf{u}_N^\sigma = (u_{N,i})_{i=1}^N \in \mathbb{R}^N$*, we can obtain the solution of* (2.25) *via* $u_N^\sigma = \sum_{i=1}^N u_{N,i}\psi_i$.

Regarding the stability of (2.26), if the reduced basis Ψ_N is orthonormal, it holds $\operatorname{cond}(\mathbf{B}_N(\sigma)) \leq \frac{\gamma(\sigma)}{\alpha(\sigma)}$ independent of N, with $\alpha(\sigma)$ and $\gamma(\sigma)$ being the coercivity and continuity constants of the bilinear form b.

From a numerical viewpoint $\mathbf{B}_N(\sigma)$ will not be sparse, but since N is usually very small, the solution of (2.26) is still very cheap compared to, e.g., the computation of a finite element approximation of the full forward problem (2.5).

We recollect two simple but important properties of the reduced basis method already familiar through the Lemmata 1.3.6 & 1.3.7: the a-posteriori error estimator for the reduced basis error, here measured in the H^1-norm $\|u - u_N\|_{H^1(\Omega)}$, and the reproduction of solutions.

Lemma 2.3.3. *(a) For $\sigma \in \mathcal{P}$ we define the residual $r(\cdot;\sigma) \in Y'$ via $r(v;\sigma) := f(v) - b(u_N, v; \sigma)$, $v \in Y$ and let $v_r \in Y$ denote the Riesz-representative of $r(\cdot;\sigma)$, i.e.,*

$$\langle v_r, v\rangle_{H^1(\Omega)} = r(v;\sigma),\ v \in Y, \quad \|v_r\|_{H^1(\Omega)} = \|r(\cdot;\sigma)\|_{Y'}.$$

Then, the error $u - u_N \in Y$ is bounded for all $\sigma \in \mathcal{P}$ by

$$\|u - u_N\|_{H^1(\Omega)} \leq \Delta_N(\sigma) := \frac{\|v_r\|_{H^1(\Omega)}}{\alpha(\sigma)}.$$

(b) For $\sigma \in \mathcal{P}$, let u, u_N be solutions of (2.5) and (2.25) and $\mathbf{e}_i \in \mathbb{R}^N$ the i-th unit vector. Then the following hold:

(i) If $u \in Y_N$ then $u_N = u$.

(ii) If $u = \psi_i \in \Psi_N$, then $\mathbf{u}_N = \mathbf{e}_i \in \mathbb{R}^N$ in Proposition 2.3.2.

Proof.

(a) See, e.g., [RHP08] or [Haa17, Propositions 2.20 & 2.24].

(b) Immediately follows from (2.5) and (2.25), see, e.g., [Haa17, Proposition 2.21].

□

We want to close this reminiscent section by commenting on the reduced basis method in a numerical setting where a fully discretized forward problem (including a finite dimensional parameter space) is given instead of (2.5).

Remark 2.3.4. *(i) The discrete forward solution takes over the role of u in this setting and the reduced basis solution approximates this discrete forward solution. As a consequence, the reduced basis error does not incorporate the approximation error that is made by the discrete forward problem and the error estimator does not include this error. This is a usual occurrence in reduced basis methods and it is assumed that the discrete forward problem is chosen well enough such that its approximation error is negligible.*

(ii) Given a discretized forward problem, the method (including the error estimator) can efficiently be implemented utilizing an offline/online decomposition, see, e.g., [RHP08, Section 7.1.3], [Haa17, Section 2.3.5] or Section 1.3.2, such that the reduced basis approximation and the error estimator can be rapidly computed and a considerable speed-up is achieved.

2.3.2 The Reduced Basis Harmonic B_z Algorithm (RBZ-Algorithm)

Let us combine Procedure 2.2.4 with a suitable termination criterion as a starting point for the development of our new method. Motivated by the fixed point discussion in Remark 2.2.5 and the convergence result in Theorem 2.2.12, we choose the logarithmic iteration error as termination criterion and formulate the following *Harmonic B_z Algorithm.*

Algorithm 4 Harmonic B_z Algorithm$(\sigma^0 = \sigma_b, \mu_0, \varepsilon, \nabla^2 B^1_{z,\star}, \nabla^2 B^2_{z,\star})$

1: $n = 0$
2: **repeat**
3: For all $\mathbf{r} \in \Omega$, calculate the vector field

$$\mathcal{V}^{n+1}(\mathbf{r}) := \begin{cases} \frac{1}{\mu_0}\left[(\sigma^n(\mathbf{r})\mathbb{A}[\sigma^n](\mathbf{r}))^{-1}\begin{pmatrix} \nabla^2 B^1_{z,\star}(\mathbf{r}) \\ \nabla^2 B^2_{z,\star}(\mathbf{r}) \end{pmatrix}\right], & \mathbf{r} \in \Omega_I, \\ (0,0)^t, & \mathbf{r} \in \Omega \setminus \Omega_I. \end{cases}$$

4: Calculate $\ln \sigma^{n+1}$ as the solution of (2.12).
5: $\sigma^{n+1} := \exp(\ln \sigma^{n+1})$
6: $n = n + 1$
7: **until** $\| \ln \sigma^n - \ln \sigma^{n-1} \|_{C(\Omega)} < \varepsilon$
8: **return** $\sigma_{BZ} = \sigma^n$

Remark 2.3.5. *(i) If $\sigma^\star$ fulfills the requirements of Theorem 2.2.12, Algorithm 4 terminates. As mentioned at the end of Section 2.2.2, Lemma 2.2.10 holds for Procedure 2.2.4 as well. Applying the triangle inequality and* (2.15) *yields*

$$\begin{aligned} \| \ln \sigma^n - \ln \sigma^{n-1} \|_{C(\Omega)} &\leq \| \ln \sigma^n - \ln \sigma^{n-1} \|_{C^{1,\alpha}(\Omega)} \\ &\leq \| \ln \sigma^n - \ln \sigma^\star \|_{C^{1,\alpha}(\Omega)} + \| \ln \sigma^{n-1} - \ln \sigma^\star \|_{C^{1,\alpha}(\Omega)} \\ &\leq C^\ddagger \left(\| \ln \sigma^n - \ln \sigma^\star \|_{C^{1,\alpha}(\Omega_c)} + \| \ln \sigma^{n-1} - \ln \sigma^\star \|_{C^{1,\alpha}(\Omega_c)} \right) \end{aligned}$$

and it follows from Theorem 2.2.12 that the last expression goes to zero as n goes to infinity. Therefore, the chosen termination criterion is reasonable although, keeping the convergence result of Theorem 2.2.12 in mind, simply running a fixed amount of repeat-loop iterations would also yield decent results.

(ii) Alternatively, an efficiently computable error estimator for $\| \ln \sigma^n - \ln \sigma^\star \|_{C^{1,\alpha}(\Omega)}$ could be used as termination criterion, see [LSW10, Theorem 2.1] for a first result in that direction.

It is our intention to develop a faster version of Algorithm 4 involving the reduced basis method presented in Section 2.3.1, where the reconstruction with the new

algorithm should retain its quality compared to Algorithm 4. Using a qualitative and cheap approximative forward solution in order to speed up the whole algorithm is intuitive, since the computationally expensive part of each iteration of Algorithm 4 is the computation of the two solutions of (2.5) (one per electrode configuration) involved in the matrix $\mathbb{A}[\sigma^n]$. One way to apply the reduced basis method would be the direct approach introduced in Section 1.4.2:

1. For each forward problem (2.5) construct a global reduced basis space, e.g., via Algorithm 2, where it is the aim of a global reduced basis space to provide accurate approximations for every parameter in the parameter domain (the desired accuracy is given by the quality condition in Theorem 2.2.12).
2. In each step of Algorithm 4, replace the forward solutions of (2.5) by the corresponding reduced basis approximations.

The offline/online decomposition mentioned in Remark 2.3.4 would guarantee the desired speed-up and as long as the quality condition in Theorem 2.2.12 is fulfilled the convergence would also be guaranteed since snapshot-based reduced basis spaces inherit the regularity from the snapshots.

In the imaging context of this chapter however, we want to recover high-resolution images of the unknown conductivity, such that a potential discrete parameter domain in a numerical setting would be very high-dimensional and as already discussed in Section 1.4.2 a global reduced basis space is out of reach for our imaging purpose.

To overcome this issue of dimensionality and to be able to tackle parameter spaces of arbitrary dimension, we proposed an adaptive reduced basis approach which aims at constructing a *locally approximating* reduced basis space. We outlined this local approach, which was based on ideas developed in [DZ07, CMW14, Las14, ZF15], for the nonlinear Landweber method in Section 1.4.3. The key idea was to simultaneously solve the inverse problem as well as adaptively enrich and therefore construct the reduced basis space. Adapting the approach to the posed inverse problem of MREIT yields the following steps.

Procedure 2.3.6 (Adaptive approach for MREIT)**.** *1. Start with two given possibly empty reduced basis spaces $Y_{N,1} = \operatorname{span}\{\Psi_{N,1}\}$ and $Y_{N,2} = \operatorname{span}\{\Psi_{N,2}\}$ (one per forward problem).*

2. Utilize the current iterate to generate snapshots for the enrichment of $Y_{N,1}$ and $Y_{N,2}$. At the beginning use σ^0.

3. Project the reconstruction algorithm on this set of reduced basis spaces. In our case this leads to Procedure 2.2.6 where $u^n_{1,N}$ and $u^n_{2,N}$ are the reduced basis approximations introduced in Definition 2.3.1 for $Y_{N,1}$ and $Y_{N,2}$ respectively.

4. Run this projected algorithm until either the current iterate is accepted as a solution to the inverse problem ($\rightsquigarrow$ termination) or the approximation quality of the reduced spaces is no longer trusted ($\rightsquigarrow$ step 2).

Basically, we abuse the ability of our inversion algorithm to find parameter values that approach the exact solution in order to determine *relevant* parameters for which we can include the snapshots into our reduced basis spaces. Based on Procedure 2.3.6, we formulate the following *Reduced Basis Harmonic B_z Algorithm* (RBZ).

Algorithm 5 RBZ($\sigma^0 = \sigma_b, \mu_0, \varepsilon_1, \varepsilon_2, \Psi_{N,1}, \Psi_{N,2}, \nabla^2 B^1_{z,\star}, \nabla^2 B^2_{z,\star}$)

$n = 0$, $Y_{N,1} = \operatorname{span}\{\Psi_{N,1}\}$, $Y_{N,2} = \operatorname{span}\{\Psi_{N,2}\}$
repeat
  $\Psi_{N,1} = \Psi_{N,1} \cup \{u_1^n\}$, $\Psi_{N,2} = \Psi_{N,2} \cup \{u_2^n\}$
  $Y_{N,1} = \operatorname{span}\{\Psi_{N,1}\}$, $Y_{N,2} = \operatorname{span}\{\Psi_{N,2}\}$
  repeat
    For all $\mathbf{r} \in \Omega$, calculate the vector field

$$\mathcal{V}_N^{n+1}(\mathbf{r}) := \begin{cases} \frac{1}{\mu_0}\left[(\sigma^n(\mathbf{r})\mathbb{A}_N[\sigma^n](\mathbf{r}))^{-1}\begin{pmatrix} \nabla^2 B^1_{z,\star}(\mathbf{r}) \\ \nabla^2 B^2_{z,\star}(\mathbf{r}) \end{pmatrix}\right], & \mathbf{r} \in \Omega_I, \\ (0,0)^t, \quad \mathbf{r} \in \Omega \setminus \Omega_I. \end{cases}$$

    Calculate $\ln \sigma^{n+1}$ as the solution of (2.13).
    $\sigma^{n+1} := \exp(\ln \sigma^{n+1})$
    $n = n + 1$
  until $\|\ln \sigma^n - \ln \sigma^{n-1}\|_{C(\Omega)} < \varepsilon_1$ **or** $\max_{j=1,2}\{\|\nabla u^n_{j,N} - \nabla u^n_j\|_{C^{0,\alpha}(\Omega)}\} > \varepsilon_2^{n+1}$
until $\|\ln \sigma^n - \ln \sigma^{n-1}\|_{C(\Omega)} < \varepsilon_1$
return $\sigma_{RBZ} = \sigma^n$

Remark 2.3.7. *(i) The initial reduced bases $\Psi_{N,1}$ and $\Psi_{N,2}$ in Algorithm 5 can be empty since they are directly enriched with the snapshots for the initial guess σ^0. Furthermore, $\Psi_{N,1}$, $\Psi_{N,2}$ are always orthonormalized to ensure numerical stability.*

(ii) If $\sigma^\star$ fulfills the requirements of Theorem 2.2.12, Algorithm 5 terminates by an argument similar to Remark 2.3.5, where ε_1 and ε_2 have to be chosen accordingly.

(iii) The formulation in Algorithm 5 is tailored around the convergence result of Theorem 2.2.12 and is not suitable for a numerical implementation: on the one hand it is difficult to handle the Hölder-norms numerically and on the other hand the criterion $\max_{j=1,2}\{\|\nabla u^n_{j,N} - \nabla u^n_j\|_{C^{0,\alpha}(\Omega_c)}\} > \varepsilon_2^{n+1}$, although ensuring the quality condition of Theorem 2.2.12 if ε_2 is chosen appropriately, is not a reasonable criterion from a reduced basis point of view. In order to check the criterion, one would have to compute the (computationally expensive) exact forward solutions u_j^n, which would defeat the purpose of a model order reduction approach.

(iv) Therefore, we will explain in the upcoming section the simplified version of the

algorithm (utilizing the error estimator introduced in Lemma 2.3.3) that was used for the numerical experiments.

2.3.3 Numerical Experiments

It is our intention to perform a short numerical comparison of Algorithms 4 & 5, including one reconstruction from exact data and one reconstruction from noisy data, where the reconstruction quality as well as the computational time will be compared. It is not our intention to verify the theoretical results from Theorem 2.2.12, such that the numerical setting below does not claim to be consistent with the requirements of the theory developed in Section 2.2.

The to-be-reconstructed conductivity is a piecewise linear approximation of the Shepp-Logan-phantom with 260×260 pixels and 1 added to the grayscale values to ensure coercivity. It is visualized in the top right of Figure 8, where in the top left the initial value $\sigma^0 = \sigma_b = 1$ can be seen. To match the phantom, we choose $\Omega := [-1,1]^2$ and $\Omega_I := \{(x,y) \mid \sqrt{x^2+y^2} < 0.95\} \subset\subset \Omega$ with electrode pairs $E_1^{\pm} := \{(\pm 1, y) \mid |y| < 0.1\}$, $E_2^{\pm} := \{(x, \pm 1) \mid |x| < 0.1\}$. For simplicity, it is $\mu_0 = 1$ and the scaling introduced in Lemma 2.2.1 is not performed. The PDEs (2.5), (2.12), and (2.13) are discretized on a triangular mesh with 135200 elements and piecewise linear finite elements are utilized for all three PDEs. As a result, the data $\nabla^2 B^1_{z,\star}$, $\nabla^2 B^2_{z,\star}$, which is generated synthetically via (2.10) where Comsol® is used for the involved PDE solutions to prevent inverse crime, is piecewise constant on the grid. The noisy data set in this comparison is generated by (trianglewise) adding 10% relative Gaussian noise to $\nabla^2 B^1_{z,\star}$, $\nabla^2 B^2_{z,\star}$ (wherever $\nabla^2 B^1_{z,\star}$ or $\nabla^2 B^2_{z,\star}$ is equal to zero, the average absolute value of $\nabla^2 B^1_{z,\star}$ or $\nabla^2 B^2_{z,\star}$ is taken as the reference value for the Gaussian relative noise). We want to emphasize that although testing the reconstruction algorithms for robustness this circumvents the problem described in Remark 2.2.5 that occurs when differentiating actual noisy B_z data (e.g., real-world measurements). In order to ensure the approximation quality of the reduced basis spaces in Algorithm 5, $\max_{j=1,2}\{\|\nabla u^n_{j,N} - \nabla u^n_j\|_{C^{0,\alpha}(\Omega)}\} > \varepsilon_2^{n+1}$ is replaced by $\max_{j=1,2}\{\Delta_{1,N}(\sigma^n), \Delta_{2,N}(\sigma^n)\} > \varepsilon_2$, where $\Delta_{j,N}(\sigma^n)$ was the rigorous reduced basis error estimator introduced in Lemma 2.3.3 with j indicating the underlying reduced basis space $Y_{N,1}$ or $Y_{N,2}$. This termination criterion is computationally cheap to evaluate and the error estimator in the $H^1(\Omega)$ norm should contain some derivative information. Finally, it is $\varepsilon = \varepsilon_1 = 10^{-6}$ as the acceptance tolerance in Algorithms 4 & 5 and $\varepsilon_2 = 10^{-3}$ for the new termination criterion. The numerical experiment is performed using Matlab® in conjunction with the library RBmatlab which can be found online[1].

As can be seen in Figure 8, all key features of the Shepp-Logan phantom are captured in the reconstructions using exact data via Algorithm 4 (center-left) and Algorithm 5 (center-right) which can visually not be distinguished. This is further reflected

[1] http://www.ians.uni-stuttgart.de/MoRePaS/software/

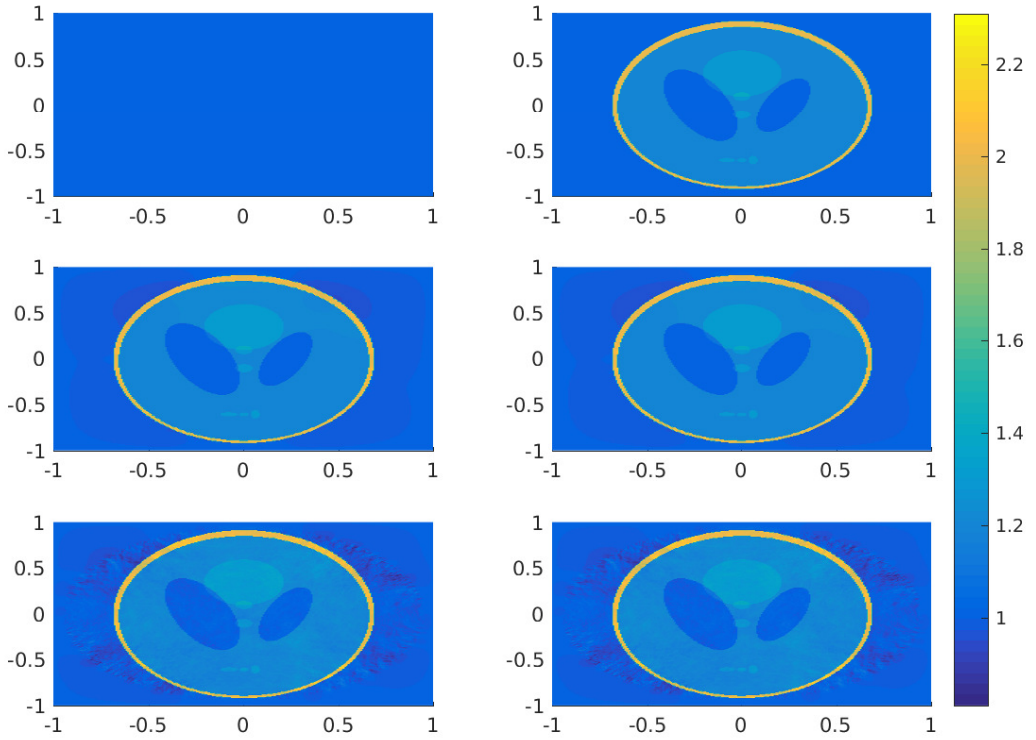

Figure 8: From top left to bottom right: σ^0 the initial guess, $\sigma^\star$ the true conductivity, σ_{BZ} the reconstruction via Algorithm 4, σ_{RBZ} the reconstruction via Algorithm 5, σ^δ_{BZ} the reconstruction from noisy data via Algorithm 4, σ^δ_{RBZ} the reconstruction from noisy data via Algorithm 5.

via

$$\frac{\|\sigma^\star - \sigma_{BZ}\|_{C(\Omega)}}{\|\sigma_{BZ}\|_{C(\Omega)}} \approx 0.092 \quad \text{and} \quad \frac{\|\sigma_{RBZ} - \sigma_{BZ}\|_{C(\Omega)}}{\|\sigma_{BZ}\|_{C(\Omega)}} \approx 5.95 \cdot 10^{-4}$$

such that a high-resolution image of the conductivity can be obtained using either of the two algorithms. Furthermore, it can be seen that the background is not exactly reconstructed, which strengthens the statement made in Remark 2.2.13.

Regarding the computational effort of the algorithms, we note that both required the same amount of 14 iterations (updates of the conductivity), resulting in 28 solutions of (2.5) for Algorithm 4. Algorithm 5 updated its reduced basis spaces 4 times, resulting in only 8 solutions of (2.5). The total computational time was 9.84 seconds for Algorithm 4 and 7.61 seconds for Algorithm 5 resulting in a speed-up of roughly 25%. Do note that both algorithms performing 14 updates of the conductivity have to solve the related PDEs (2.12) and (2.13) 14 times. In our reduced basis approach the PDE (2.13) remains untouched, and one could introduce

a third reduced basis space to include this PDE in the adaptive space enrichment procedure as well. Although this should result in further speed-up, the theoretical foundation via Theorem 2.2.12 would then be lost.

Having a look at σ_{BZ}^{δ} (bottom left of Figure 8) and σ_{RBZ}^{δ} (bottom right of Figure 8), the reconstructions via Algorithms 4 & 5 using the noisy data set, we observe that the key features of the phantom remain intact and note that

$$\frac{\|\sigma^{\star} - \sigma_{BZ}^{\delta}\|_{C(\Omega)}}{\|\sigma_{BZ}^{\delta}\|_{C(\Omega)}} \approx 0.13 \quad \text{and} \quad \frac{\|\sigma_{RBZ}^{\delta} - \sigma_{BZ}^{\delta}\|_{C(\Omega)}}{\|\sigma_{BZ}^{\delta}\|_{C(\Omega)}} \approx 9.12 \cdot 10^{-4}.$$

The computational effort in this noisy scenario and the speed-up obtained were basically the same as in the noiseless case such that we omit the exact numbers.

2.4 Conclusion

The B_z-based Magnetic resonance electrical impedance tomography problem can be solved using the existing Harmonic B_z Algorithm. The convergence theory for the algorithm in the two-dimensional setting was extended to include the case when an approximative forward solution of the underlying partial differential equation is used instead of the exact forward solution. This novel result ensures actual numerical convergence of the algorithm and enables the combination of it with innovative numerical methods. The reduced basis method, a model order reduction technique, was presented and a reduced basis version of the Harmonic B_z Algorithm was developed in order to speed up the algorithm. In a numerical example (including noisy data) a high-resolution image of the Shepp-Logan phantom was reconstructed. Both algorithms achieved a satisfactory approximation quality and the novel Reduced Basis Harmonic B_z Algorithm achieved a speed-up of around 25%.

Bibliography

[AF03] R.A. Adams and J.J.F. Fournier. *Sobolev Spaces*. Pure and Applied Mathematics. Elsevier Science, 2003.

[AGL11] Andy Adler, Romina Gaburro, and William Lionheart. Electrical Impedance Tomography. In *Handbook of Mathematical Methods in Imaging*, pages 599–654. Springer, 2011.

[AR04] Giovanni Alessandrini and Edi Rosset. Volume bounds of inclusions from physical EIT measurements. *Inverse Problems*, 20(2):575–588, 2004.

[BMNP04] Maxime Barrault, Yvon Maday, Ngoc Cuong Nguyen, and Anthony T. Patera. An 'empirical interpolation' method: application to efficient reduced-basis discretization of partial differential equations. *Comptes Rendus Mathematique*, 339(9):667–672, 2004.

[CIN99] Margaret Cheney, David Isaacson, and Jonathan C. Newell. Electrical Impedance Tomography. *SIAM review*, 41(1):85–101, 1999.

[CMW14] Tiangang Cui, Youssef M Marzouk, and Karen E Willcox. Data-driven model reduction for the Bayesian solution of inverse problems. *International Journal for Numerical Methods in Engineering*, 102(5):966–990, 2014.

[DH15] M. A. Dihlmann and B. Haasdonk. Certified PDE-constrained parameter optimization using reduced basis surrogate models for evolution problems. *COAP, Computational Optimization and Applications*, 60(3):753–787, 2015.

[dHQS15] Maarten V. de Hoop, Lingyun Qiu, and Otmar Scherzer. An analysis of a multi-level projected steepest descent iteration for nonlinear inverse problems in Banach spaces subject to stability constraints. *Numerische Mathematik*, 129(1):127–148, 2015.

[DZ07] Vladimir Druskin and Mikhail Zaslavsky. On combining model reduction and Gauss-Newton algorithms for inverse partial differential equation problems. *Inverse Problems*, 23(4):1599–1610, 2007.

[EHN96] Heinz Werner Engl, Martin Hanke, and Andreas Neubauer. *Regularization of inverse problems*, volume 375. Springer Science & Business Media, 1996.

[EPR10] Jens L. Eftang, Anthony T. Patera, and Einar M. Rønquist. An "*hp*"

Certified Reduced Basis Method for Parametrized Elliptic Partial Differential Equations. *SIAM Journal on Scientific Computing*, 32(6):3170–3200, 2010.

[GH18] Dominik Garmatter and Bastian Harrach. Magnetic Resonance Electrical Impedance Tomography (MREIT): Convergence and Reduced Basis Approach. *SIAM Journal on Imaging Sciences*, 11(1):863–887, 2018.

[GHH16] Dominik Garmatter, Bernard Haasdonk, and Bastian Harrach. A Reduced Basis Landweber method for nonlinear inverse problems. *Inverse Problems*, 32(3):035001, 2016.

[GT98] David Gilbarg and Neil S. Trudinger. *Elliptic partial differential equations of second order*. springer, 1998.

[Haa17] Bernard Haasdonk. Reduced Basis Methods for Parametrized PDEs–A Tutorial Introduction for Stationary and Instationary Problems. *Chapter in Model Reduction and Approximation: Theory and Algorithms*, pages 65–136, 2017.

[Had14] Jacques Hadamard. *Lectures on Cauchy's problem in linear partial differential equations*. Courier Corporation, 2014.

[Han97] Martin Hanke. A regularizing Levenberg - Marquardt scheme, with applications to inverse groundwater filtration problems. *Inverse Problems*, 13(1):79–95, 1997.

[Han14] Martin Hanke. A Note on the Nonlinear Landweber Iteration. *Numerical Functional Analysis and Optimization*, 35(11):1500–1510, 2014.

[HDO11] Bernard Haasdonk, Markus Dihlmann, and Mario Ohlberger. A training set and multiple bases generation approach for parameterized model reduction based on adaptive grids in parameter space. *Mathematical and Computer Modelling of Dynamical Systems*, 17(4):423–442, 2011.

[HKL+13] K. C. Hoang, B. C. Khoo, G. R. Liu, Ngoc C. Nguyen, and Anthony T. Patera. Rapid identification of material properties of the interface tissue in dental implant systems using reduced basis method. *Inverse Problems in Science and Engineering*, 21(8):1310–1334, 2013.

[HNS95] Martin Hanke, Andreas Neubauer, and Otmar Scherzer. A convergence analysis of the Landweber iteration for nonlinear ill-posed problems. *Numerische Mathematik*, 72(1):21–37, 1995.

[HSZ14] Jan S. Hesthaven, Benjamin Stamm, and Shun Zhang. Efficient greedy algorithms for high-dimensional parameter spaces with applications to empirical interpolation and reduced basis methods. *ESAIM: Mathematical Modelling and Numerical Analysis*, 48(1):259–283, 2014.

[IK94] K. Ito and K. Kunisch. On the Injectivity and Linearization of the Coefficient-to-Solution Mapping for Elliptic Boundary Value Problems.

Journal of Mathematical Analysis and Applications, 188(3):1040 – 1066, 1994.

[Kno99] Ian Knowles. Uniqueness for an elliptic inverse problem. *SIAM Journal on Applied Mathematics*, 59(4):1356–1370, 1999.

[KNS08] B. Kaltenbacher, A. Neubauer, and O. Scherzer. *Iterative Regularization Methods for Nonlinear Ill-Posed Problems*. Radon Series on Computational and Applied Mathematics. De Gruyter, 2008.

[KPSW06] Ohin Kwon, Hyunchan Pyo, Jin Keun Seo, and Eung Je Woo. Mathematical framework for B_z-based MREIT model in electrical impedance imaging. *Computers & Mathematics with Applications*, 51(5):817–828, 2006.

[KSS09] Barbara Kaltenbacher, Frank Schöpfer, and Thomas Schuster. Iterative methods for nonlinear ill-posed problems in Banach spaces: convergence and applications to parameter identification problems. *Inverse Problems*, 25(6):065003, 2009.

[Las14] Oliver Lass. *Reduced order modeling and parameter identification for coupled nonlinear PDE systems*. PhD thesis, Universität Konstanz, 2014.

[Lio04] William Lionheart. EIT reconstruction algorithms: pitfalls, challenges and recent developments. *Physiological measurement*, 25(1):125–142, 2004.

[LSSW07] Jijun Liu, Jin Keun Seo, Mourad Sini, and Eung Je Woo. On the Convergence of the Harmonic B_z Algorithm in Magnetic Resonance Electrical Impedance Tomography. *SIAM Journal on Applied Mathematics*, 67(5):1259–1282, 2007.

[LSW10] Jijun Liu, Jin Keun Seo, and Eung Je Woo. A Posteriori Error Estimate and Convergence Analysis for Conductivity Image Reconstruction in MREIT. *SIAM Journal of Applied Mathematics*, 70(8):2883–2903, 2010.

[LX11] Jijun Liu and Huilin Xu. Reconstruction of biologic tissue conductivity from noisy magnetic field by integral equation method. *Applied Mathematics and Computation*, 218(6):2647–2660, 2011.

[NGI88] J.C. Newell, David G. Gisser, and David Isaacson. An electric current tomograph. *IEEE Transactions on Biomedical Engineering*, 35(10):828–833, 1988.

[Ngu05] Ngoc C. Nguyen. *Reduced-Basis Approximation and A Posteriori Error Bounds for Nonaffine and Nonlinear Partial Differential Equations: Application to Inverse Analysis*. PhD thesis, Singapore-MIT Alliance, National University of Singapore, 2005.

[NRHP10] Cuong Nguyen, Gianluigi Rozza, D. B. Phuong Huynh, and Anthony T.

Patera. Reduced basis approximation and a posteriori error estimation for parametrized parabolic PDEs; Application to real-time Bayesian parameter estimation. *Large Scale Inverse Problems and Quantification of Uncertainty*, (Chapter 8):151–178, 2010.

[OLW+03] Suk Hoon Oh, Byung Il Lee, Eung Je Woo, Soo Yeol Lee, Min Hyoung Cho, Ohin Kwon, and Jin Keun Seo. Conductivity and current density image reconstruction using harmonic B_z algorithm in magnetic resonance electrical impedance tomography. *Physics in Medicine and Biology*, 48(19):3101–3116, 2003.

[RHP08] Gianluigi Rozza, DBP Huynh, and Anthony T. Patera. Reduced basis approximation and a posteriori error estimation for affinely parametrized elliptic coercive partial differential equations. *Archives of Computational Methods in Engineering*, 15(3):229–275, 2008.

[Ric81] Gerard R. Richter. An Inverse Problem for the Steady State Diffusion Equation. *SIAM Journal on Applied Mathematics*, 41(2):210–221, 1981.

[Rie03] A. Rieder. *Keine Probleme mit Inversen Problemen: Eine Einführung in ihre stabile Lösung*. Vieweg+Teubner Verlag, 2003.

[SAS17] Yizhuang Song, Habib Ammari, and Jin Keun Seo. Fast Magnetic Resonance Electrical Impedance Tomography with Highly Undersampled Data. *SIAM Journal on Imaging Sciences*, 10(2):558–577, 2017.

[Sch98] Otmar Scherzer. An iterative multi level algorithm for solving nonlinear ill-posed problems. *Numerische Mathematik*, 80(4):579–600, 1998.

[SCI92] Erkki Somersalo, Margaret Cheney, and David Isaacson. Existence and Uniqueness for Electrode Models for Electric Current Computed Tomography. *SIAM Journal on Applied Mathematics*, 52(4):1023–1040, 1992.

[SGZ+05] Rosalind Sadleir, Samuel Grant, Sung Uk Zhang, Byung Il Lee, Hyun Chan Pyo, Suk Hoon Oh, Chunjae Park, Eung Je Woo, Soo Yeol Lee, Ohin Kwon, et al. Noise analysis in magnetic resonance electrical impedance tomography at 3 and 11 T field strengths. *Physiological measurement*, 26(5):875–884, 2005.

[SJLW11] Jin Keun Seo, Kiwan Jeon, Chang-Ock Lee, and Eung Je Woo. Non-iterative harmonic B_z algorithm in MREIT. *Inverse Problems*, 27(8):085003, 2011.

[SW11] Jin Keun Seo and Eung Je Woo. Magnetic Resonance Electrical Impedance Tomography (MREIT). *SIAM review*, 53(1):40–68, 2011.

[SYWK03] Jin Keun Seo, Jeong-Rock Yoon, Eung Je Woo, and Ohin Kwon. Reconstruction of conductivity and current density images using only one component of magnetic field measurements. *IEEE Transactions on Biomedical Engineering*, 50(9):1121–1124, 2003.

[Uhl09] Gunther Uhlmann. Electrical impedance tomography and Calderón's problem. *Inverse problems*, 25(12):123011, 2009.

[UVZ14] Karsten Urban, Stefan Volkwein, and Oliver Zeeb. Greedy sampling using nonlinear optimization. In Alfio Quarteroni and Gianluigi Rozza, editors, *Reduced Order Methods for Modeling and Computational Reduction*, volume 9 of *MS&A - Modeling, Simulation and Applications*, pages 137–157. Springer International Publishing, 2014.

[VPRP03] Karen Veroy, Christophe Prud'homme, Dimitrios V. Rovas, and Anthony T. Patera. A Posteriori Error Bounds for Reduced-Basis Approximation of Parametrized Noncoercive and Nonlinear Elliptic Partial Differential Equations. In *Proceedings of the 16th AIAA computational fluid dynamics conference*, volume 3847, pages 2003–3847, 2003.

[WS08] Eung Je Woo and Jin Keun Seo. Magnetic resonance electrical impedance tomography (MREIT) for high-resolution conductivity imaging. *Physiological measurement*, 29(10):R1–R26, 2008.

[ZF15] Matthew J. Zahr and Charbel Farhat. Progressive construction of a parametric reduced-order model for PDE-constrained optimization. *International Journal for Numerical Methods in Engineering*, 102(5):1111–1135, 2015.

Zusammenfassung

Partielle Differentialgleichungen (PDGLn) sind das Mittel der Wahl um die verschiedensten Sachverhalte, welche wir heutzutage in der Physik, der Biologie und anderen Wissenschaften beobachten, mathematisch zu beschreiben. Für gewöhnlich ist der aktuelle Zustand, z.B. anhand von Parametern, bekannt und man möchte eine zugehörige physikalische Größe bestimmen. Obwohl dieses sogenannte *Vorwärtsproblem* für sich gesehen interessant und dessen korrekte Modellierung und numerische Lösung für viele Industrie- und Wirtschaftszweige äußerst relevant ist, beschäftigt sich diese Arbeit mit sogenannten *inversen Problemen für partielle Differentialgleichungen*. Im inversen Kontext ist die physikalische Größe (z.B. durch eine Messung) bekannt und man interessiert sich für die zugrunde liegenden Parameter.

Wir betrachten das folgende Modellproblem, wobei Ω den Gegenstand von Interesse bezeichnet: zu einer in Ω gegebenen Wärmeleitfähigkeit σ (dem Parameter) soll die zugehörige Wärmeverteilung u (die physikalische Größe) bestimmt werden, sodass die folgende PDGL erfüllt ist

$$\nabla \cdot (\sigma \nabla u) = 1 \quad \text{in } \Omega \qquad u = 0 \quad \text{on } \partial\Omega. \tag{3.1}$$

Dabei bezeichnet $\partial\Omega$ den Rand des Gebiets Ω. Das zugehörige *inverse Modellproblem* lautet: bestimme zu einer über Ω gegebenen Temperaturverteilung u den zugehörigen Wärmeleitkoeffizienten σ, sodass (3.1) erfüllt ist.

Hadamard [Had14] formulierte einst folgende Bedingungen für ein *wohlgestelltes* mathematisches Problem: Existenz einer Lösung, Eindeutigkeit einer Lösung und die stetige Abhängigkeit der Lösung von den Daten (kleine Fehler in den Daten resultieren lediglich in kleinen Fehlern in der Lösung). Weiterhin schlug Hadamard vor sich nur mit wohlgestellten Problemen zu beschäftigen und Probleme bei denen mindestens eines der Kriterien nicht erfüllt ist, sogenannte *schlechtgestellte* Probleme, zu ignorieren. Da viele wichtige inverse Probleme partieller Differentialgleichungen (unter anderem das vorgestellte Modellproblem) schlechtgestellt sind, ist diese Ansicht offenbar nicht mehr zeitgemäß und es stellt sich die Frage, wie solche Probleme dennoch effizient und stabil gelöst werden können. Dabei sei angemerkt, dass die Schlechtgestelltheit oft dadurch auftritt, dass das dritte Kriterium verletzt ist, sodass kleine Fehler in den Daten zu beliebig großen Fehlern in der Rekonstruktion, der Lösung des inversen Problems, führen können.

Ein einfacher Ansatz wäre es, zu einem geratenen Parameter die zugehörige Lösung der PDGL zu bestimmen, diese mit den beobachteten Daten zu vergleichen und diesen Vorgang so lange zu wiederholen bis eine PDGL-Lösung die beobachteten Daten

zufriedenstellend approximiert. Abgesehen davon, dass das Raten eines Parameters keine effiziente Strategie ist, schlägt der Ansatz fehl, sobald das inverse Problem schlecht gestellt ist und die Daten durch Messfehler belastet sind. Dennoch hat dieser Ansatz etwas mit vielen modernen Lösungsalgorithmen von inversen Problemen gemein: um das inverse Problem zu lösen muss das zugehörige Vorwärtsproblem teilweise sehr häufig gelöst werden. Sogenannte *Regularisierungsmethoden*, siehe z.B. [KNS08, EHN96, Rie03] für eine Einführung, verwenden einerseits ausgefeilte Strategien um den gesuchten Parameter zu finden und sind andererseits in der Lage auch im Fall von gestörten Daten eine stabile Lösung zu finden.

Das frequentierte Lösen der zum inversen Problem gehörigen PDGL ist sehr zeitaufwendig und damit die grundlegende Motivation für diese Arbeit. Wir wollen Lösungsverfahren von inversen Problemen beschleunigen, indem wir die für die Vorwärtslösung benötigte Rechenzeit verringern. Genauer gesagt wollen wir anstatt der Vorwärtslösung eine Approximation an diese verwenden, welche kostengünstig zu berechnen ist. Somit werden wir Verfahren entwickeln, welche eine Kombination aus diesem Ansatz der approximierten Vorwärtslösung und bestehenden Lösungsverfahren sein werden. Für die Bestimmung einer kostengünstigen Approximation an die Vorwärtslösung verwenden wir die *Reduzierte Basis Methode*, eine Modellreduktionstechnik.

Zu einer parametrisierten PDGL, sei dies beispielsweise (3.1) mit $\sigma \in \mathcal{P}$ dem Parameter im Parameterraum $\mathcal{P}$ und $u^\sigma \in Y$ der zugehörigen Lösung im Lösungsraum Y, gibt es eine dazugehörige Lösungsmannigfaltigkeit $\mathcal{M} := \{u^\sigma \mid \sigma \in \mathcal{P}\}$. Das Ziel der klassischen Reduzierten Basis Methode ist es einen niedrigdimensionalen globalen *Reduzierte Basis Raum* (RB-Raum) $Y_N \subset Y$ zu konstruieren welcher die Mannigfaltigkeit $\mathcal{M}$ approximiert. Die Galerkinprojektion von u^σ auf Y wird dann als *Reduzierte Basis Lösung* (RB-Lösung) u_N^σ bezeichnet. Oftmals ist der RB-Raum die lineare Hülle sogenannter *Snapshots*, das sind Beispiellösungen der PDGL zu bestimmten, für das Problem relevanten, Parametern. Abbildung 9 zeigt eine schematische Darstellung der Reduzierten Basis Methode und wir verweisen auf [RHP08, Haa17] für eine ausführliche Übersicht der Methode.

Kehren wir zu unserem schlechtgestellten inversen Modellproblem zurück. In Kapitel 1 dieser Arbeit wird das nichtlineare Landweber-Verfahren, siehe z.B. [HNS95, Han14] für eine tiefgreifende Untersuchung dieses einfachen iterativen Regularisierungsverfahrens, verwendet, um das inverse Modellproblem zu lösen. Weiterhin wird eine neue Methode entwickelt, welche das nichtlineare Landweber-Verfahren mit der Reduzierten Basis Methode verknüpft. Ein *direkter Ansatz* um die beiden Methoden zu verknüpfen wäre: konstruiere einen globalen RB-Raum für die zugrunde liegende PDGL (3.1) und ersetze alle im Landweber-Verfahren vorkommenden Vorwärtslösungen durch entsprechende RB-Lösungen. Offenkundig basiert dieser Ansatz auf der Möglichkeit einen globalen RB-Raum zu konstruieren.

Beim inversen Modellproblem möchte man jedoch ein hoch aufgelöstes Bild der Wärmeleitfähigkeit rekonstruieren, sodass dies in der numerischen Behandlung auf

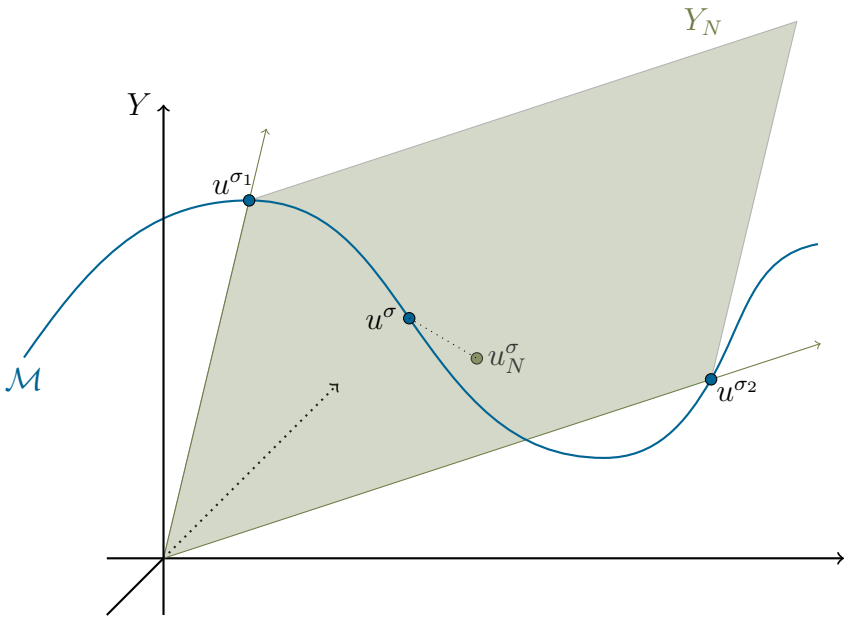

Abbildung 9: Schematische Darstellung der Reduzierten Basis Methode. Der RB-Raum Y_N ist die lineare Hülle der Snapshots u^{σ_1}, u^{σ_2}. Weiter ist u_N^{σ}, die Reduzierte Basis Approximation von u^{σ}, als die orthogonale Projektion von u^{σ} auf Y_N dargestellt.

einen hochdimensionalen Parameterraum führt, da ein Pixel des Bildes einer Dimension des Parameterraumes entspricht. In Kapitel 1 wird erörtert, warum man für solch einen komplexen und hochdimensionalen Parameterraum keinen globalen RB-Raum mehr konstruieren kann, womit der direkte Ansatz für uns nicht mehr in Frage kommt. Das bringt uns zum ersten Hauptresultat dieser Arbeit: der Entwicklung eines allgemeinen Ansatzes, welcher es erlaubt, die Reduzierte Basis Methode im Kontext von hochdimensionalen Parameterräumen bei der Bildrekonstruktion zu verwenden. Als Resultat werden wir neue Verfahren erhalten, welche bestehende Lösungsverfahren für (schlechtgestellte) inverse Probleme mit einem *adaptiven Reduzierte Basis Ansatz* verbinden, dessen Grundzüge wir im Folgenden erläutern wollen.

Iterative Regularisierungsverfahren wie das Landweber-Verfahren geben eine Folge von Iterierten aus, welche mit dem Startwert beginnt und mit der exakten Lösung des inversen Problems oder einer Approximation derselben endet. In jedem Fall befinden sich alle Elemente dieser Folge in einem a-priori unbekannten Teil des Parameterraumes $\mathcal{P}$, womit sich die zugehörigen PDGL-Lösungen ebenfalls in einem a-priori unbekannten Teil der Lösungsmannigfaltigkeit $\mathcal{M}$ befinden. Um diese Vorwärtslösungen durch geeignete Reduzierte Basis Approximationen zu ersetzen genügt es also einen *lokalen Reduzierte Basis Raum* zu konstruieren, welcher lediglich diesen a-priori unbekannten Teil der Mannigfaltigkeit (anstatt ganz $\mathcal{M}$) approximiert. Wie

kann man aber einen solchen lokalen RB-Raum konstruieren, wenn der zu approximierende Teil von $\mathcal{M}$ und der dazugehörige Teil von $\mathcal{P}$ a-priori unbekannt sind? Um dieses Problem zu lösen, werden wir uns die Eigenschaft des Lösungsverfahrens des inversen Problems zu Nutze machen, neue Parameter zu finden, welche der Lösung des inversen Problems dienlich sind. Wir geben die folgenden Schritte als Grundlage unseres adaptiven Reduzierte Basis Ansatzes an:

1. Sei ein RB-Raum Y_N gegeben, so projiziere den Lösungsalgorithmus des inversen Problems auf diesen RB-Raum.
2. Generiere mit Hilfe dieses projizierten Verfahrens neue Iterierte bis entweder eine Iterierte das inverse Problem löst oder bis der RB-Raum Y_N erweitert werden muss.
3. Im ersten Fall wird das Verfahren beendet, im zweiten Fall wird die zur aktuellen Iterierten gehörige Vorwärtslösung verwendet, um den RB-Raum Y_N zu verbessern. Danach wird mit dem ersten Schritt fortgefahren.

In Kapitel 1 wird diese Idee sorgfältig ausgearbeitet mit dem Resultat des neuartigen *Reduzierte Basis Landweber-Verfahrens*. In einer numerischen Untersuchung wird dieses neue Verfahren mit dem ursprünglichen Landweber-Verfahren verglichen. Es wird sich herausstellen, dass das neuartige Verfahren um mehr als eine Ordnung schneller ist, wobei es numerisch dasselbe Bild wie das ursprüngliche Verfahren liefert. Abbildung 10 stellt eine Vorschau der Resultate bezüglich dieser Ähnlichkeit der Rekonstruktionen dar.

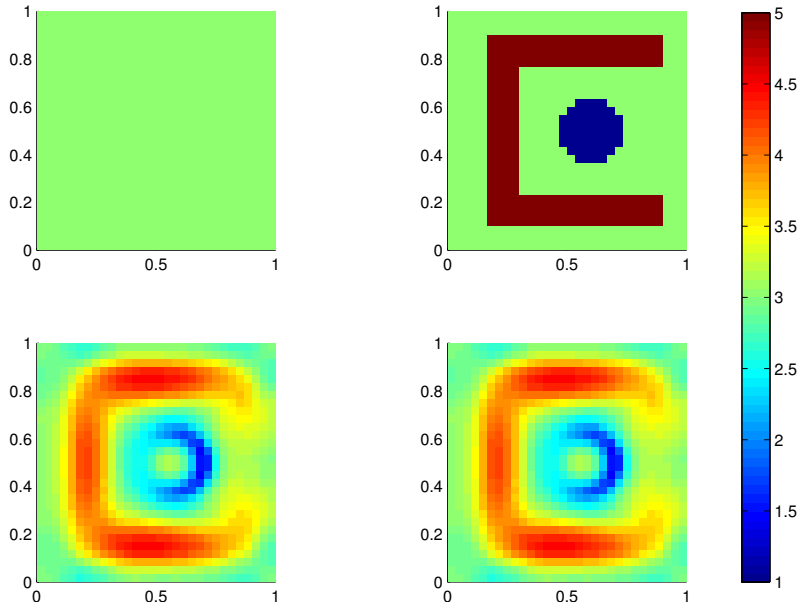

Abbildung 10: Der Startwert (oben links), die exakte Lösung (oben rechts), die Rekonstruktionen mit dem Reduzierte Basis Landweber-Verfahren (unten links) und dem Landweber-Verfahren (unten rechts).

Magnet Resonanz Elektrische Impedanztomographie

Im zweiten Kapitel dieser Arbeit soll der zuvor entwickelte adaptive Reduzierte Basis Ansatz auf ein komplexes und praxisrelevantes Problem angewandt werden. Vor allem soll die dadurch entstehende neue Methode mit Hinblick auf Konvergenz theoretisch ausführlich untersucht werden. Daher widmet sich der zweite Teil dieser Arbeit dem Problem der Magnet Resonanz Elektrischen Impedanztomographie (MREIT).

Bei der MREIT handelt es sich um ein Bildgebungsverfahren, welches während der letzten drei Jahrzehnte entwickelt wurde. Dabei wird ein Gegenstand, an welchen Elektroden angeheftet sind, in einen Kernspintomographen gelegt und es ist das Ziel des Verfahrens die elektrische Leitfähigkeit des Gegenstandes zu bestimmen. Die dazu benötigten Daten werden folgendermaßen gewonnen: indem Strom an einer der Elektroden angelegt wird, wird ein Stromfluss erzeugt, welcher wiederum eine Änderung der Magnetflussdichte $\mathbf{B} = (B_x, B_y, B_z)$ induziert. Diese kann mit Hilfe des Kernspintomographen gemessen werden, wodurch man einen vollen Satz innerer Daten zur Hand hat, sodass hoch aufgelöste Bilder der elektrischen Leitfähigkeit des Gegenstandes rekonstruiert werden können.

Die Idee der MREIT entspringt der Elektrischen Impedanztomographie (EIT), siehe z.B. [CIN99, NGI88, AGL11, Lio04, Uhl09] für eine ausführliche Übersicht der Methode, wobei die elektrische Leitfähigkeit des Gegenstandes mit Hilfe von Strom-zu-Spannungsmessungen, welche an den Elektroden durchgeführt werden, rekonstruiert werden soll. Da kein Kernspintomograph benötigt wird ist der Aufbau der EIT wesentlich einfacher, allerdings ist das zugehörige inverse Problem überaus schlecht gestellt und nichtlinear, sodass die Auflösung der Bildrekonstruktionen oftmals sehr gering ist. Dieser Nachteil der EIT ist die historische Motivation zur Entwicklung der MREIT.

Wir werden in dieser Arbeit die B_z-basierte MREIT untersuchen. Dabei wird angenommen, dass mit B_z nur eine Komponente des Magnetfeldes $\mathbf{B}$ bekannt ist wobei die z-Richtung die Richtung des Hauptmagnetfeldes des Kernspintomographen bezeichnet (möchte man das komplette Magnetfeld messen, so muss der Gegenstand im Tomographen rotiert werden, was in der Praxis oft unmöglich ist). Seo u.a. [SYWK03] haben mit dem *Harmonischen B_z Algorithmus* ein numerisches Lösungsverfahren für dieses B_z-basierte inverse Problem der MREIT entwickelt und wir weisen darauf hin, dass dieser Algorithmus seitdem ausführlich untersucht wurde, siehe z.B. [OLW$^+$03, KPSW06, WS08, LSSW07, LSW10, SW11] und die darin enthaltenen Quellen.

Wir untersuchen dieses praxisrelevante Problem mit dem Harmonischen B_z Algorithmus als Lösungsverfahren und beweisen mit Theorem 2.2.12 ein Konvergenzresultat welches die bestehende Konvergenztheorie, siehe [LSSW07, LSW10], zu einem approximativen Harmonischen B_z Algorithmus hin erweitert. Dabei hängt es nicht davon ab welche Art von Approximation an die Vorwärtslösung der entsprechenden

PDGL man verwendet, solange diese einer Regularitäts- und einer Qualitätsbedingung genügt. Damit folgt das zweite Hauptresultat dieser Arbeit: die numerische Konvergenz des Harmonischen B_z Algorithmus. Wir möchten dabei hervorheben, dass Konvergenzresultate im Bereich der inversen Probleme (sofern es sie gibt) meistens die Kenntnis der exakten Vorwärtslösung annehmen, sodass keine numerische Konvergenz des zugehörigen Verfahrens folgt (in einer numerischen Implementation wird stets eine Approximation an die Vorwärtslösung verwendet). Somit ist Theorem 2.2.12 ein Schritt hin zur numerischen Konvergenz anderer Lösungsverfahren von inversen Problemen.

Da das theoretische Resultat von der Art der Approximation nicht abhängt, erhalten wir ebenfalls die Konvergenz des neuartigen *Reduzierte Basis Harmonischen B_z Algorithmus*, welcher die Kombination unseres adaptiven Reduzierte Basis Ansatzes und des Harmonischen B_z Algorithmus ist. In einer kurzen numerischen Untersuchung stellen wir fest, dass dieser Reduzierte Basis Harmonische B_z Algorithmus schneller als der Harmonische B_z Algorithmus ist, wobei die Qualität der Rekonstruktion gleichbleibend ist. Somit funktioniert unser adaptiver Reduzierte Basis Ansatz also auch angewandt auf dieses komplexe praxisrelevante Problem. Abbildung 11 stellt eine Vorschau der Resultate im Bezug auf die Qualität der Rekonstruktion dar wenn keine Messfehler vorliegen, wobei wir in der eigentlichen Untersuchung auch fehlerbehaftete Messdaten berücksichtigen.

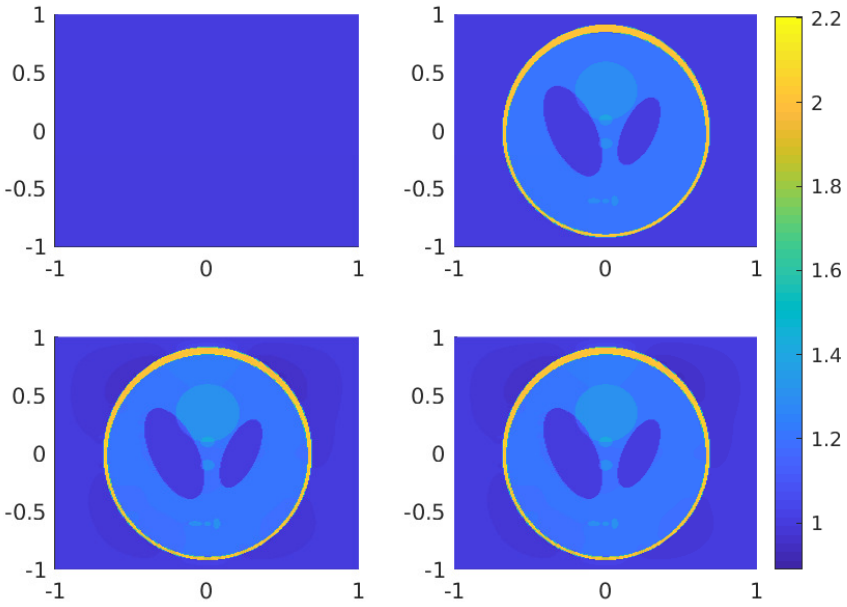

Abbildung 11: Der Startwert (oben links), die exakte Lösung (oben rechts), die Rekonstruktionen mit dem Harmonischen B_z Algorithmus (unten links) und dem Reduzierte Basis Harmonischen B_z Algorithmus (unten rechts).